Spectral and Temporal Control of Broadband Pulses to Enable Multi-TW Peak Power Coherently-combined Fiber Laser Arrays

by

Siyun Chen

A dissertation submitted in partial fulfillment
of the requirements for the degree of
Doctor of Philosophy
(Electrical and Computer Engineering)
in The University of Michigan
2021

Doctoral Committee:

Professor Almantas Galvanauskas, Chair
Professor Igor Jovanovic
Mr. John Nees
Professor Herbert Winful

Siyun Chen

chensyun@umich.edu

ORCID iD: 0000-0002-6350-8472

ACKNOWLEDGEMENTS

I would like to thank Prof. Galvanauskas for his valuable insight and support. My work would've turned out very differently without his patience and unconditioned trust throughout the years. I learnt a great deal from him on scientific mindset and career path as well.

I would like to thank my committee John Nees, Prof. Jovanovic and Prof. Winful for their help and guidance on my projects over the years. I also want to express my gratitude for my colleagues, Matthew Whittlesey, Lauren Cooper, Alexander Rainville, Mingshu Chen, Chris Pasquale, Yifan Cui, Weizhi Du, Yu Bai, Yanwen Jing, Hanzhang Pei, John Ruppe, Morteza Sheikhsofla, Cheng Zhu and I-Ning Hu, for their help and contribution on both the work and life. They are an integral part of this project and I owe them a lot.

I want to thank our collaborators Qiang Du, Russell Wilcox and Tong Zhou at Lawrence Berkeley National Lab, Jay Dawson at Lawrence Livermore National Lab, Frank Wise and Pavel Sidorenko at Cornell University, and Yariv Shamir and Shaul Pearl at SOREQ- nuclear research center at Israel.

Finally, I want to thank all of my friends here at Ann Arbor for the years of time we've spent together.

TABLE OF CONTENTS

LIST OF FIGURES

Figure

ABSTRACT

Coherent beam combining of fiber laser arrays is promising to potentially generate multi-TW peak power and multi-KW average power optical pulses, which are desired for various scientific and industrial applications, such as the next generation laser plasma accelerators, and secondary radiation sources. Coherent Pulse Stacking Amplification (CPSA) technique, a temporal pulse combining approach, which enables two orders of magnitude higher pulse energies from a single fiber amplifier than the traditional CPA approach, is currently emerging as a key technique enabling practical power scaling of fiber laser arrays.

This thesis develops some theoretical and experimental aspects of amplifying broadband ultrashort pulses with the CPSA technique. Exploiting the previous work by others, which established foundations of the CPSA technique, this current thesis addresses various issues arising in high energy CPSA and fiber Chirped Pulse Amplification (CPA) associated with broadband pulses, such as compensation of gain narrowing in a high energy Yb-doped fiber amplifier chain, dispersion engineering to compensate large amounts of higher-order material dispersion in the system, and compensating individual pulse distortions in an amplified CPSA stacking burst occurring at highly saturated energy extraction in the final stages. As a result, this thesis demonstrates the potential for achieving much shorter pulse durations with a fiber-based system, well beyond the current state-of-the-art.

In more detail, research and development work presented in this thesis consists of the following main thrusts. First, we developed several high-energy pulse amplification fiber models to explore the broadband pulse performance, and to calibrate numerical model predictions with experimental measurements, which was later extensively used in the other research thrusts of this thesis. Second, we proposed and developed a method to overcome amplitude shaping effects in individual pulses from strong gain saturation in high energy fiber amplifiers by actively controlling in-burst pulse shapes and phase profiles, which included experiments demonstrating gain saturation compensation at multi-mJ pulse energies from a large core fiber amplifier. Furthermore, we explored gain narrowing effects with increasing, and very high -100-150dB, gain in fiber systems, and demonstrated entire gain narrowing compensation for reaching 40-100fs pulses in the CPSA system, with the gain equivalent to ~10mJ energy amplification, which is well beyond what has been previously demonstrated in the state-of-the-art. Finally, we proposed and experimentally demonstrated a novel dispersion compensation approach to accurately compensate all the relevant higher-order dispersion terms for compressing CPSA system output pulses down to this sub-100fs range.

In summary, this thesis provides the theoretical foundations and experimental validation of several new concepts, that enable broadband CPSA technique. When combined with coherent spatial combining, this broadband CPSA technique is key for developing multi-TW peak power laser systems, with pulse durations in sub-100fs range that are needed by the majority of high-intensity laser-matter interaction applications.

CHAPTER 1

Introduction and Motivations

1.1 Background

Lasers were born out of 1950s thanks to the contributions from many research groups worldwide, who broadened our knowledge on the basic principles of light generation of coherent diffraction-limited laser beams. The theory of Maxwell electromagnetic radiation was developed by Maxwell in 1873. The scientific foundations of light generation amplification were developed (and later awarded the for) by Townes, Basov and Prokhorov, who received the Nobel Prize in 1964 for laying the quantum theory for oscillators and amplifiers [1]. Based on this, in 1960, Theodore Maiman introduced a ruby laser [2]. Since then, there have been significant advance in terms of fundamental work and laser technique development, which also enabled practical laser applications in a variety of different fields, such as scientific studies, medical and commercial laser applications [3].

There has been a strong demand for lasers that generate high peak power and high average power optical pulses, as required by multiple applications such as laser material processing, medicine, neutron generation, etc. [4]. Next generation laser plasma accelerators, for example, will require laser sources that are able to generate multi-TW peak power (30-100 fs pulse duration, >0.1-10 J pulse energy) and 10-100 kw average power laser pulses [5]. However, currently mature high-

power laser technologies are subjected to many technological limitations that inhibit pushing average powers of high-intensity lasers further.

One of the most important limitation for higher pulse energies are nonlinear effects that distort the signal, or even cause optical damage due to high optical intensity. In fiber laser systems, which is the topic of this thesis, nonlinearity can cause stronger effects than in solid-state lasers because the signal has longer interaction length, and the beam is confined in a small cross-sectional area. One of the most import technique developed to reduce or avoid nonlinear effects is Chirped Pulse Amplification (CPA), introduced by Strickland and Mourou in 1985, and which won the Nobel Prize in 2018 [6]. CPA allows the peak power to increase by five orders of magnitude without involving nonlinear issues. This is achieved by stretching seed pulse to reduce the peak power before amplification. Thus, the pulse can be amplified to higher energy level by a factor similar to the stretching factor. After amplification, the pulse is compressed down to the bandwidth-limited duration. However, in order to reach TW peak powers with fiber lasers many further improvements are needed. To extract maximum energy from gain media at the stored energy limit, longer pulse duration (10-100ns) are necessary, while the current stretching and compressing techniques allow to stretch the signal to only 1-2 ns due to the practical size constraints of the stretching and compressing optical components.

In recent years, Coherent Pulse Stacking Amplification (CPSA) was introduced to further extend the pulse duration, and thus achievable pulse energy, by temporal combining [7]. Instead of a single input pulse, CPSA starts with a burst of pulses which are modulated to have specific amplitude and phase waveforms. The pulses in the burst are stretched to 1 ns and then sent into a

set of amplification stages. After amplification, the burst is sent into a sequence of free-space interferometers where the pulses in this burst are stacked to a single pulse. A compressor then compresses this single pulse down to the bandwidth-limited pulse duration. CPSA has the potential to stack > 100 pulse without requiring complex arrangement. This would correspond to amplifying a 100 ns stretched pulse duration in CPA systems. This thesis is dedicated to optimizing the CPSA system to accommodate broadband pulses for reaching very short pulse durations, and for improving stacking efficiency of such pulses at high energies. Thus, it lays the foundation that will enable development of multi-TW peak power fiber laser systems.

Apart from pulse energy scaling, very short pulse durations are also very important for achieving multi-TW peak power laser pulses. There are two aspects that need to be optimized in order to generate short pulses: broad spectral bandwidth, and accurate dispersion control. First, there has to be enough spectral content to obtain short pulses, and so the laser system should be designed and implemented carefully in order to avoid significant spectral narrowing. In high energy laser systems, the main phenomena affecting the spectral bandwidth are the gain saturation, and the gain narrowing. Gain saturation induces time-dependent gain on the pulses. This is because the gain is determined by the upper-level ion population in the gain medium, which is depleted along the propagating pulse burst as it travels in the gain medium. For chirped pulses whose spectral shape is similar to its temporal shape, this time-dependent gain occurs due to the saturation-induced changes in the gain spectrum that the different pulses in the burst encounter. As this thesis will show, gain saturation compensation is necessary for Coherent Pulse Stacking Amplification (CPSA), since this time-dependent gain will shape different pulse differently. This is detrimental to the CPSA technique, which requires identical pulse shapes across the burst. Gain narrowing

also occurs, reducing spectral bandwidth of the amplified signals. To achieve very short pulses of less than ~100fs, the required spectral bandwidth typically exceeds the residual gain bandwidth after multiple amplification stages, due to the non-flat Yb-doped fiber gain curve is with respect to wavelength. For example, to achieve multi-mJ pulse energies, the total gain in the fiber CPA or CPSA system can reach higher than 100dB. Such high gain can narrow amplified pulse spectrum by approximately ten times longer. Therefore, it becomes necessary to compensate gain narrowing effects in such systems in order to achieve <100fs pulse durations.

Broadband pulses are very sensitive to the residual dispersion of the fiber laser system [8]. Higher-order residual dispersion terms can very detrimentally affect the final compressed pulse duration and its shape. But accurately controlling dispersion to have different dispersion orders compensated nearly to zero is a significant technical challenge. Typical 2nd to 4th phase orders from dispersion (β_2 to β_4) need to be considered, and for very broadband pulses, 5th phase order may also need to be addressed. Dispersive components such as stretchers, compressors and gain mediums usually have different phase order ratios (β_3/β_2, β_4/β_2) and thus compensating all the orders at the same time is very difficult. This is especially true for high power fiber laser systems, where the cumulative total fiber length is usually tens of meters. This induces a large amount of different dispersion orders, thus making dispersion compensation for achieving bandwidth-limited pulse durations much harder.

This thesis work consists of three main components. First, in-burst pre-shaping for gain saturation control in Coherent Pulse Stacking Amplification (CPSA) is demonstrated, to enable high-fidelity pulse stacking under strong saturation conditions in the final amplification stages. Second, gain

narrowing in Yb-doped fiber laser systems is explored and analyzed, and a birefringent plate based spectral filter is designed, and implemented to compensate gain narrowing for very high total gains. Third, the issues related to dispersion are analyzed, and a novel dispersive device is designed based on controlled optical aberrations is proposed and demonstrated. This dispersion compensator can be used to match the phase orders of different combinations of diffraction-grating stretchers, compressors, and optical fibers for achieving sub-100 fs compressed pulses.

1.2 Fiber Chirped Pulse Amplification (FCPA) and its Limitations

Chirped Pulse Amplification (CPA) was introduced by Strickland and Mourou in 1985 for amplifying optical pulses to high energy without optical damage or nonlinear signal distortion. As figure 1.1 shows, an ultrashort input pulse is temporally stretched by an optical stretcher to significantly reduce the peak power. The stretcher imprints a large amount of chromatic dispersion onto the pulse due to the different propagation distances travelled by different wavelengths. In the process a spatially chirped pulse is produced, which after the second pass through the stretcher is unchirped spatially and exits the stretcher as a single diffraction-limited beam. Thus, the stretched pulse duration is proportional size grating separation, as well as to the transverse size of the largest diffraction grating in the stretcher. The stretched pulse is then sent to the amplifier and is amplified to high energy levels, while maintaining peak powers below the threshold for significant nonlinear effects. After amplification, this pulse goes through a dispersive compressor to remove the temporal chirp. The dispersion provided by the compressor has a similar magnitude but opposite

sign than that of the stretcher. So, the pulse is compressed down to the similar duration as the input pulse. To obtain bandwidth-limit pulse duration, which is the shortest pulse duration a pulse signal can have, the compressor dispersion should match well that of the stretcher, plus that of the gain medium. This is a challenge for broadband signals, because sensitivity to the dispersion mismatch increases with the increasing pulse bandwidth.

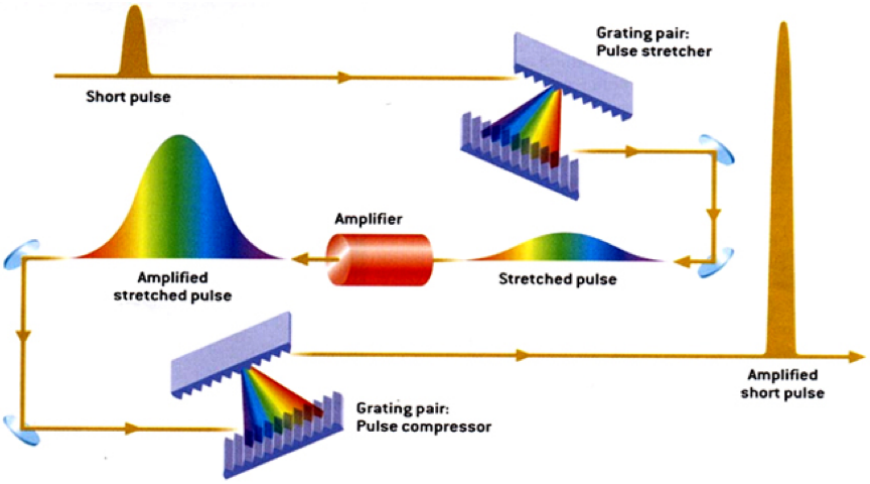

Figure 1.1 Chirped Pulse Amplification [6]

The maximum extracted energy, and so the highest achievable pulse energy in FCPA (Fiber Chirped Pulse Amplification) is determined by the stored energy in a gain medium. Since longer pulse durations have lower peak powers, which enables higher amplified energy, most of the stored energy should be extractable with the sufficiently long pulses, which for fiber-based systems >100 ns. With current stretching and compressing techniques laser pulses can be stretched to approximately 1-2 ns but achieving longer stretched pulses is impractical. Since the stretching factor is proportional to the stretcher/compressor grating size, very long stretched durations would require impossibly large grating. This has inspired new innovations to overcome the limitation due to the limited CPA stretched-pulse durations.

1.3 Coherent Beam Combining Techniques

Coherent beam combining techniques are a promising path in developing high power and high intensity lasers, since they enable to overcome the limitations in individual laser systems, thus, to enable much higher energies and powers than any of today's laser sources can reach. Coherent beam combining generally means combining the optical outputs from multiple fiber lasers in an array. There are mainly two types of beam combining techniques: spatial beam combining and temporal beam combining. Spatial beam combining involves multiple fiber amplifiers in an array to increase the output average power and pulse energy proportionally to the number of the parallel amplification channels. For a typical fiber amplifier, the achievable pulse energy is 0.1-1 mJ. Spatial beam combining allows to directly increase this number by the factor of the number of channels. To reach >1 J pulse energy by spatially combining FCPA laser systems, it requires 10^4 -10^5 channels at the mJ to sub-mJ level each. This complexity can introduce many technical issues and can be of limited practical use.

Temporal beam combining means combining a number of pulses in time domain. In a single fiber amplifier, a burst rather than a single pulse is amplified and then the pulses in this burst are stacked to a single pulse by free-space optical components. One of the temporal beam combining techniques is Divided Pulse Amplification (DPA) [9]. A single pulse is split into multiple pulses by polarization-control components (polarizing beam splitters, waveplates and delay-lines) before amplification. The time-separated pulses are then amplified so that this is equivalent to increasing the pulse duration. After amplification, the pulses are combined back to a single pulse by similar polarization-control components. This technique has the potential to extend the pulse duration and

reach higher energy level than a single nanosecond pulse can do. But the limitation is that spatial splitting does not have enough degrees of freedom to control saturation processes in the final amplification stages. Furthermore, when the pulse number goes up, the total length of the delay-lines increases proportionally. Having this splitting setup both before and after the amplification stages consumes large space and is not easy to arrange. In this thesis, Coherent Pulse Stacking Amplification (CPSA) is chosen to push the energy limit. Since CPSA relies on electronically controlled pulse burst formation, it can achieve full control of the saturation processes in high energy fiber amplifiers. Additionally, the total roundtrip length of the stackers is only half of that of the DPA systems.

1.4 Coherent Pulse Stacking Amplification (CPSA)

Coherent Pulse Stacking Amplification, also called temporal pulse combing, is an extension of Chirped Pulse Amplification technique [7]. This temporal scaling technique consists of two parts. One is pulse modulation that picks up a burst from the pulse train output of an oscillator and tailors the amplitude and phase of each of the pulses to have the desired waveform. The other is a sequence of free-space interferometers that stacks this burst into a single pulse. This technique further increases the pulse duration by 10-1000 times in the fiber amplifiers based on CPA systems, and allows to fully extract the stored energy. Compared to the complexity of using only the spatial beam combining, where 10-1000 fiber arrays must be combined and controlled, CPSA allows orders-of-magnitude smaller numbers of parallel amplification channels in a fiber array, is thus more compact and easier to implement.

One of the critical requirements for CPSA is that the amplitude and phase of individual pulses in the burst must be identical, in order to achieve high fidelity pulse stacking. In high power fiber amplifiers gain saturation shapes pulses in both temporal and spectral domains, which can limit the extractable energy due to its shaping effects. Thus, gain saturation control becomes necessary.

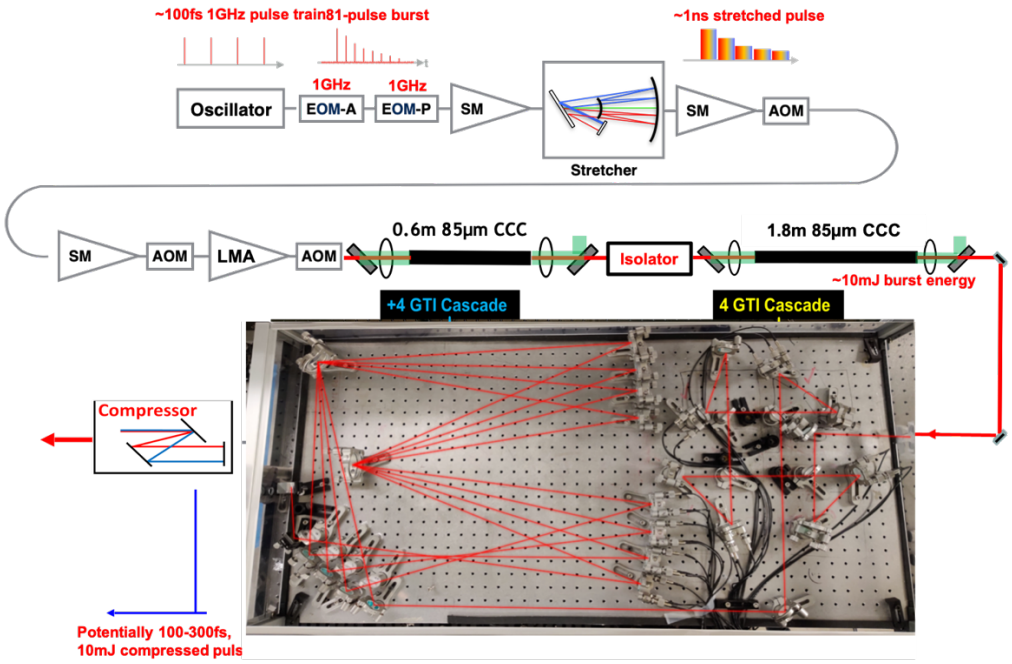

Figure 1.2 Experimental setup of the CPSA system.

1.5 Gain Narrowing Compensation

To achieve TW peak power laser pulses, 30-60 nm signal bandwidth (50-100 fs pulse duration) is required of the laser system. Gain narrowing is one of the most detrimental effects that prohibits

achieving sub-fs pulses, because it narrows spectral bandwidth with increasing gain. When the input energy is much lower than the saturated energy of the fiber amplifier, the gain seen by the seed is a small signal gain, which can be expressed as:

$$G(\lambda) = \exp\left[\sigma(\lambda)\Delta NL\right] \tag{1.1}$$

$$G_{dB}(\lambda) = 4.34 \times \sigma(\lambda)\Delta NL \tag{1.2}$$

Where, $\sigma(\lambda)$ is the emission cross section, ΔN is the conversion and L is the fiber length. In Yb-doped fiber amplifiers, 1030 nm has the peak emission cross section, corresponding to the highest gain. Let λ_0 = 1030 nm and assume the input spectrum is flat-top, the output spectrum is:

$$I_{out}(\lambda) = I_{in}G_{dB}(\lambda) = 4.34I_{in} \times \sigma(\lambda)\Delta NL \tag{1.3}$$

The FWHM of the bandwidth can be obtained by calculating 3dB point:

$$I_{out}(\lambda_{3dB}) = 4.34I_{in} \times \sigma(\lambda_0)\Delta NL - 3 = 4.34I_{in} \times \sigma(\lambda_{3dB})\Delta NL \tag{1.4}$$

$$\Delta\lambda = 2\lambda_{3dB} = \sigma^{-1}\left(\frac{4.34I_{in}\times\sigma(\lambda_0)\Delta NL-3}{4.34\Delta NL}\right) = \sigma^{-1}\left(\frac{I_{in}\times G(\lambda_0)-3}{4.34\Delta NL}\right) \tag{1.5}$$

Since $\lambda_0 = 1030$ nm is where the maximum value of the emission cross section is, the emission cross section decreases as the wavelength is away from λ_0. Therefore, $\Delta\lambda$ decreases as the gain $G(\lambda_0)$ increases.

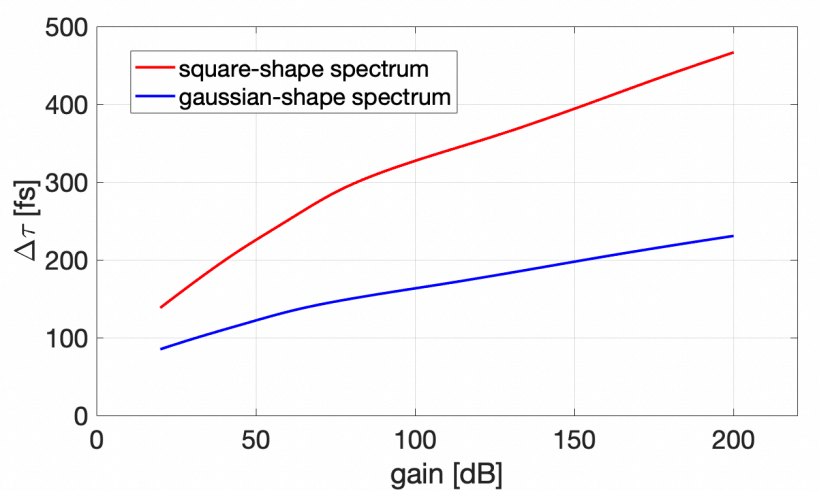

Figure 1.3 Bandwidth-limit pulse duration dependency on the total gain in an Yb-doped fiber amplifier system

Figure 1.3 shows the bandwidth-limited pulse duration at different total-gain values for a flat-top and a gaussian-shaped input spectrum. In a CPA system, where the seed spectrum is truncated by the hard-edge of optical components in the stretcher (such as diffraction-grating edges), the spectrum can be square-shaped. To achieve 0.1-1 J pulse energy, >100 dB gain is necessary and so the available pulse duration is only 300-500 fs, achievable without gain narrowing compensation.

This thesis demonstrates a method to equalize the gain by using spectral filters to pre-shape the seed spectrum and shows that 50-100 fs compressed pulse durations are achievable for >150 dB total gain. This proves the feasibility of TW peak power fiber laser systems, with >1 J pulse energies and pulse durations in this 50-100fs range.

1.6 Dispersion Management

CPA is well-established in high peak power solid state and fiber lasers, where it uses diffraction gratings to stretch and compress ultrashort pulses [10]. Various fiber-based stretchers were also proposed and demonstrated for fiber CPA system, such as specially designed fiber stretchers [11], [12], and fiber Bragg gratings. However, there are still many issues that remain to be addressed. For instance, when a fiber stretcher is used to stretch the seed in the front end, it higher-order dispersion orders might be not matched by a grating compressor, thus limiting the achievable stretched pulse duration for ~100fs to only ~100 ps. Thus, the achievable amplified pulse energy is quite low in such a system.

Second, high power fiber laser systems generally consist of a sequence of fiber amplification stages and so the total fiber length is long (e.g., 30-50 m). Such long fiber length requires a large mismatch between the stretcher and the compressor to compensate the large amount of fiber dispersion. Even using stretchers and compressors that have matched phased orders, for example, stretchers and compressors that have the same pair of gratings, this mismatch induces uncompensated large magnitudes of higher order dispersion that prohibits compressing the pulses down to sub-100 fs duration.

A new device having the potential to provide controllable and independent phase orders is desired to achieve TW peak power fiber laser systems. The novel device that is discussed in the following is an aberration-based controllable dispersion compensator that has tunable 2^{nd}, 3^{rd} and 4^{th} order phases over a large value range. This compensator can be used either in a CPA system working

with different combinations of stretchers and compressor, or a fiber delivery system to compensate fiber dispersion.

CHAPTER II

Modeling of High Energy Fiber Amplification

2.1 Background

Numerical simulation of fiber amplification is always important for exploring the physical foundation and providing guidance on system design and experimental implementation. On the other hand, fiber modeling is also valuable for examining current theoretical assumptions and conclusions. Modeling of fiber amplification can be complex due the involvement of many different light signals such as signal, pump and amplified spontaneous emission (ASE). It is generally a three-dimensional problem, which also need to consider light signals in temporal and spatial domains. In addition, for short pulses, the spectral domain involving multiple effects such as wavelength-dependent gain and dispersion, also need to be included. According to the time dependence of the signal and the pump, fiber amplifiers can be characterized within two categories: continuous-wave amplifiers (CW) and pulsed amplifiers [13]. CW amplifiers imply that the fiber is continuously or quasi-continuously pumped and the signal is continuously generated or amplified. Therefore, the CW fiber amplification model is independent of time and is a function of position along the fiber only. Once the input signal and pump power values are given, solving CW amplification equations is basically a process of solving a boundary value problem (BVP) of first-order ordinary differential equations (ODEs) [13]–[15]. Pulsed amplifiers are amplifiers deal with pulsed signals, and the pump can be either continuous or pulsed. So, pulsed amplification models should depend on both time and position coordinates, which is an initial-boundary value

problem of partial differential equations (PDEs) [16]. Neither of these two models can be solved analytically, and numerical methods must be implemented. There have been many methods developed for solving CW and pulsed amplifier equations. In this thesis work, a CW amplifier model is solved using the shooting method [15], and the finite difference method is chosen to obtain the solution of pulse amplifier model [16]. Both or the models are built for Yb-doped single-mode Chirally-Coupled-Core (CCC) fiber amplifiers, because they are the fibers used in all the experiments [17]. But the used theoretical framework and developed numerical models are applicable to any single-mode Yb-doped and other rare-earth ion-doped fiber amplifiers.

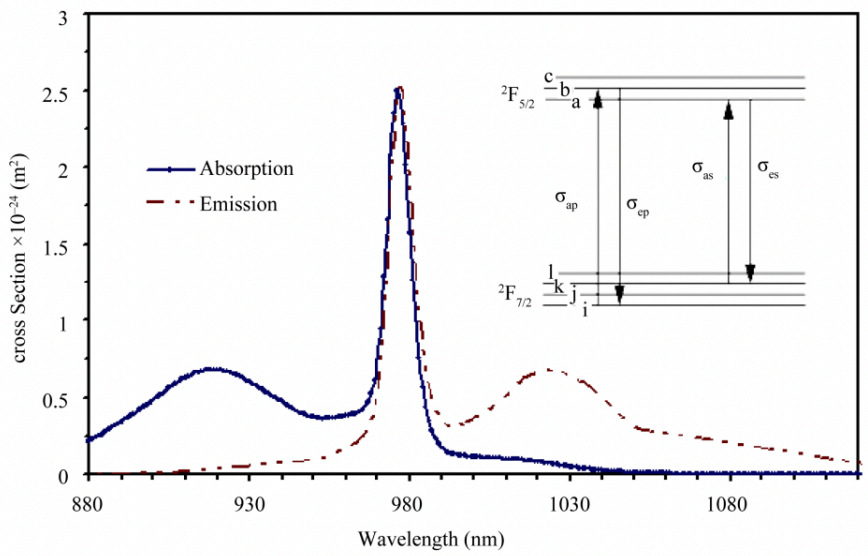

Figure 2.1 Cross sections of Yb3+ and its energy levels [18].

2.2 Yb3+ Atomic Rate Equation

Yb3+ ion has a simpler energy level structure compared to other rare-earth ions (e.g., Nd3+, Er3+ and Tm3+). It is a quasi-two level system: coupling the 2F_(7/2) ground state level, and the 2F_(5/2) excited state level. The rate equation can be written as:

$$\frac{dN_2(z,t)}{dt} = \sum_{k=1}^{k} \frac{1}{hcA_k} \Gamma_k \lambda_k [\sigma_a(\lambda_k) N_1(z,t) - \sigma_e(\lambda_k) N_2(z,t)] P_k^{\pm}(z,t) - \frac{N_2(z,t)}{\tau} \quad (2.1)$$

$$N_1(z,t) = N - N_2(z,t) \quad (2.2)$$

$N_1(\mathrm{z},\mathrm{t})$ and $N_2(\mathrm{z},\mathrm{t})$ is the lower and upper ion concentrations, N is the total ion concentrations in the fiber amplifier, $\sigma_a(\lambda_k)$ and $\sigma_e(\lambda_k)$ is the absorption and emission cross section which are functions of wavelength. λ_k corresponding to different wavelength channels, where k = 1, 2 …, K, and K is the number of wavelengths. The pump wavelength is denoted by λ_p, the signal wavelength is λ_s, and λ_{ase} is amplified spontaneous emission (ASE) wavelength. It should be noted that each of λ_p, λ_s, and λ_{ase} can comprise multiple different-wavelength channels. We assume that there are m pump channels, n signal channels, and the ASE band consists of one channel, each channel being defined by its spectral width Δλ. Therefore, total number of channels is K = m + n + 1. $P_k^{\pm}(z,t)$ is the power for each *k-th* wavelength channel. $P_k^{+}(z,t)$ means this spectral section is propagating forward with the same direction of the pump, while $P_k^{-}(z,t)$ is propagating backward with respect to the pump direction. τ is the life time of the upper level ions. A_k is the mode area of each channel. $\Gamma_k$is the overlap factor between the two corresponding modes. If we assume the doping area is uniformly doped by Yb^{3+} with doping radius a_0, then the doping concentration as a function of radius is

$$\rho(r) = \begin{cases} \rho_0 & for \quad r \leq a_0 \\ 0 & for \quad r > a_0 \end{cases} . \tag{2.3}$$

The overlap factor between the doping and a specific mode, which has the mode radius ω_k is,

$$\Gamma_k = 1 - \exp\{-(\frac{a_0}{\omega_k})^2\} \tag{2.4}$$

It should be noted that the two-level structure for Yb3+ is a simplified description. The two Yb3+ energy levels are not single levels. The lower one has 4 sublevels, and the upper one has 3. The manifolds are split by the Stark effect, which is induced by a ligand field generated by the charge distribution in the host glass. Ion distribution between each manifold is determined and stabilized by intramanifold thermalization. Figure 2.1 shows the absorption and emission cross sections of Yb3+at room temperature. Transitions A and B correspond to the pumping processes at 975nm and 910nm. Transition D represents the main amplification area centered at around 1030nm. Withing the short signal-wavelength range, the sublevels are very close to the ground state. In this case, the Yb3+ fiber system operates as a quasi-three-level system, without gain threshold. For wavelengths longer than ~1040nm, the Yb3+ fiber system operates as a quasi-four-level system.

2.3 Amplified Spontaneous Emission Calculation and Power Evolution Equations

Amplified spontaneous emission (ASE) can have a significant effect on laser or amplifier performance. For a fiber amplifier in particular, ASE is the most import factor that limits the stored energy, and thus determines the achievable pulse energy. Therefore, an accurate calculation of ASE is necessary for majority of amplifier configurations. The source of ASE is spontaneous emission (SE), which emits photons when an excited ion spontaneously returns to the ground state.

A small part of spontaneous emission is coupled into fiber modes, and then amplified while propagating along the fiber. In a fiber amplifier, ASE can propagate in two directions: forward (moving in the same direction as the pump), and backward (moving in the opposite direction as the pump).

Within an infinitely small volume dV, the number of spontaneously generated photons that have frequency between υ and υ + δυ are [19]:

$$dn(\upsilon) = h\upsilon d\upsilon \frac{g(\upsilon)}{\tau}\frac{d\Omega}{4\pi} dV_k \int N_2(r,\theta)\overline{\psi_k}(r,\theta) r dr d\theta \tag{2.5}$$

Here $g(\upsilon)$ is the lineshape function, τ is the upper-level lifetime, and $d\Omega$ is the solid angle. $dV_k = A_k dz = \pi\omega_k^2 dz$ is the infinitely small volume. $\overline{\psi_k}(r,\theta) = \frac{\psi_k(r,\theta)}{\int \psi_k(r,\theta) r dr d\theta}$ is the normalized mode amplitude profile. h is the Plank constant. For the fundamental mode,

$$\mathrm{d}\Omega = \frac{\lambda_k^2}{n_0^2 \pi \omega_0^2} \tag{2.6}$$

The lineshape is:

$$g(\upsilon) = \frac{8\pi n_0^2 \tau \sigma_e(\upsilon)}{\lambda_k^2} \tag{2.7}$$

The integration part is,

$$\int N_2(r,\theta)\overline{\psi_k}(r,\theta) r dr d\theta = n_2 \Gamma_k \tag{2.8}$$

Thus, the number of ions that are coupled into the fiber mode is,

$$dn(\upsilon) = 2h\upsilon d\upsilon\sigma_e(\upsilon)n_2\Gamma_k = 2\Gamma_k\sigma_e(\lambda)n_2\frac{hc^2}{\lambda_k^3}\Delta\lambda \tag{2.9}$$

Adding this ASE term into the power evolution equations, we have

$$\pm\frac{\partial P_p^{\pm}(z,t)}{\partial z} + \frac{1}{V_p}\frac{\partial P_p^{\pm}(z,t)}{\partial t} = -\Gamma_p\left[\sigma_a(\lambda_p)N_1(z,t) - \sigma_e(\lambda_p)N_2(z,t)\right]P_p^{\pm}(z,t) - \alpha(\lambda_p)P_p^{\pm}(z,t)$$

$$\begin{aligned}\pm\frac{\partial P_s^{\pm}(z,t)}{\partial z} + \frac{1}{V_s}\frac{\partial P_s^{\pm}(z,t)}{\partial t} &= -\Gamma_s[\sigma_a(\lambda_s)N_1(z,t) - \sigma_e(\lambda_s)N_2(z,t)]P_s^{\pm}(z,t) - \alpha(\lambda_s)P_s^{\pm}(z,t)\\ &\quad + 2\sigma_e(\lambda_s)N_2(z,t)\frac{hc^2}{\lambda_s^3}\Delta\lambda \pm \frac{\partial P_{ase}^{\pm}(z,t,\lambda_k)}{\partial z} + \frac{1}{V_s}\frac{\partial P_s^{\pm}(z,t,\lambda_k)}{\partial t}\\ &= -\Gamma_s[\sigma_a(\lambda_k)N_1(z,t) - \sigma_e(\lambda_k)N_2(z,t)]P_{ase}^{\pm}(z,t,\lambda_k)\\ &\quad - \alpha(\lambda_k)P_{ase}^{\pm}(z,t,\lambda_k) + 2\sigma_e(\lambda_k)N_2(z,t)\frac{hc^2}{\lambda_k^3}\Delta\lambda\end{aligned} \tag{2.10}$$

2.4 Continuous-wave (CW) Fiber Amplification Model

For the continuous-wave (CW) model, the derivative of the t term in equation (2.10) is zero and the problem becomes boundary-value problem of first-order ODEs. In this case, the equations are,

$$\begin{aligned}\pm\frac{\partial P_p^{\pm}(z)}{\partial z} &= -\Gamma_p\left[\sigma_a(\lambda_p)N_1(z) - \sigma_e(\lambda_p)N_2(z)\right]P_p^{\pm}(z) - \alpha(\lambda_p)P_p^{\pm}(z) \pm \frac{\partial P_s^{\pm}(z)}{\partial z}\\ &= -\Gamma_s[\sigma_a(\lambda_s)N_1(z) - \sigma_e(\lambda_s)N_2(z)]P_s^{\pm}(z) - \alpha(\lambda_s)P_s^{\pm}(z) + 2\sigma_e(\lambda_s)N_2(z)\frac{hc^2}{\lambda_s^3}\Delta\lambda \pm \frac{\partial P_{ase}^{\pm}(z,\lambda_k)}{\partial z}\\ &= -\Gamma_s[\sigma_a(\lambda_k)N_1(z) - \sigma_e(\lambda_k)N_2(z)]P_{ase}^{\pm}(z,\lambda_k) - \alpha(\lambda_k)P_{ase}^{\pm}(z,\lambda_k)\\ &\quad + 2\sigma_e(\lambda_k)N_2(z)\frac{hc^2}{\lambda_k^3}\Delta\lambda\end{aligned} \tag{2.11}$$

The boundary conditions for different spectral channels are,

$$P_p^+(0) = forward\ pump\ power, \quad P_p^-(L) = backward\ pump\ power \tag{2.12}$$

$$P_s^+(0) = forward\ seed\ power, \quad P_s^-(L) = \ backward\ seed\ power \tag{2.13}$$

$$P_{ase}^+(0, \lambda_k) = 0, \ \ P_{ase}^-(L, \lambda_k) = 0 \tag{2.14}$$

The shooting method [15] is implemented to solve this problem. The ODEs are solved using the Runge–Kutta method from z = 0 to z = L. For backward propagating light, whose value is known at z = L, the equation is solved using a guess as the initial condition. Then, the calculated output power for each channel with this "guess" initial value is compared to its boundary value, and a new guess value is generated, depending on the error magnitude. The initial guess values are updated for each iteration, until the boundary conditions for all the channels are satisfied. Thus, the closeness of guessed initial values to the correct values plays a critical role in whether the algorithm is converging, and what is the convergence speed. For high energy fiber amplification, the calculated output is more sensitive to the initial value due to high gain. Thus, initial guess value must be very close to the real conditions for achieving convergence of the algorithm. Using experimentally measured data as guesses for the initial conditions, is one good strategy. Using an estimated value obtained from analytical theory, is another option, although it may not work for high energy conditions.

2.5 Pulsed Fiber Model

For pulsed lasers, which generate time varying signals, numerical modeling must deal with both temporal and spatial domains. The finite difference method (FDM) converts the partial-differential equations (2.10) to a set of linear equations, which can be efficiently solved by numerical methods [20], [21]. The time and spatial domains are discretized into points, each separated by the step size h, and the partial-derivative terms are converted to the finite differences based on each of these points. A small value of h is necessary to minimize the truncation errors, which is the fundamental error of the finite difference method approximation. However, the small step size increases computational speed proportionally with the number of steps. Therefore, h size should be chosen carefully, accounting for specific computational conditions, and the required error magnitudes.

The model described above works well for long pulses, with variable pulse shapes. Gain saturation is accounted for by calculating time-varying upper-level ion populations, which imprint time-dependent gain onto optical pulses. For short pulses with broadband bandwidths, gain also varies across the spectral window, and dispersion also needs to be considered in some modeled situations. Thus, modeling of short pulse amplification must include spectral domain. The slip-step Fourier method is widely used, which switches between time and spectral domain at each propagation step [8]. However, the gain can only be considered in either time or spectral domain, but not in both. This problem can be solved by assuming a specific relationship between time and spectral domains. This method works well for strongly chirped pulses, because the spectral components is nearly linearly distributed over time domain. In this way, both time and spectral-dependent gain can be

calculated in time domain only. Another method can be used to calculate gain saturation, and spectral-dependent gain at the same time by splitting the pulse into multiple temporal sections at each step, and then transforming each section into the frequency domain. The size of each temporal section should be so small enough, so that the gain saturation is very week within each of them. At the end of each step, the temporal sections are combined into a single pulse, and then moved to the next step. This method, however, has a heavy computational load.

2.6 Model Calibration

In the reported experimental CPSA system, 1.9m of CCC fiber is used as the final power amplification stage. It has 85μm core diameter, and 42-55μm mode-field-diameter (MFD). 42μm MFD was used for all the calculations in this thesis. The cladding size is 420μm. Lifetime is chosen to be 770 μs. The ion concentration is $5 \cdot 10^2 3$ m^3. The pumping wavelength is either 976nm, or 915nm. The ASE band is from 1010nm to 1070nm, and is divided into 12 channels, with the spectral width of $\Delta\lambda$ = 5nm each. The experimentally measured coupling efficiency of the pump is 88%. The signal is an 81ns-long burst, produced at 10-50KHz repetition rate. Each burst has 81 1ns-long pulses with either 10nm or 30nm spectral bandwidth.

At the beginning, the CW fiber model is run to calculate the initial inversion conditions in the fiber amplifier prior to sending the seed. The boundary values of pump (input pump power), signal (zero), and ASE (zero) are chosen. The calculated outputs are the upper-level ion distribution along the fiber, and ASE and pump output powers and spectra. The upper-level ion distribution can be used to calculate the stored energy and the small-signal gain, which provide insight about the

performance and limitations of laser amplifiers in terms of high energy extraction. Then the pulsed model is run, taking the upper-level ion distribution as the initial condition, with the seed burst as the initial-boundary value of the signal. It provides the output burst and phase profile at the end of the fiber. Both fiber models are calibrated using experimentally measured data, which are the stored energy, small signal gain and output signal power.

Stored energy is the total photon-flux energy that a fiber amplifier can generate, which mainly depends on pump power and ASE. Stored energy can be calculated as

$$E_{store} = h\upsilon A_{mode} \int_0^L (N_2(z) - N_1(z))dz = h\upsilon A_{mode}(n'_2 - n'_1) \qquad (2.15)$$

Here A_{mode} is the mode area. n'_2 and n'_1 are the ion concentrations in the upper and lower sublevels, integrated along the fiber. Small signal gain is the gain of a fiber amplifier experienced by a small input signal, which is small enough not to significantly change the inversion, thus, not to cause any gain saturation. The small signal gain is measured by injecting 50 μw cw seed power and dividing the output power by the seed power. It can be numerically calculated as [22],

$$g_{ss} = \exp\left(\int_0^L \sigma_e(\lambda_0)(N_2(z) - N_1(z))dz\right) = \exp\{\sigma_e(\lambda_0)(n'_2 - n'_1)\} \qquad (2.16)$$

The ion distribution between sublevels is determined by the condition of equilibrium,

$$A_{nr}^{-} N_u = A_{nr}^{+} N_{u-1} \qquad (2.17)$$

A_{nr}^{-} and A_{nr}^{+} are nonradiative rate, and N_u and N_{u-1} are concentrations in sublevel u and $u-1$. Then,

$$\frac{N_u}{N_{u-1}} = \frac{A_{nr}^{+}}{A_{nr}^{-}} = \exp\left(-\frac{\Delta E_u}{K_B T}\right) \tag{2.18}$$

where $\Delta E_u = E_u - E_{u-1}$. The ion concertation on sublevel u can be obtained using

$$N_u = \frac{\exp\left[-(E_u - E_1)/K_B T\right]}{\sum_{n=1}^{g} \exp\left[-(E_n - E_1)/K_B T\right]} N_{total} \tag{2.19}$$

The ion distribution of each energy level can be obtained by plugging in each sublevel energy-level values. The distribution for sublevel b and e is,

$$N_b = 0.05 N_1 \tag{2.20}$$

$$N_e = 0.97 N_2 \tag{2.21}$$

T is room temperature, N_2 and N_1 are the total number of ions in the upper and lower energy levels respectively. Therefore, the stored energy, and the small signal gain can be expressed as,

$$E_{store} = h\upsilon A_{mode}(0.97 n'_2 - 0.05 n'_1) \tag{2.22}$$

$$g_{ss} = \exp\{\sigma_e(\lambda_0)(0.97 n'_2 - 0.05 n'_1)\} \tag{2.23}$$

To calibrate the numerical model, the parameters are tweaked within the reasonable range, until the calculated outputs match the experimental data. However, perfect matching of all the simulated data with the experimental data could not be achieved. The discrepancies have two aspects. One is the slopes of the stored energy, and of the small signal gain dependencies vs the pump power.

The other is the threshold where the signal becomes transparent, i.e., achieves gain = 1. The slope is mainly determined by absorption and emission cross sections, and the overlapping factors. Since the mode field diameter is smaller than the core size, the overlapping factor for the signal is always equal to 1. The overlapping factor for the pump, which is determined by pump beam propagation in the double clad fiber, as well as the absorption and emission cross sections, need to be tweaked to match the experimentally measured slope. A good matching is achieved when the emission cross section is reduced from the published value by a factor of 2, and the pump diameter is a little larger than the injected pump diameter due to diffraction in the cladding (provided the incident pump beam is smaller than the cladding). The uncertainty in emission cross section data was measured and analyzed in [23], [24]. This inaccuracy comes from the limited reliability of the McCumber relation. The absorption cross section data is measured experimentally, and so is reliable. Then the McCumber relation is used to calculate the emission cross section from the measured absorption cross section. The unreliability of the McCumber relation computation generally induces 50% inaccuracy and this number is similar to the factor used to modify the emission cross section in the model. The discrepancy of threshold can come from several sources. Pump loss due to pump leakage can directly reduce the inversion, and thus increase the threshold. Another source of error in the threshold may be radial amplified spontaneous emission, which can also consume the inversion, and thus to increase the threshold. In single-mode fibers, doped area diameter is only 5-7μm. Within this small distance, the spontaneous emission in the radial direction can hardly be amplified. However, in 85μm-CCC fibers, or large mode area fibers (LMA) with >25μm core diameters, the radial spontaneous emission can be amplified to some degree, and thus to consume upper-level populations.

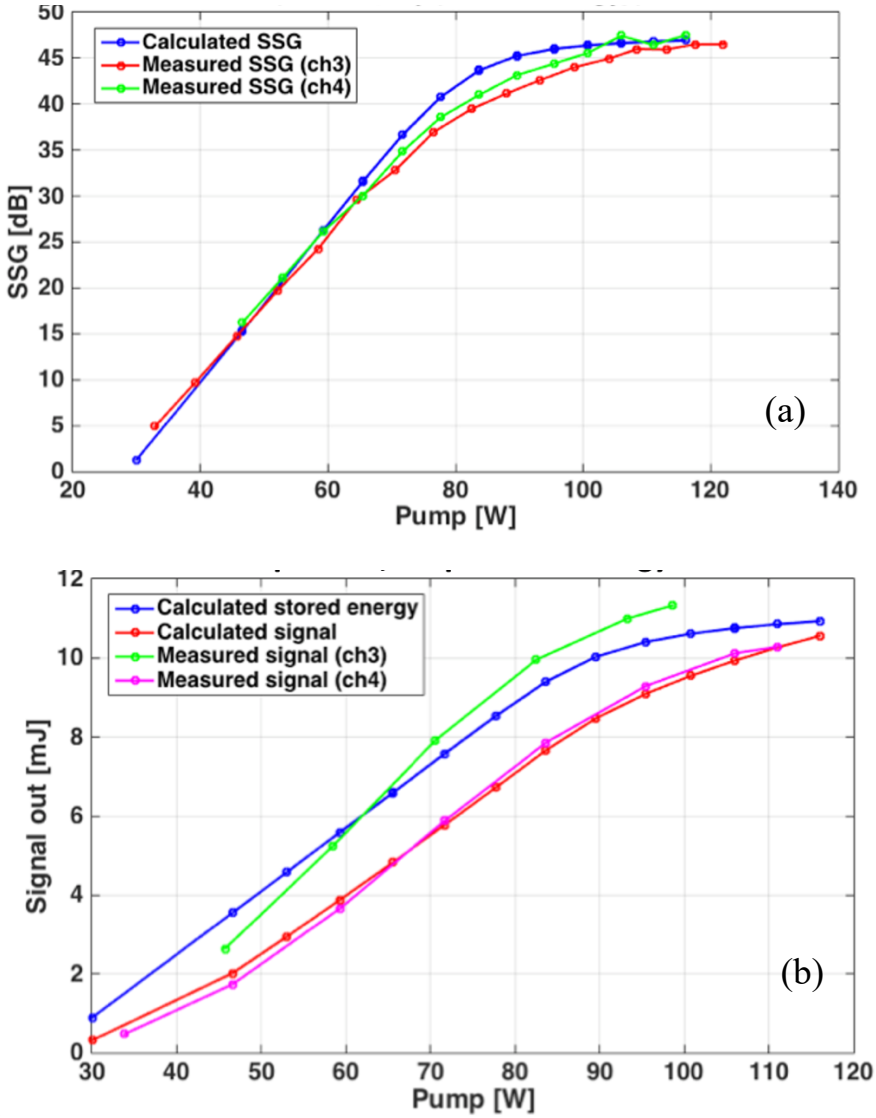

Figure 2.2 Comparison of experimental data and simulated data after model calibration for 1.9m 85µm-CCC-fiber: (a) small signal gain with 50µw input ASE power; (b) amplified burst energy with a 250µJ input burst of 81 1ns-stretched pulses (10nm @ 1037nm):

Figure 2.2 shows the comparison between the experimental data, and the simulated data, obtained with the above described recalibrated parameters. In this experiment, a small signal gain is measured by sending a very low power signal into a 1.9m 85µm-CCC-fiber. The seed power should be so low, that it could influence the ion population inversion. In figure 2.2 (b), the

amplified burst energy is measured at different pump powers of up to 110W. The 250μJ seed burst has 81 1ns-stretched pulses, with 10nm spectral bandwidth centered at 1037nm. To match the measured small signal gain and the output signal energy, the emission cross section data in the numerical code is changed to be 0.45 times of the original emission cross section data. Also, the pump power is reduced by 10W, which is the value assumed to correspond to the pump loss due to pump leakage or radial amplification. The stored energy is also calculated and compared to the measured output energy. According to the simulation result, higher than 10mJ burst energy can achieved in a fiber amplifier with 11mJ stored energy. This means 90% of the stored energy can extracted by the burst, which has been previously achieved with coherent pulse stacking amplification technique.

CHAPTER III

In-burst Pulse Reshaping for Gain-saturation Compensation, to Enable High-fidelity Pulse Stacking at High Energies

The key advantage of the coherent pulse stacking amplification is that it enables nearly a complete stored energy extraction from a fiber amplifier, while a fiber-based CPA is limited by the onset of fiber nonlinearities at high peak powers to extracting only 1-2% of stored energy. Consequentially, unlike the fiber CPA where saturation is negligible, gain saturation in the final stages of a fiber CPSA system are very strong and must be addressed. As is shown in [25], stacking-burst output from a strongly saturated fiber amplifier must have individual amplitudes of pulses in the burst follow a certain prescribed profile, for achieving equal nonlinearity induced phase-shifts between all the pulses in the amplified burst. However, this previous work did not consider that the gain spectrum seen by each individual broadband pulse in the amplified burst can also vary along the burst under the conditions of strong saturation, i.e. previous work only considered saturated-amplification stacking in the monochromatic limit. For broadband pulses saturated amplification can produce variation in temporal shapes and in nonlinearly induced phase-shift profiles between different pulses in the stacking burst, which detrimentally affects pulse stacking fidelity at the system output. This chapter presents our work on identifying these individual-pulse distortion effects in the saturated-amplification stacking of broadband pulses, and then developing a technique to compensate them, thus enabling high-fidelity (i.e. high stacking efficiency and low pre-pulse contrast) stacking at the highest achievable pulse energies.

3.1 Coherent Pulse Stacking Amplification Technique

Coherent Pulse Stacking Amplification (CPSA) is a temporal beam combining technique that overcomes ultrashort-pulse energy limitations of Fiber Chirped Pulse Amplification (FCPA) systems. In a FCPA system, pulses are stretched in the time domain by a stretcher before amplification to reduce the peak power. Broadened pulses are amplified to high energies and then compressed down to close to bandwidth-limited duration by a compressor. However, diffraction-grating based stretchers and compressors are limited to stretched pulse durations of up to ~1-2ns. Increasing this stretched duration by, for example, an order of magnitude, would require corresponding increase in a diffraction grating size, which is technologically unfeasible. This is the main limitation on achievable pulse energy because 1-2ns stretched pulse duration allows extraction of only 1-2% of the stored energy. The CPSA technique overcomes this limitation by amplifying > 10-100 ns duration burst of 10-100 pulses and combining this burst to a single pulse after amplification, which therefore enables full extraction of the stored energy from a fiber amplifier.

CPSA technique consists of the following steps: stacking-burst formation, pulse stretching, amplification, pulse stacking, and compression. A stacking burst is formed from a 1GHz mode-locked ultrashort pulse train, which is "carved-up" into ~10 - ~100 pulse bursts, with a certain prescribed burst-amplitude profile, and with each individual pulse in the burst "imprinted" with a certain pulse phase. The ultrashort pulses in the burst are stretched to 1ns each, which, due to 1ns separation between 1GHz repetition rate pulses, effectively produces a 10-100ns duration burst. This signal is then amplified in a sequence of fiber amplification stages where nearly 100% of the stored energy extracted in the final amplifier. Beam combining in the time domain is achieved by

utilizing a sequence of free-space Gires–Tournois Interferometers (GTI), which can coherently stack into a single high-energy pulse a burst of ~10-100 amplified pulses. At the system output the stacked pulse is compressed back to the short duration by a grating-based compressor. Coherent time domain combining in the stacker is achieved by active roundtrip-phase control in each GTI, and by the phase profile imprinted during stacking-burst formation in the front of the system. Burst amplitude profile is usually chosen to compensate strong gain saturation effects occurring in the final amplification stages, as described in more detail further in the text.

A GTI cavity is a linear optical resonator that consists of one partially reflecting front mirror, and one or more ~100% reflectivity mirrors forming a roundtrip cavity. Using more than one HR mirror allows one to configure a GTI as a ring cavity, conveniently separating input and output beams. There are two parameters needed for each GTI cavity in a stacker: the reflectivity of the partially reflecting front mirror, and the roundtrip cavity phase. The pulse stacking process can be explained as a reverse process of sending a single pulse into a sequence of GTI cavities. The pulse is split into a transmitted and a reflected pulse at each partially reflecting front mirror and the transmitted pulse enters the cavity, and undergoes reflection and transmission at the front mirror after each roundtrip. Thus, the output signal is a burst of pulses separated by one roundtrip time of the GTI cavity. The amplitudes and phases of the pulses in the output burst are determined by the GTI parameters (front mirror reflectivity and cavity phases). Pulse stacking is the reversed process of a single pulse passing through the GTI cavities. The desired phase profile of the burst from a GTI can be obtained by calculating the cavity impulse response [25].

Each individual GTI cavity can stack approximately 2 pulses, and N equal-length cavities can stack approximately 2N pulses. One example of the pulse stacking configuration is a sequence of 4 equal-length GTI cavities, schematically shown in Figure 3.1 (top) [25]. The cavity's lengths are equal to the roundtrip length of the mode-locked oscillator. This particular configuration is designed to stack 9 equal-amplitude pulses, and figure 3.1 (bottom) illustrates the reversibility of the pulse stacking process. The prescribed burst stackable into a single pulse is the time reverse of the stacker impulse response. In the real stacker, where mirrors are not exactly 100% reflective, the small loss makes the system not exactly reversible. However, since in practice mirror losses are very small, using impulse response for design and analysis yields sufficiently accurate results. However, stacking 100 pulses one would need ~50 equal-length GTI cavities, which is not practical. Fortunately, a small number of non-equal length GTI cavities can be configured to stack a large number of cavities. For example, if the pulse stacker has N+N multiplexed cavities that has N equal-length cavities with the cavity length equal to the roundtrip length of the oscillator and N equal-length cavities (identical to the first. Set of cavities) with the length equal to 2N roundtrip length of the oscillator, this multiplexed configuration can stack $4N^2$ pulses. One example of such a multiplexed configuration is a sequence of 4+4 multiplexed cavities for stacking 81 pulses that is shown in figure 3.2. The burst of 81 pulses is stacked into 9 pulses first when going through the first sequence of 4 small cavities, and then the 9 pulses are stacked again into a single pulse at the second sequence of 4 long cavities. The first 4 cavities are equal in length to the roundtrip length of the mode-locked oscillator, and the 4 longer cavities are 9 times longer than the small cavities. In the experiment, we use this 4+4 multiplexed configuration to stack 81 pulses. We choose to use a 1 GHz Yb-doped fiber oscillator as a seed source for the CPSA system because its pulses are separated by 1ns, so that after stretching to ~1ns these pulses form a nearly continuous pulse. Since

the oscillator pulse repetition rate defines the smallest roundtrip length in a GTI stacker, this 1ns pulse separation in the burst provides a compact solution for the GTI stacker layout. In the experiment, the pulses are usually stretched to 800-900ps leaving a gap of ~100ps between the pulses. for the 1GHz oscillator, the four smallest cavities have 30 cm roundtrip length, and four larger cavities have 2.7 m roundtrip length. The total path length in this 4 + 4 stacker is 12m, which is arranged on an optical breadboard in a folded configuration with a compact 61cm×91cm footprint.

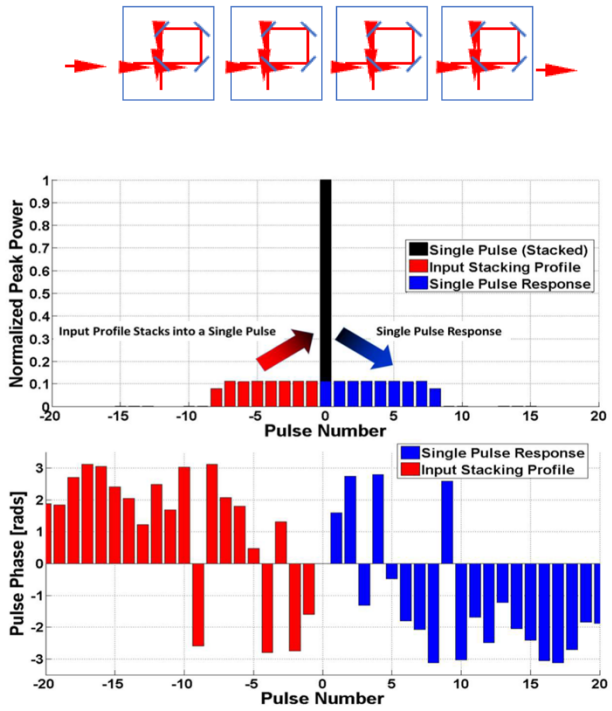

Figure 3.1 (top) schematic of pulse stacker with 4 equal-length cavities; (bottom) (this plot is taken from [25], Figure 2.1) Time reversibility of the coherent pulse stacking process: time reverse of system's impulse response is the stacking burst. This stacking is accomplished using a sequence of 4 lossless GTIs with parameters chosen to stack a burst containing ~9 equal intensity pulses. The pulse intensities are shown in the top graph and the pulse phases are shown in the bottom graph.

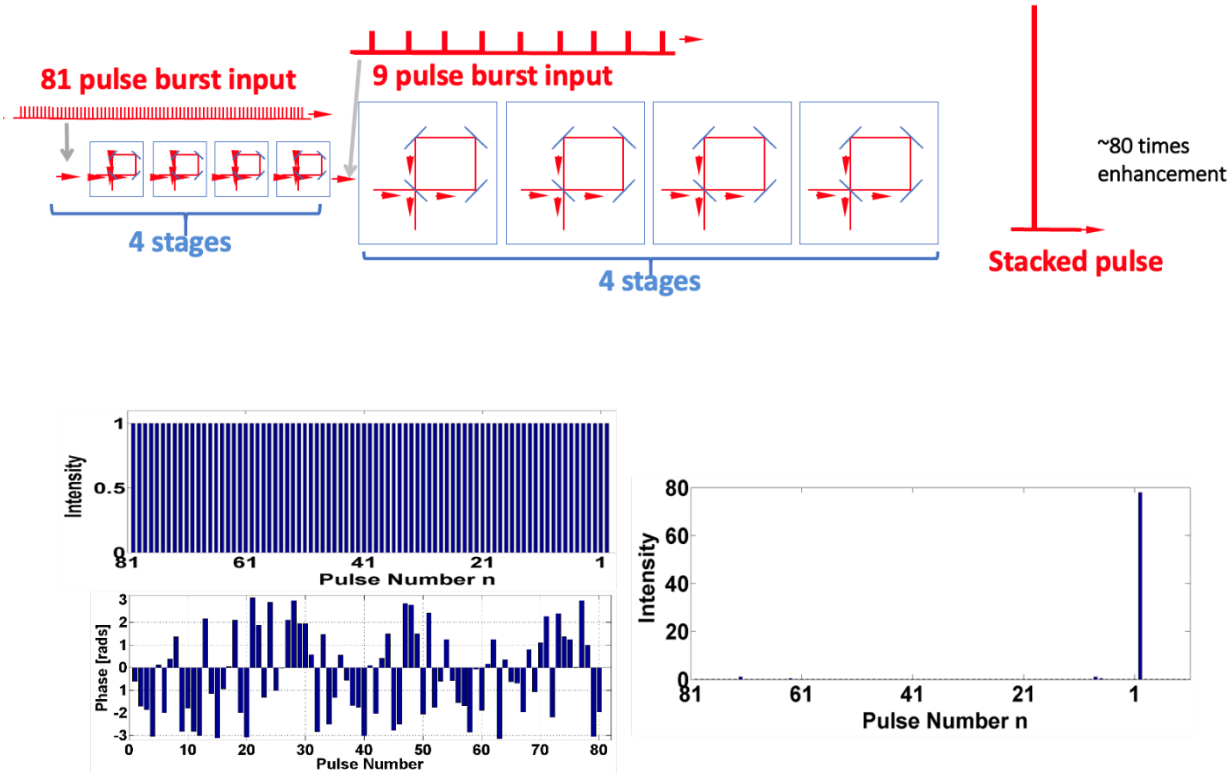

Figure 3.2 Schematic design of the 4+4 multiplexed GTI stacker (top figure), and an example of 81 equal amplitude stacking burst and its phases (lower figure left), with its staking result shown on the lower right figure.

Since pulse stacking relies on coherent addition of pulses, each pulse in the stacking burst must have identical amplitude and phase profiles. Any pulse-to-pulse variation in either shape or phase profile reduces coherent combining efficiency and pre-pulse contrast. One source of distortions in the CPSA system is the nonlinearity-induced phase profile across each pulse accumulated in the final amplification stage due to the high peak power. When nonlinearity-induced phase-shifts in final amplification stages are negligible in a low-energy CPSA system, an equal amplitude burst profile is an optimum one as an amplified stacking burst. However, in a high-energy system, when there are significant nonlinearity-induced phase shifts in the final amplifier, a strong gain

saturation typically occurs as well. But, for strongly saturated fiber amplifiers, gain saturation induces time-varying gain along the pulse burst, which, for reasons explained in detail below, results in dissimilar nonlinearity among the individual pulses in an equal-amplitude stacking burst at the output. This pulse-to-pulse varying nonlinearity induces different phase-profile distortions for different pulses in the burst. Therefore, the burst must be shaped before amplification in such a way as to equalize nonlinearity in order to achieve high-fidelity pulse stacking.

For certain simplifying assumptions, the required "equal nonlinearity" burst profile can be calculated analytically [25]. However, as discussed later, due to the simplifying assumptions this analytical solution is only approximate. The exact calculation of the required burst profile for achieving an equal-nonlinearity amplified stacking-burst profile can be achieved via numerical simulations using the pulsed fiber model presented in Chapter 2, as discussed later in this Chapter. At high energy amplification, the gain is time-varying along the burst and the pulses in the front of the burst see higher gain while the pulses in the end of the burst see lower gain. This is because as each pulse is sent into the fiber and amplified, it depletes upper-level ions and thus reduces the gain seen by the next pulse. The gain as a function of time can be expressed as [26]:

$$G(t) = 1 + [G_0 - 1]e^{-\int_0^t \frac{I_{out}(t')}{U_{sat}} dt'} \tag{3.1}$$

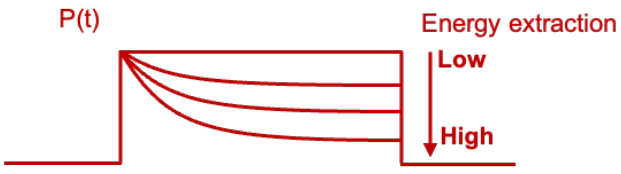

Figure 3.3 Amplitude-decaying burst profile under the condition of gain saturation

I_{out} is the output intensity, U_{sat} is the saturation fluence of the amplifier, and G_0 is the small signal gain. This time-varying gain decreases along the burst and, as illustrated in figure 3.3, the gain decays faster when more stored energy is extracted, and so gain saturation is stronger. Instead of equal-amplitude pulses in the amplified burst (assume the input burst is equal-amplitude) in low energy laser system, the amplified burst from the saturated fiber amplifier has a rapidly-decaying shape. Also, this non-equal gain produces non-equal nonlinearity-induced phase-shifts across the burst. This effect can be explained by the following equations:

$$L_{eff}(t) = \frac{L}{\ln[G(t)]}\left[1 - \frac{1}{G(t)}\right] \tag{3.2}$$

$$\emptyset_{NL}(t) = \frac{2\pi}{\lambda} n_2 \int_0^L I(t,z)dz \propto L_{eff}(t) \tag{3.3}$$

Figure 3.4 Increasing nonlinear phase profile under the condition of gain saturation

$L_{eff}(t)$ is the effective fiber length, L is the real fiber length, n_2 is the nonlinear refractive index and $I(t,z)$ is the intensity at z position as a function of time. Equation (3.2) shows that the effective length is inversely dependent on the gain magnitude. The effective length is shorter when the gain is higher. In equation (3.3), the nonlinear phase accumulated along the fiber with length L is calculated by the integration of the intensity over the fiber length. The value of this integration is proportional to the effective length, and so the nonlinear phase is also proportional to the effective

length. Since higher gain corresponds to shorter effective fiber length, and the nonlinear phase is proportional to effective fiber length, the accumulated nonlinear phase value grows exponentially along the burst (figure 3.4). The slope is deeper with more substantial saturation. It should be noted that since the first point of the burst sees the shortest effective fiber length, it has the minimum phase value compared to other points in the burst, and so this equal-nonlinearity burst would also have the minimum nonlinearity. The burst profile $I_{out}(t)$ can be solved analytically [25], when the inversion along the fiber can be assumed to be constant, i.e., signal gain is simply an exponential function, although different for each pulse in the burst due to amplifier gain saturation varying within the burst. With this assumption, equation (3.3) can be written as equation (3.4), and also $\emptyset_{NL}(t)$ should be constant with time since we seek the equal nonlinearity burst profile. The output burst intensity that has equal nonlinear phase across the burst can be calculated from equation (3.1), (3.2) and (3.4) and is shown in equation (3.5),

$$\phi_{NL}(t) = n_2 k_0 I_{out}(t) L_{eff}(t) \tag{3.4}$$

$$I_{out}(t) = \frac{\left\{\frac{\phi_{NL}}{n_2 k_0 L}\right\} \ln[G_0] \exp\left[\frac{-\phi_{NL}}{n_2 k_0 L U_{sat}} t\right] G_0^{\exp\left[\frac{-\phi_{NL}}{n_2 k_0 L U_{sat}} t\right]}}{G_0^{\exp\left[\frac{-\phi_{NL}}{n_2 k_0 L U_{sat}} t\right]} - 1} \tag{3.5}$$

In reality, pulses deplete population inversion to a lesser degree at the amplifier input rather than its output, and the inversion along the fiber is not constant, resulting in per-pulse gain along the fiber slower than an exponential growth. To more accurately calculate the burst profile for equal nonlinearity, equation (3.3) needs to be numerically solved and we can use the fiber model developed in Chapter 2 to do this.

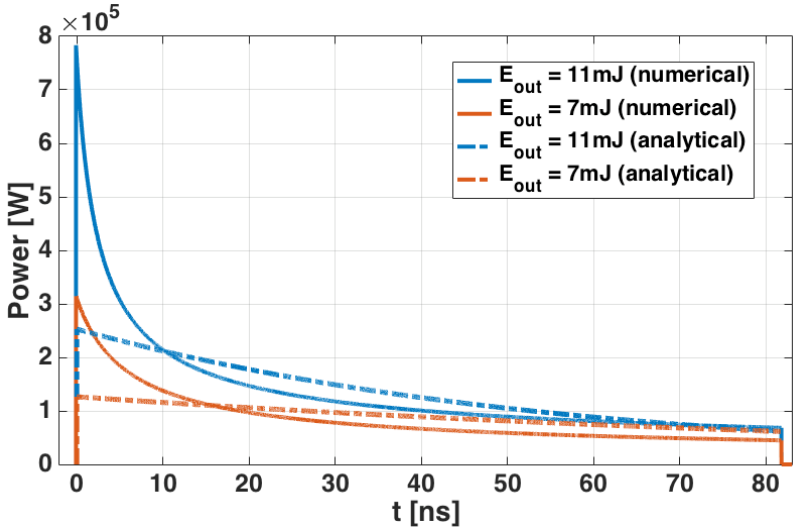

Figure 3.5 Comparison of output burst profile calculated by numerical and analytical method. The signal is $\lambda = 1037\text{nm}$. The fiber is 85μm-CCC with 1.9m length.

The output bursts calculated by numerical and analytical methods are compared in figure 3.5. The rate of burst amplitude decrease is higher for higher burst energy because larger energy extraction produces stronger gain saturation. For the same energy, the analytical solution presents weaker saturation because the gain is assumed to be exponentially increasing, while the saturated gain grows slower along the amplifier. The numerical model provides a more accurate solution and is a good guide to explore and control the gain saturation effects in fiber amplifiers.

For illustration of the earlier arguments, we used the numerical model to simulate and compare the nonlinear phase profile of the amplified burst that has equal-amplitude pulses to the one that has decaying amplitude profile. Figure 3.6 (a) shows the output burst profile for a 10mJ burst, that has equal amplitude pulses in the burst, and figure 3.6 (b) shows its nonlinear phase, calculated assuming signal wavelength of 1037 nm and negligible bandwidth of the chirped pulse. This demonstrates that an equal amplitude stacking burst profile can produce non-equal (and large)

nonlinear phase-shifts, detrimental for pulse stacking. The decaying burst profiles in figure 3.6 (c) are the desired stacking burst profile, because they have equal nonlinear phase across the burst shown in figure 3.6 (d). These profiles are usually identified as “equal nonlinearity bursts”.

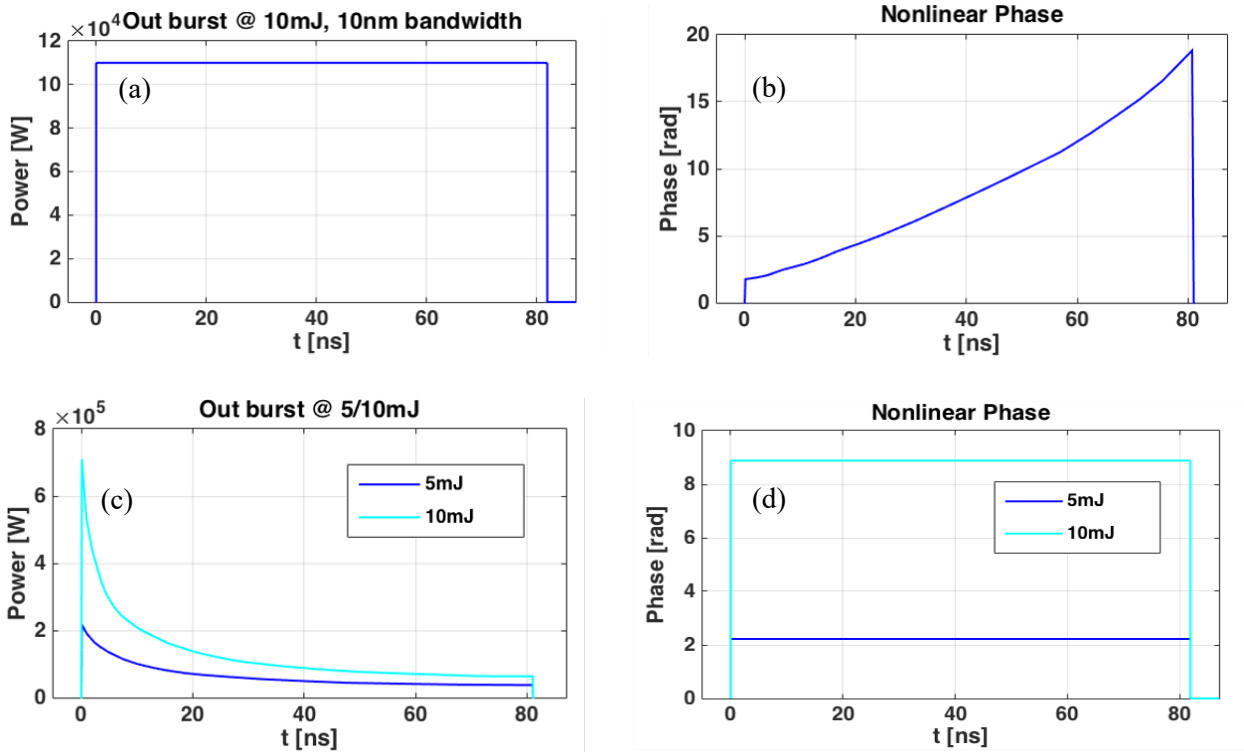

Figure 3.6 (a) (b) equal amplitude burst profile and its non-equal nonlinear phase; (c) (d) desired burst profile for enabling equal nonlinearity across the burst for 5 and 10mJ, and their equal nonlinear phase profile.

3.2 Coherent Pulse Stacking Amplification (CPSA) Experimental Setup

Figure 3.2 shows an example of an actual CPSA experimental setup without in-burst re-shaping. 1 GHz pulse train is generated from a Yb-doped fiber-based oscillator. The pulses have 35nm

(FWHM) spectral bandwidth and ~60 fs bandwidth-limited duration. A pair of 1 GHz electro-optic waveguide modulators (an amplitude modulator and a phase modulator) right after the oscillator are used to modulate the amplitude and phase of the pulse train, to create a properly shaped and phased stacking burst. For a strongly saturated fiber system to achieve high energy extraction, the initial burst intensity should strongly increase along the burst so that the nonlinearities across the burst are equal after burst is reshaped after all amplification stages into a rapidly decaying profile. The phase modulator is for adding the desired phases onto each pulse to make it stackable. Since the pulses are 1GHz and the electro-optic modulators are also 1GHz, the amplitude and phase of the modulated pulses are flat across each pulse, and there is no in-pulse modulation. The modulated burst is then sent into a diffraction-grating-based stretcher, where the pulses are stretched from hundreds of femtoseconds to nearly 1 ns. The grating has 1740/mm groove density. The spectral bandwidth is cut to 10 nm by the hard edges of gratings, lenses, and mirrors inside the stretcher. The stretched burst goes through multi-stage pre-amplifiers and is then amplified to millijoules level burst energy in the final power stage. The final power stage is a 1.8 m long fiber [17] with an 85 μm core diameter. After amplification, the burst is sent into a 4+4 sequence of GTI cavities, where it is stacked into a single pulse. This single pulse is then compressed to a short duration by a diffraction-grating compressor in a folded configuration with a single 1740/mm grating.

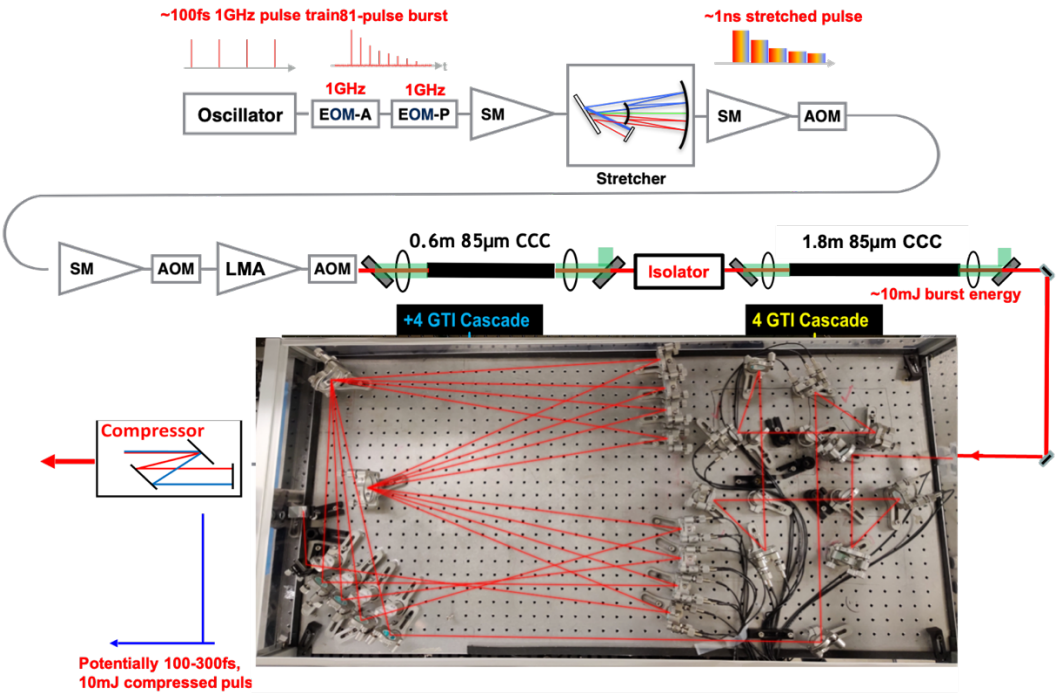

Figure 3.7 Experimental configuration of CPSA system

It has been experimentally demonstrated that when 81 pulses are picked up as a burst, 10 mJ burst energy is achieved at the final CCC power stage at 1 kHz repetition rate. By utilizing the fiber amplification model mentioned in Chapter 2, the stored energy in this CCC fiber can be calculated to be ~ 11 mJ for this particular amplifier. This means 90% energy extraction efficiency was achieved, far beyond what can be achieved using fiber CPA only.

3.3 Effects of Gain Saturation on the Amplified Stacking Burst

It is instrumental for further discussion to first describe the details of the stacking burst formation at the front of the system, and also the details of that burst format. The initial pulse train (figure 3.8(a)) is generated by a 1GHz repetition rate mode-locked Yb-doped fiber oscillator producing 60fs pulses at > 300mW average power. These short pulses are stretched to ~10ps when

propagating along a 10m single-mode passive fiber and then sent to a 1GHz amplitude electro-optic modulator and a 1GHz phase electro-optic modulator for creating a properly amplitude-shaped and phase-modulated stacking bursts required for pulse stacking. (Pulses are initially fiber-stretched to reduce peak power, for avoiding detrimental nonlinear effects in theses waveguide-based EOMs). In an idealized picture, operation of both 1GHz amplitude and phase electro-optic modulators (A-EOM and P-EOM) can be represented as a sequence of rectangular functions/time windows, each 1ns wide, and all immediately adjacent to each other. Each EOM thus imprints constant amplitudes (A-EOM) or phases (P_EOM) over each pulse in a stacking burst. Each stacking burst contains finite number of pulses, carved out of the infinite pulse train from the mode-locked seed oscillator. Although, in reality, the time window of electro-optic modulators has limited rise and fall time, they still imprint fixed amplitude and phase values across each pulse because the pulse duration is much shorter than the 1ns time window of electro-optic modulators, and by positioning each pulse in the center of each window, they can always be outside the range of time-window rise and fall times. These modulated pulses are each stretched to ~900ps by the grating-based stretcher, inserted after the EOMs, so that nearly adjacent pulses are produced in the burst (with only ~100ps "gaps" between the stretched pulse), which minimizes the overall length of all the GTI-cavities, and thus minimizes the size of the pulse stacker. The stretcher provides a large magnitude of positive chirp onto each pulse and, as illustrated in figure 3.8 (b), the pulse is strongly chirped with the longer wavelength travels faster than shorter wavelength. Then, this 81ns quasi-continuous signal with 81 1ns stretched pulses is amplified in the single-mode amplifiers, a 25μm-LMA stage and two 85μm-CCC stages. The amplitude profile of the stacking burst is selected to be such, that it would produce at the output of the final 85μm-CCC stage, ~10mJ

stacking burst with equal nonlinearity across the burst. This final amplified burst is then sent to the pulse stacker and the compressor for stacking and compression.

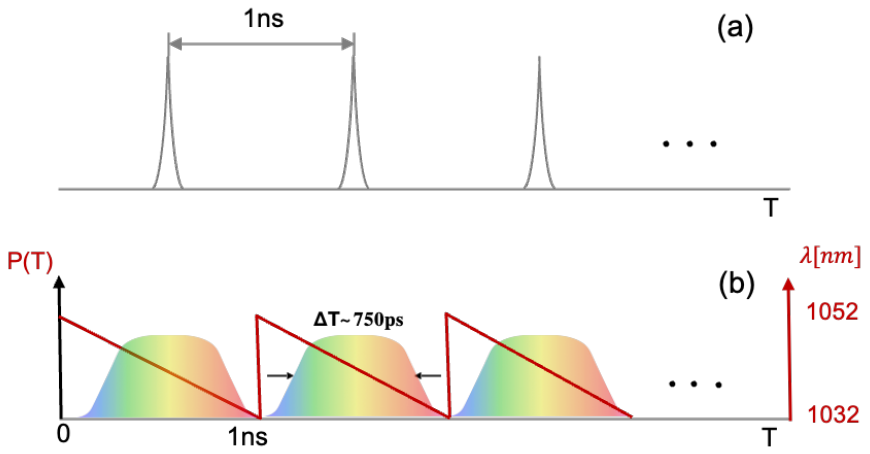

Figure 3.8 Schematic of (a) short pulses output of the oscillator separated by 1ns; (b) stretched 1ns-pulses that are positively chirped with 10nm bandwidth centered at 1037nm.

Until now, when talking about the amplitude and phase profile of the stacking burst, we only considered a "monochromatic limit", i.e., did not consider effects of gain saturation on the amplitude and phase shape within each broadband pulse. As we show next, broadband pulses in the burst undergo individual-pulse amplitude and phase profile changes during amplification in the final strongly-saturated amplifier stage.

It is straightforward to show that, under strong saturation conditions, individual broadband pulses experience amplitude reshaping, which depends on the position of the pulse in a stacking burst. Such reshaping results from the fact that amplifier gain is a wavelength-dependent function, and that increasing degree of gain saturation affects gain at different wavelengths differently. This is illustrated in figure 3.9, which shows how a Yb-doped fiber amplifier gain spectrum changes under

different degrees of saturation. As discussed in Chapter 2, the energy levels of Yb^{3+} are split into several sublevels, and different sublevels corresponds to different spectral region. When there is no saturation, the gain is highest at 1030nm, and gradually decreases with longer wavelengths, approximately following the spectral dependence of Yb^{3+} ion emission cross-section. Without saturation, this affects amplified pulse spectra, and thus their temporal shape, identically for all the pulses in the burst. When the amplifier is saturated, then, with increasing degree of saturation, the population at shorter wavelengths decreases faster than at longer wavelengths. Therefore, gain saturation reshapes its spectral shape by shifting the gain peak to the longer wavelengths, causing corresponding change in the individual amplified pulses, which experience increasing degree of gain saturation from the start towards the end of the burst. Because the spectra of the individual pulses change differently, so do their temporal shapes, which are related to their spectra via Fourier transformation. Since pulse stacking is based on coherent interference between each pulse, the stacking burst with different pulse shapes would have lower combining efficiency at the end of the CPSA system.

In order to understand of how gain saturation affects phase-profile of individual pulses in a burst differently, we need to remember that, in a final amplifier stage, individual pulses are stretched from ~100fs to approximately 1ns duration, i.e., are very strongly chirped. The temporal shape of a strongly chirped pulse is similar to its spectral shape, and as figure 3.10 illustrates, changes on the spectral shape induces similar changes in its temporal shape [27]. Therefore, the stretched-pulse spectral reshaping resulting from saturation-induced gain-shift produces similar reshaping in the temporal stretched-pulse shape. And each pulse shape is reshaped differently across the amplified burst because each spectrum is reshaped differently by a different degree of gain

saturation along the burst. Consequently, the nonlinearity-induced phase distortions imprinted onto each pulse are also different across the burst since the accumulation of nonlinear phase-shifts is proportional to the temporal intensity and the gain magnitude, both of them varying between the pulses.

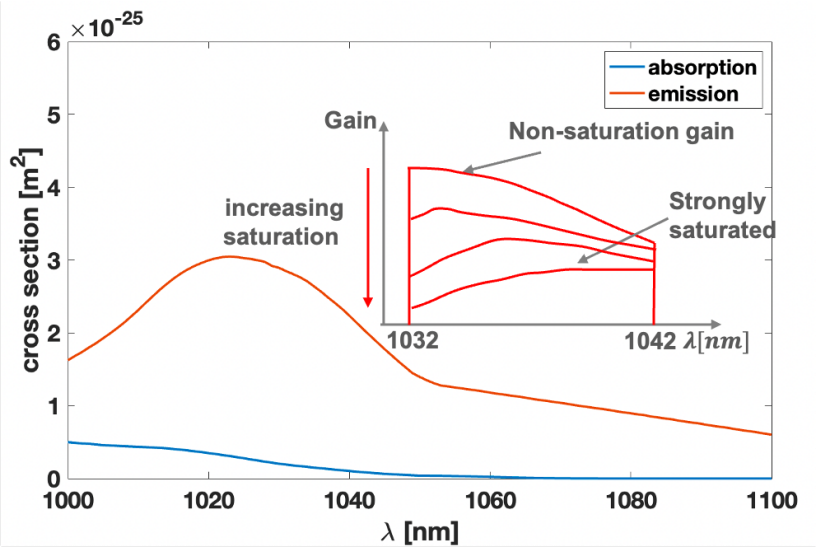

Figure 3.9 Cross sections of a Yb-doped fiber amplifier and its gain spectrum changes due to saturation.

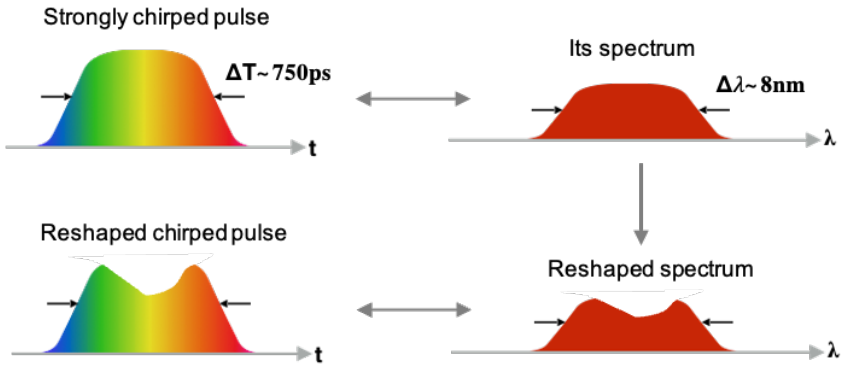

Figure 3.10 The similarity between temporal and spectral shape of a strongly chirped pulse

To visualize gain saturation and gain narrowing effects on individual pulse shapes and phase-shifts across the burst output from the final amplifier, let's use the pulse fiber model discussed in Chapter 2 to simulate broadband pulse amplification under strong saturation. The seed burst has 81 pulses at 1GHz repetition rate, and each pulse is positively chirped to 1ns duration with 10nm centered at 1037 nm. The pulse shape is assumed to be flat-top with sharp edges which is an idealization of a typical "square-like" shape of a stretched optical pulse, with spectral edges truncated by sharped-edged transmission window of a diffraction-grating based stretcher. The seed burst is pre-shaped to ensure that the amplified burst follows the equal nonlinearity profile. Then, this input burst is sent to an 85μm-CCC fiber amplifier with 1.9m fiber length and amplified to 11mJ burst energy. The numerically calculated output burst profile, and the accumulated nonlinear phases of individual pulses in the output burst from the fiber amplifier are plotted in figure 3.11. One can immediately notice that pulse shapes across the stacking burst are indeed strongly varying along the burst. It is also evident that, although equal nonlinearity-induced phase shift is achieved (if to look at the 1st point of each pulse), the phase-shifts within each pulse are different, and this shaping effect is stronger toward the end of the burst where gain saturation is stronger. We can conclude here that, at high degrees of energy extraction with broadband pulses, it is necessary to develop methods for compensating these detrimental amplitude and phase profile distortions of individual pulses along the amplified stacking burst.

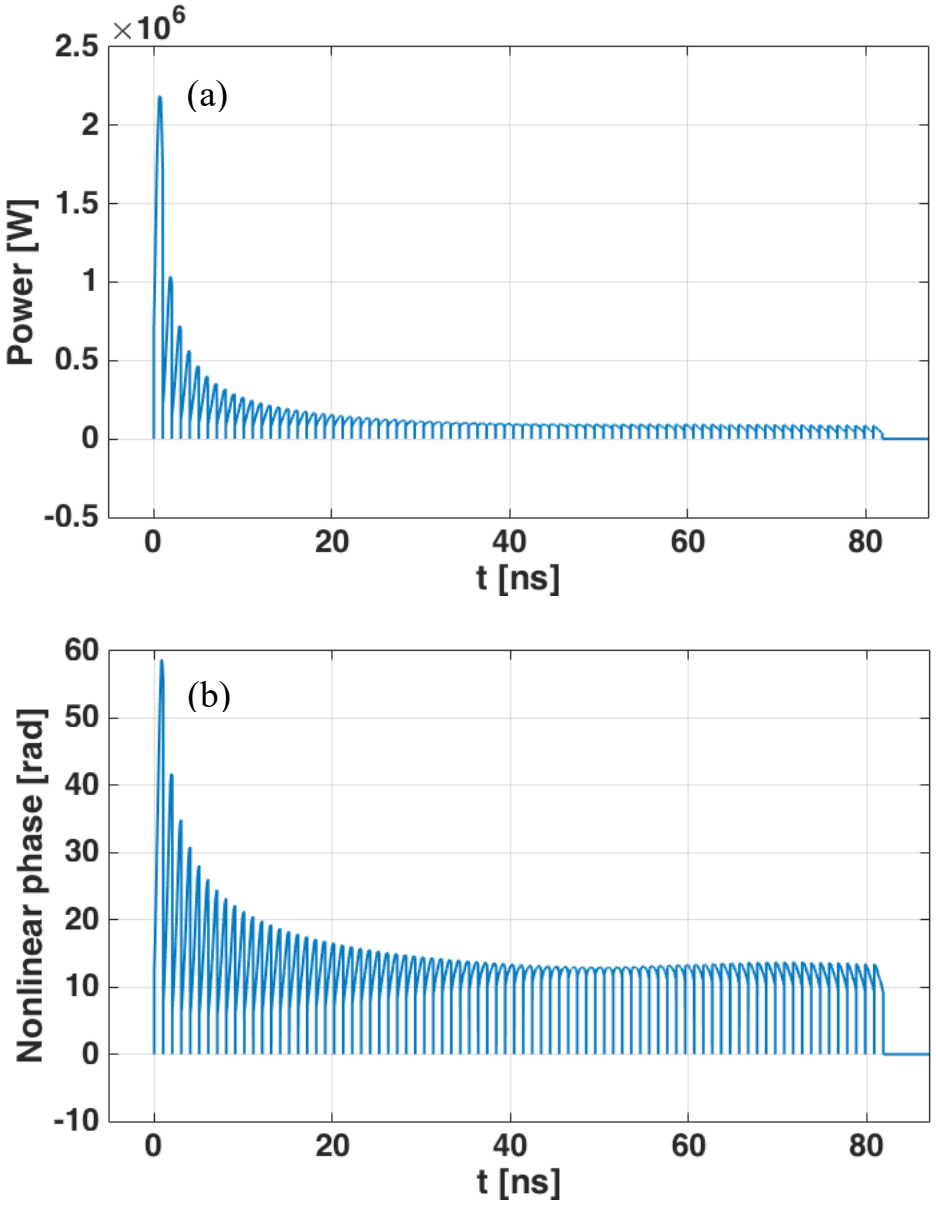

Figure 3.11 Burst amplitude (a) and nonlinear phase profile (b) with each pulse (10nm @ 1037nm) re-shaped differently by gain saturation and gain narrowing effects, from 1.9m 85μm-CCC for 11mJ burst energy.

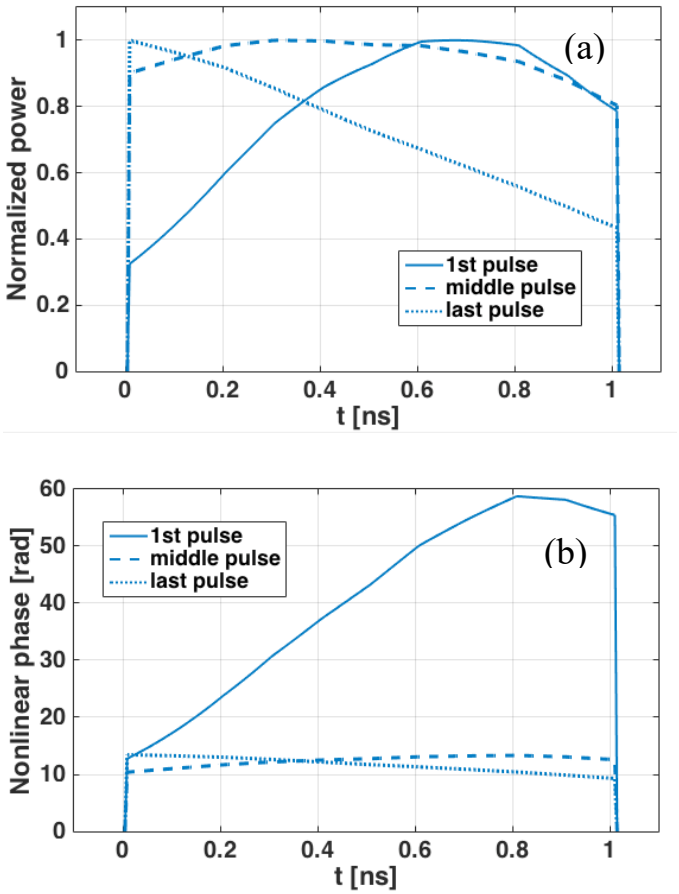

Figure 3.12 Comparison of pulse amplitude and nonlinear phases between individual pulses in the burst shown in figure 3.11.

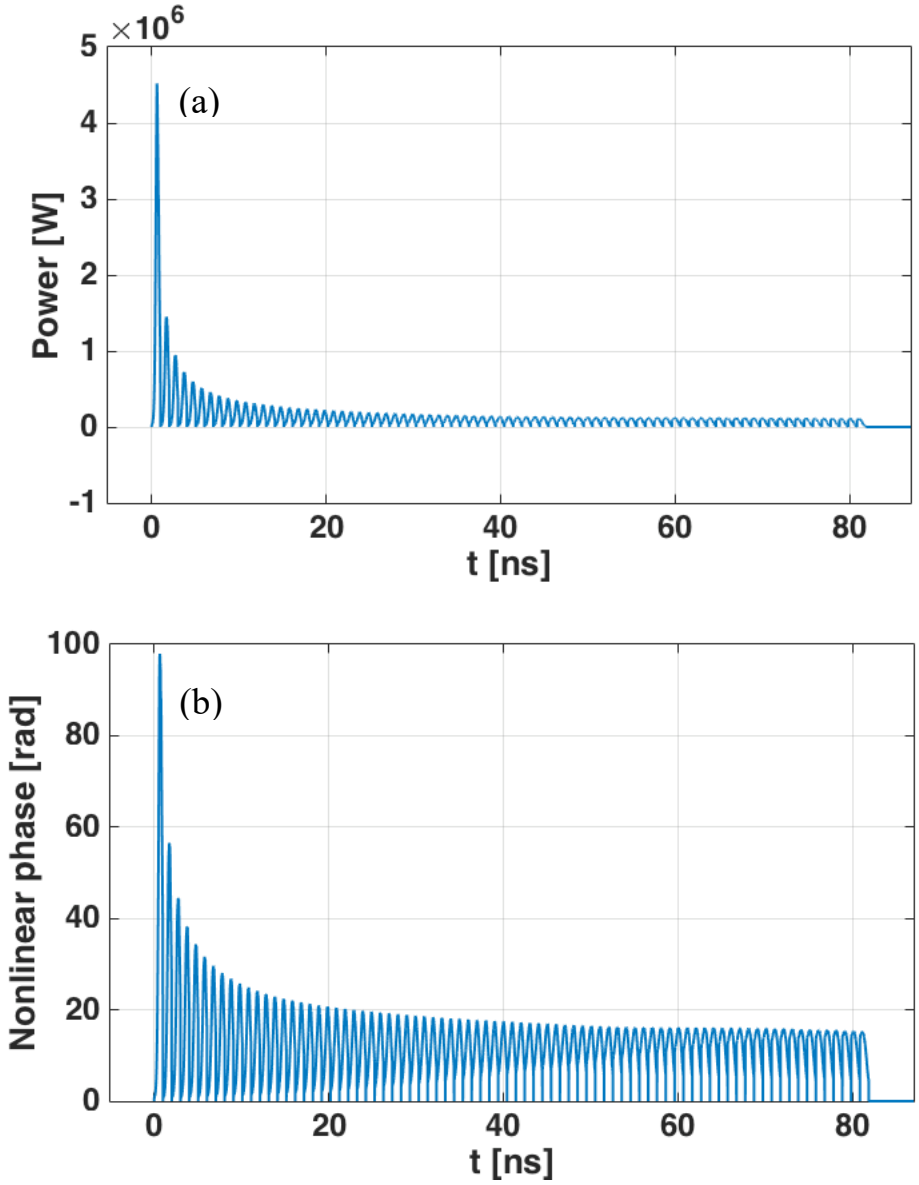

Figure 3.13 broadband burst amplitude (a) and nonlinear phase profile (b) with each pulse (30nm @ 1037nm) re-shaped differently by gain saturation and gain narrowing effects, from 1.9m 85µm-CCC for 11mJ burst energy.

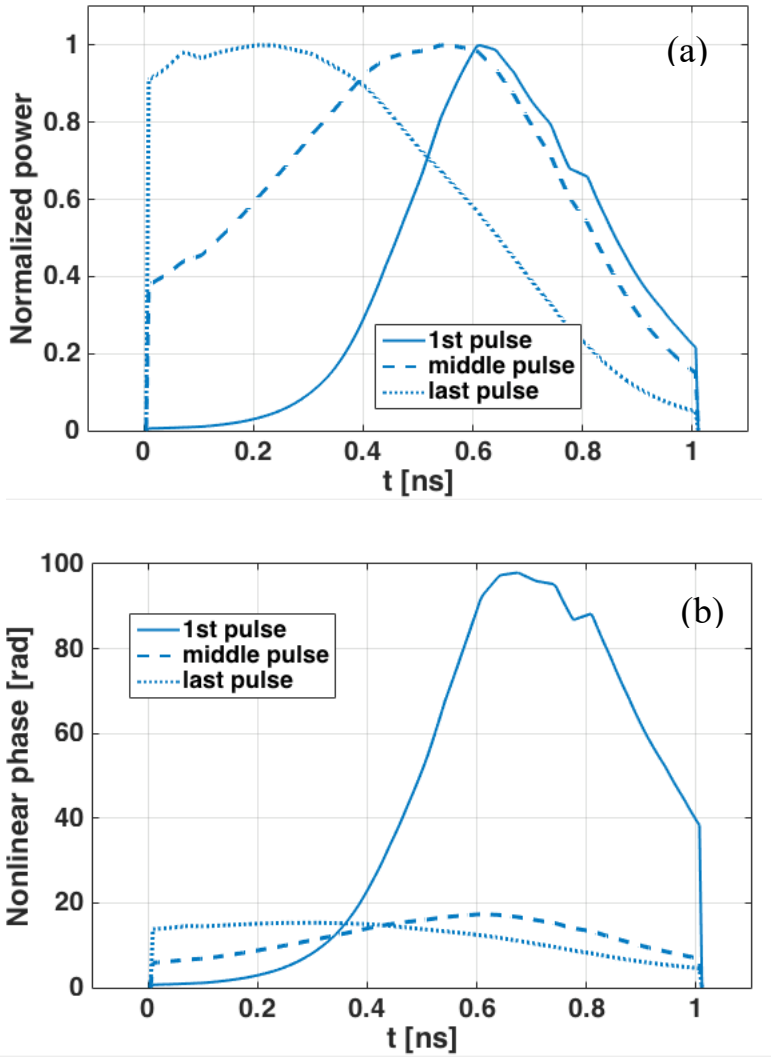

Figure 3.14 Comparison of 30nm bandwidth pulse amplitude and nonlinear phases between individual pulses in the burst shown in figure 3.13.

3.4 Gain Saturation Compensation with In-burst Individual Pulse Amplitude or Phase Profile Control

Since, as was shown in the previous section, individual-pulse distortions, occurring due to varying along the burst saturation, are also linked to individual-pulse phase distortions, one can expect that achieving equal-shape individual pulses, in an equal-nonlinearity burst profile would be sufficient

for compensating both amplitude distortion, as well as phase distortion effects. In this section, we numerically equalizing individual pulse shapes and then compare the nonlinear phase profile between the pulses to see the feasibility of pulse amplitude control.

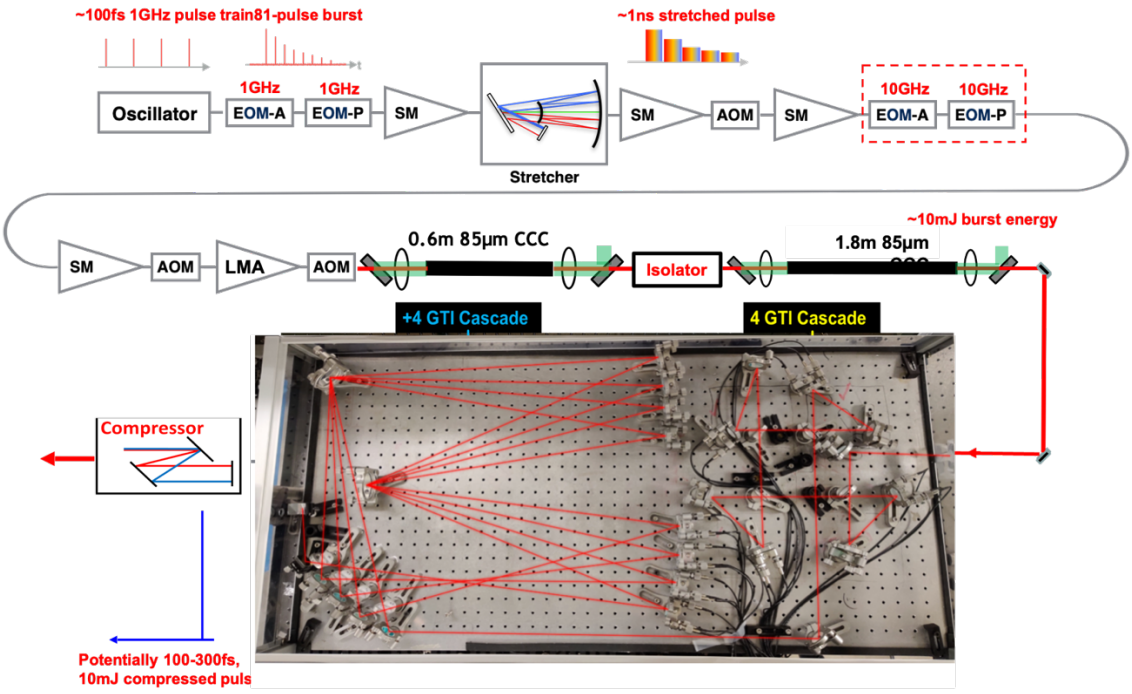

Figure 3.15 CPSA system configuration with in-burst amplitude pre-shaping

Equal-shape individual pulses in the amplified burst can be achieved by pre-shaping each individual pulse shapes in the seed burst, provided that there is a mapping between temporal shape and spectral shape as illustrated in figure 3.10. When the temporal shape is tailored to have a curtain shape, the spectral shape is also changed to have similar shape, and thus pre-shaping each pulse shapes in the seed burst is equivalent to modulate each spectral shape for overcoming spectral shaping effects from gain saturation. To equalize the pulse shapes across the amplified burst in the

modeling, a gradient descent-based optimization loop is implemented. The input amplitudes of each pulse are updated until a flat-top pulse shape output from the fiber amplifier is achieved. Here, we assume that the pulse amplitudes can be adjusted continually and smoothly. The output pulses can have any arbitrary shape as long as they are identical and are not necessary to be flat-top. Flat-top output pulses are chosen here because it has the broadest pulse duration and thus it is an optimal choice for achieving short pulse duration at the end of the CPSA system. The simulated results of output burst profile and nonlinear phase are shown in figure 3.16. When we control the pulse amplitudes to equalize the pulse shapes in the output burst, the nonlinearity-induced phase-shifts still varies between individual pulses. This is because the nonlinearity-induced phase-shift is determined by the pulse intensity and the gain (equation (3.2) and (3.3)) and in-burst amplitude reshaping doesn't equalize the gain across an individual pulse.

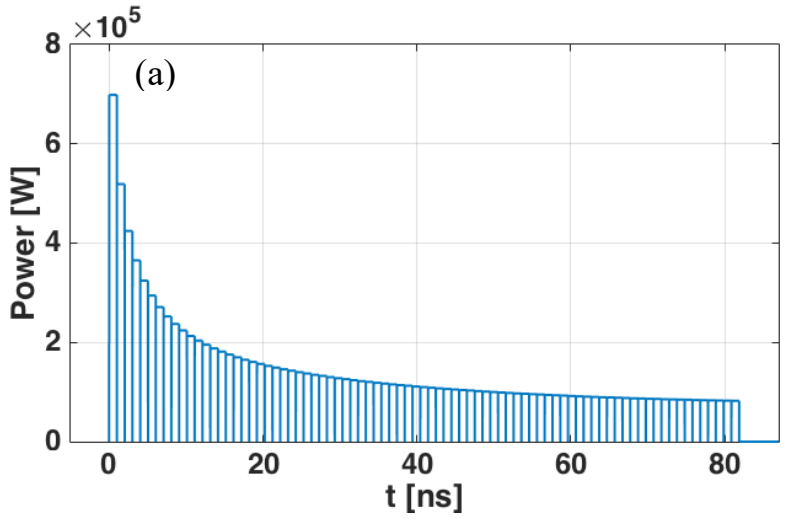

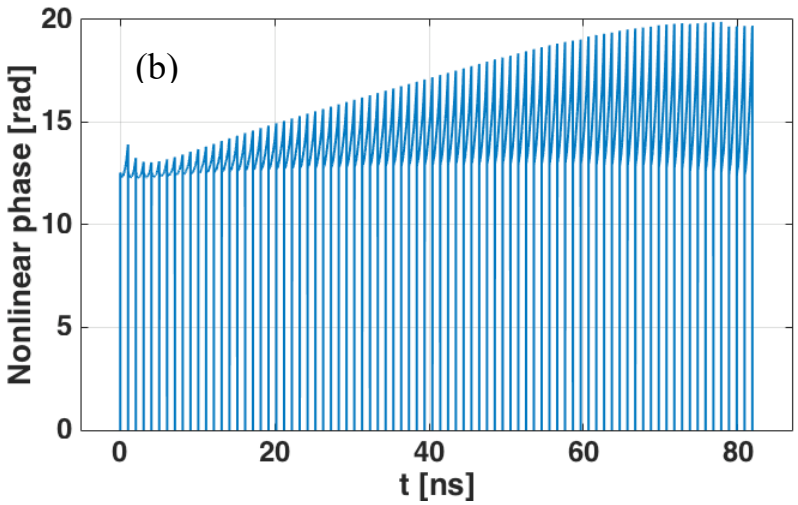

Figure 3.16 burst amplitude (a) and nonlinear phase profile (b) with in-burst amplitude reshaping. Each pulse has 10nm bandwidth centered 1037nm. The burst is amplified in 1.9m 85μm-CCC for 11mJ burst energy.

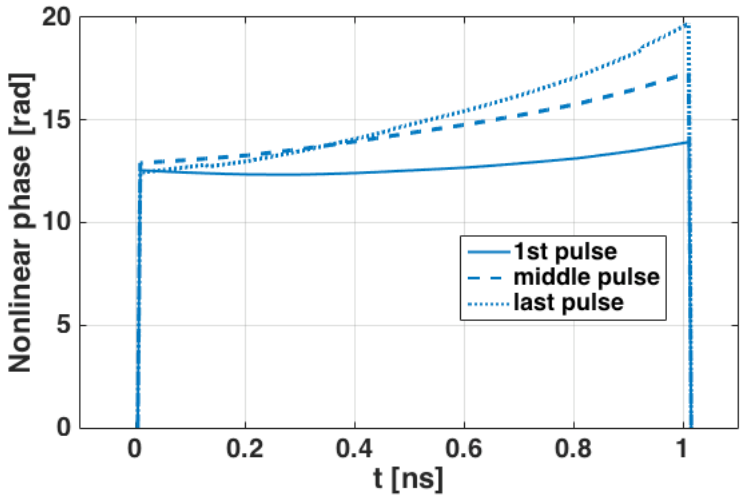

Figure 3.17 Comparison of nonlinear phase shapes between individual pulses in the burst shown in figure 3.16

We already demonstrated that having in-burst amplitude control to achieve identical pulse shapes in the burst cannot correct the deviations of nonlinear phase between individual pulses. It is a good

practice then to simulate the condition where each pulse shape over the input burst into the final amplifier is pre-shaped to achieve equal nonlinearity-induced phase shifts and compare the pulse shapes in the output burst. In this simulation, the pulse amplitudes of each pulse in the input burst are updated until the nonlinear phase equals to that of the first data point in the burst. At the output, the nonlinear phase is not only the same across the burst but also flat within each pulse while the output pulse shapes deviate from each other. The temporal shapes of the 1st and 81st pulse in the output burst is compared in figure 3.18. The simulation is done for two bandwidths: 10nm and 30nm, to see the effects of spectral bandwidth on pulse shape distortion. According to the numerical results, the pulse shapes in the output burst are different and broader bandwidth pulses have more deviations from each other.

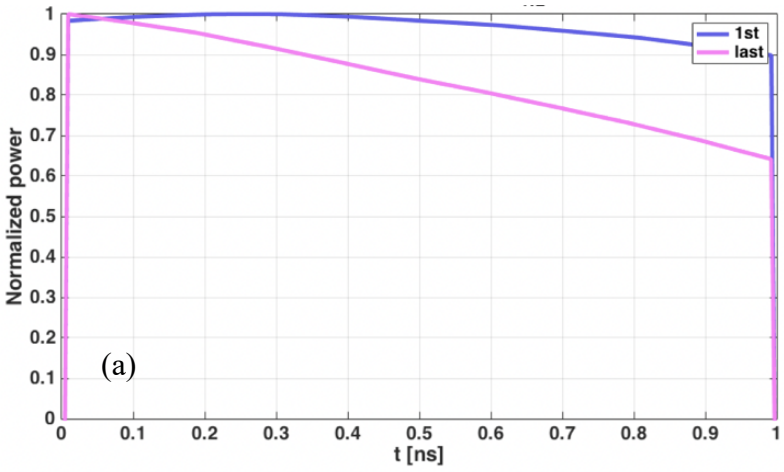

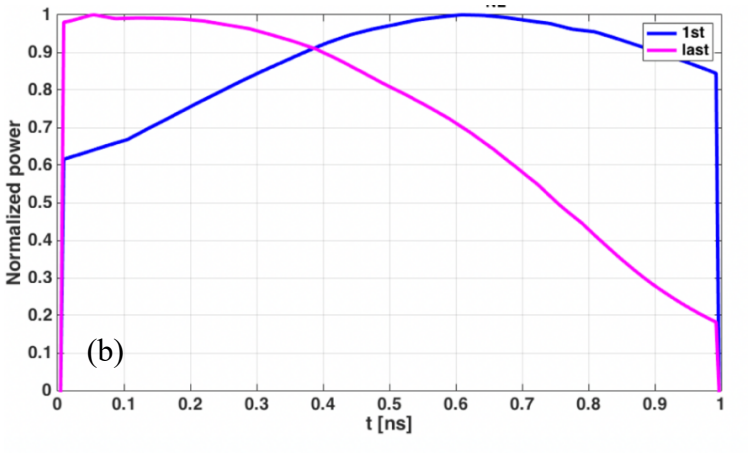

Figure 3.18 Pulse shape comparison of 1st and 81st pulse for (a) 10nm @1037nm and (b) 30nm @1037nm when the pulse amplitudes are controlled to have equal nonlinearity within each pulse across the burst

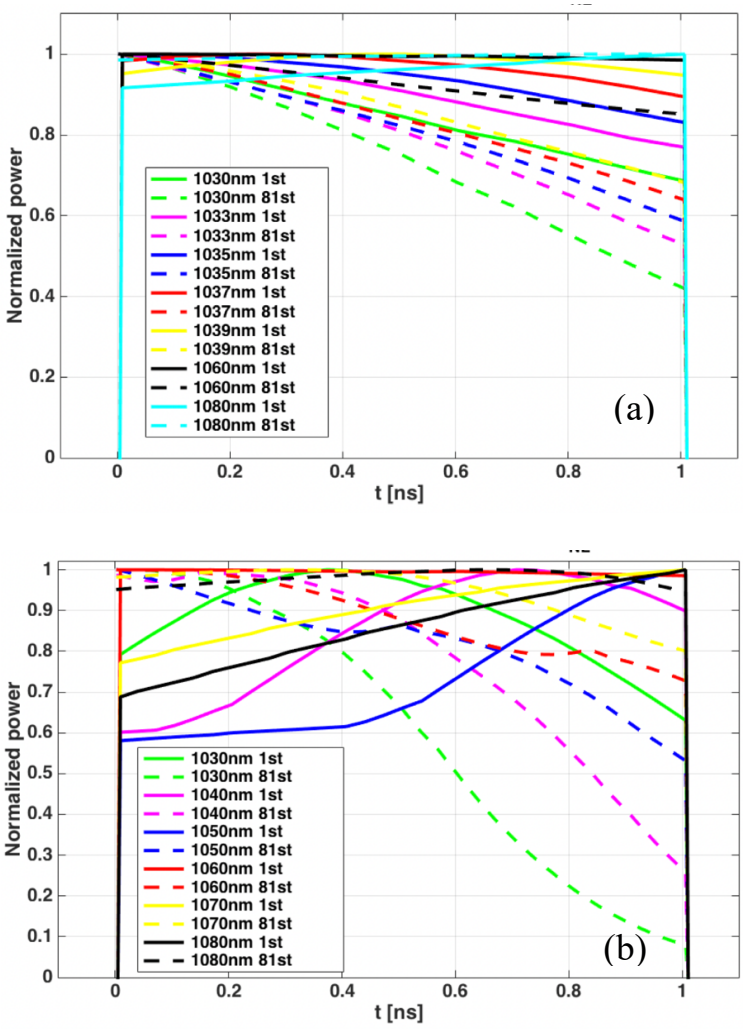

Figure 3.19 Differences between pulses in the amplified burst dependence on central wavelength for (a) 10nm, and (b) 30nm bandwidth pulses.

3.5 Full Compensation of Gain Saturation with In-burst Individual Pulse Amplitude and Phase Profile Control

Based on the above analysis, we conclude that identical pulse shapes and phase profiles, with peak phase values being equal between all the pulses across the stacking burst cannot be achieved by either in-burst pulse amplitude or phase control alone. Simultaneous control of both in-burst pulse shapes and phase profiles are necessary for achieving this. To have both in-burst pulse shape and phase controls in the experiment, as shown in the experimental setup (figure 3.15), we insert another pair of electro-optic modulators that is faster than 1GHz so that they can modulate multiple points on each individual stretched (and thus spectrum-to-time mapped) pulse, provided that the fast modulators are positioned after the stretcher to modulate each 1ns stretched pulses. Figure 3.20 shows the simulated results of amplitude and phase burst profiles with both in-burst pulse shapes and phase profile controls. This confirmed that flat-top pulse shapes and equal phase profiles is achievable, when we have perfect control for both amplitude and phase within individual pulses. In the real case, we have limited number of control points on the pulse shape and phase profile due to the limited bandwidth of electronics, which leads to pulse amplitude and phase shape distortions. But the equal-shape and equal-phase pulse profiles in the stacking burst shown in 3.20 can be approximately achieved if very fast electronics are implemented.

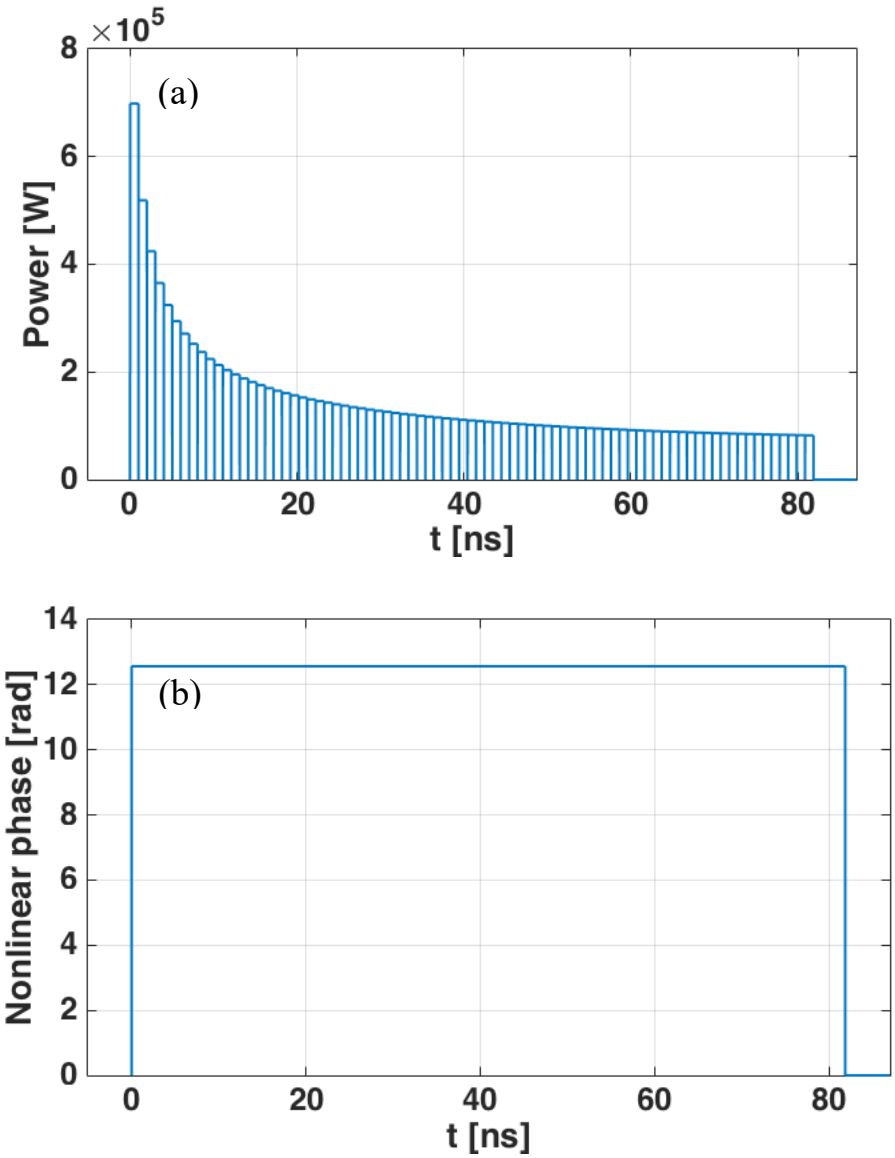

Figure 3.20 one example of desired stacking burst profile with 11mJ burst energy and equal-nonlinearity phase profile in 1.9m 85μm-CCC fiber for achieving high-fidelity pulse stacking amplification

3.6 Limitations on the Accuracy of Controlling Pulse Shape and Phase Profile due to Electronic Bandwidth and Sampling Rate Limitations

We have demonstrated that individual pulse shape and phase profile distortions induced by gain saturation can be in principle fully compensated by in-burst amplitude and phase reshaping.

However, this assumes that an arbitrarily precise and fast control can be achieved. In reality, there is significant control-electronics constraints, primarily expressed as limited bandwidth of electronics. In the experiment, the modulating waveform is generated from a Digital to Analog Converter (DAC) in the form of voltage and sent to the fast amplitude and phase electro-optic modulators, which tailor the signal proportional to this waveform. A DAC is a device that converts discrete digital signals to continuous analog signals. This conversion process is not perfectly linear due to the finite bandwidth of the DAC. A bandwidth-limited DAC only allows a finite bandwidth to convert without loss. The frequency components higher than half of the bandwidth are filtered out, which leads to distortions on analog signals. Another distortion effects due to the finite bandwidth of the DAC is the limited digital sampling rate on 1ns time. Due to this limited sampling rate, the DAC cannot produce an electrical signal equivalent to the desired continuous amplitude or phase value at each point, and thus results in modulated errors on the signal.

Figure 3.21 shows the process of calculating the distorted waveform due to the finite bandwidth of the DAC. The DAC used for this calculation is AD9174 with 5GHz bandwidth. Figure 3.21 (a) shows the ideal input waveform for 81 pulses, that can have identical pulse shape and equal nonlinear phase after being amplified to 10mJ. The red curve in Figure 3.21 (a) is the digital input waveform sent to the DAC. It is a step-shaped curve, and the sampling rate determines the spacing between two adjacent steps. For the 5GHz sampling rate, there are five different points in the 1ns time window. Thus, a 1ns pulse can have five different steps. The last point in each pulse must be set to be zero to separate adjacent pulses. This step-shaped waveform is Fourier Transformed to the frequency domain, and Figure 3.21 (b) shows the frequency components corresponding to the step-shaped waveform. A perfect low-pass filter with a hard-cutoff edge is assumed to filter the

frequency components higher than 2.5GHz. The specific shape of the low-pass filter is dependent on the particular DAC design used, can have variety of shapes. The passband can drop before the point at half of the bandwidth and go to zero after this point. The time domain picture, corresponding to the truncated frequency domain is shown in Figure 3.21 (d). Bandwidth-limited DAC distorts the pulse shape, and distorts the real input waveform compared to the ideal one. As shown below, this input burst profile that the real DAC modulates, leads to the amplified burst with non-identical pulse shapes and phase profiles.

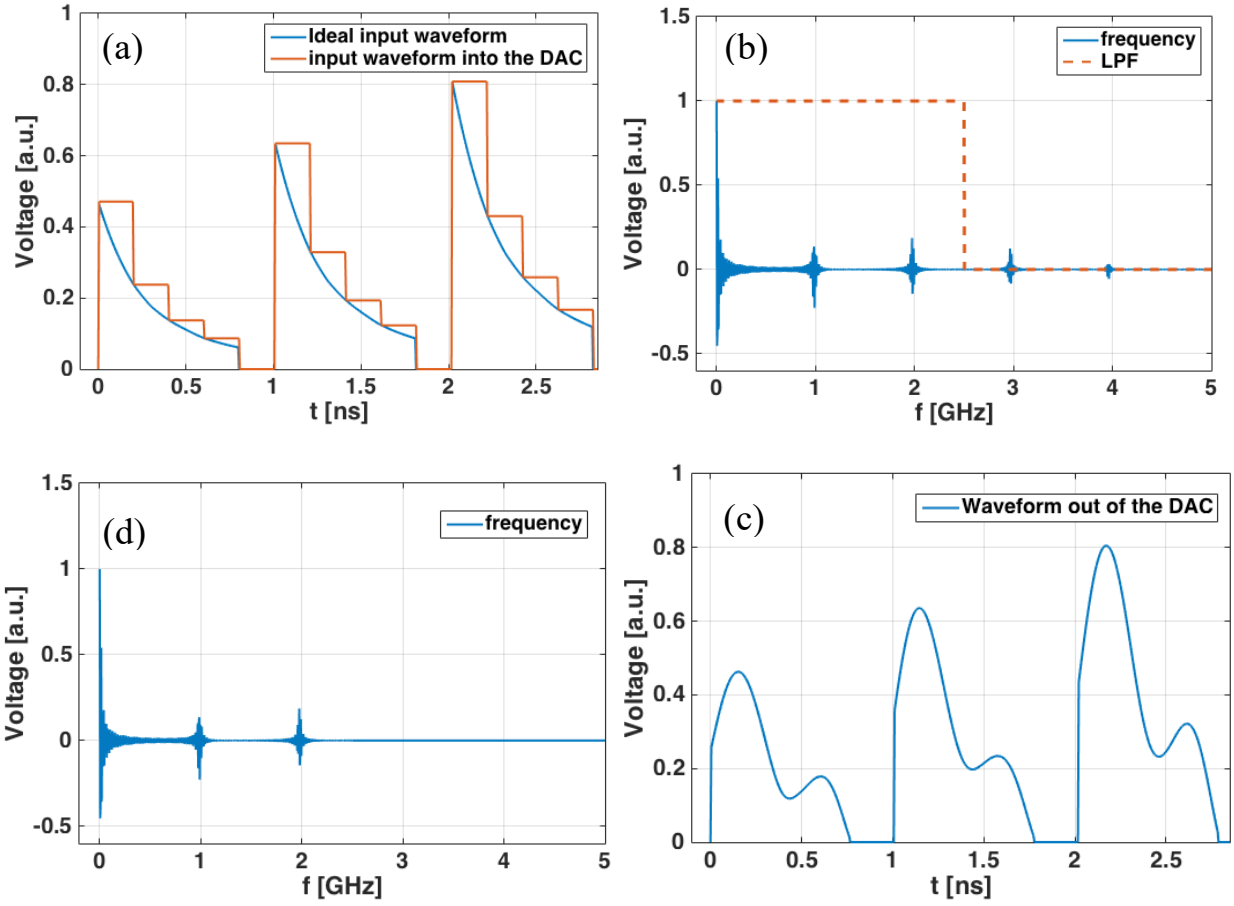

Figure 3.21 Calculation of phase shape distortion due to the finite sampling rate and limited bandwidth of the electronics.

Figure 3.22 (a) and (b) show the amplified burst and nonlinear phase profile with 10mJ burst energy. The pulse shape is not flat-top due to the modulated input pulse shape. The phase profile of each individual pulse also varies across the burst. The amplitude and phase shapes of individual pulses are shown in figure 3.23. 1st, 41st, and 81st pulses are chosen to represent the effect of unwanted modulation on the front end, middle area, and back end of the burst. Pulses in the middle and the back of the burst have similar shapes, while pulse shapes in the front are very different because front-end pulses experience higher gain than other pulses. The nonlinear phase of the first pulse has a more modulated shape, and has a much higher value than the middle and the last pulses. This would be detrimental to pulse stacking efficiency, and pre-pulse contrast, and need to be addressed.

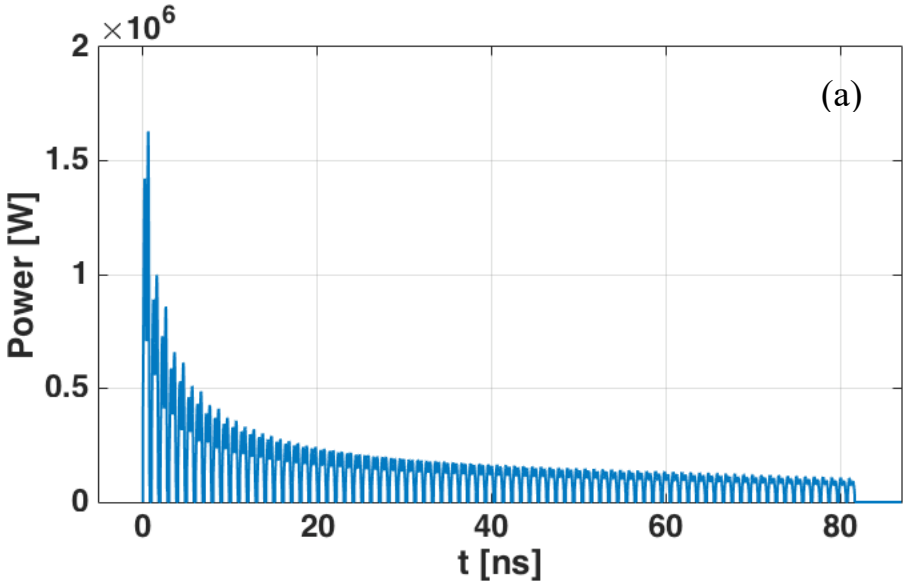

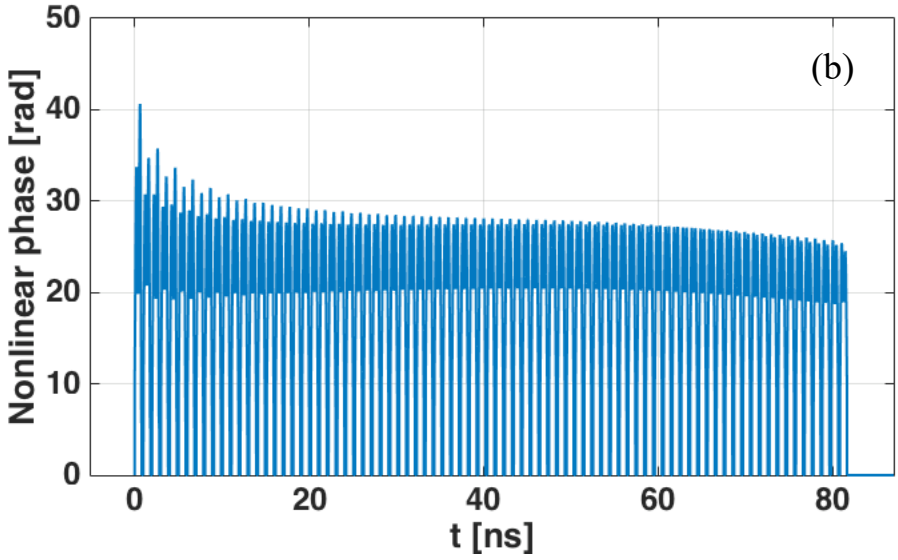

Figure 3.22 The amplitude and nonlinear phase profile across the burst calculated with 5GHz sampling rates

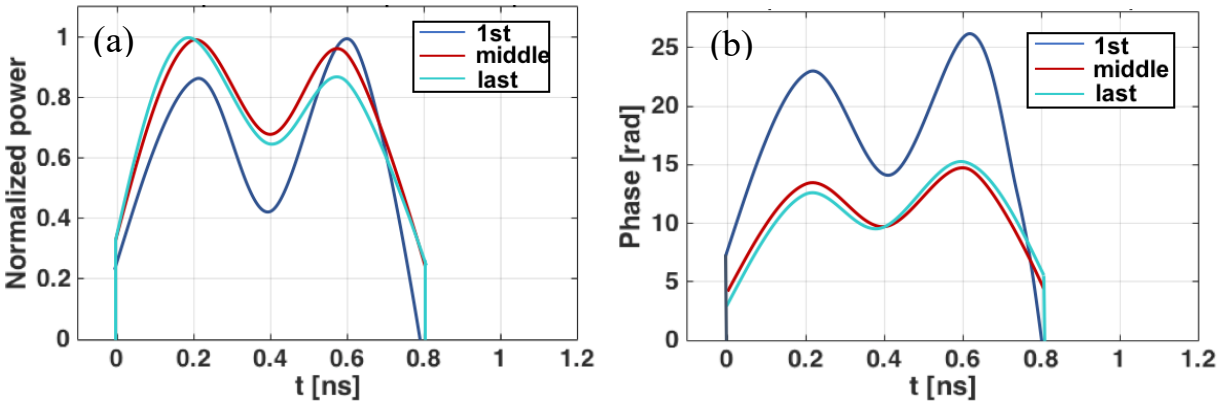

Figure 3.23 Comparison of individual pulse amplitude and nonlinear phase profiles in the amplified burst shown in figure 3.22

3.7 Correction of Modulation Errors on Individual Pulse Amplitude Shape and Phase Profile from Electronics Limitations by an Optimization Feedback Loop

We have demonstrated that flat-top pulses and flat-top phase profiles in the stacking burst are optimal for high-fidelity pulse stacking, and such pulse shapes and phase profiles in principle can be achieved by in-burst pulse shape and phase reshaping. The limited accuracy of pulse shape and individual phase profile control from limited bandwidth electronics makes flat-top pulses and flat-top phase profiles not easy to achieve in the real experiment. Instead, we aim to obtain identical pulse shapes and equal phase profiles across the burst using the finite bandwidth electronics. To achieve this goal, the differences of pulse shapes and nonlinear phase profiles across the burst due to the limited controlling accuracy of real electronics need to be corrected, and this correction can be achieved by implementing a feedback loop based on stochastic parallel gradient descent (SPGD) algorithm [28].

The SPGD method is a "hill climbing algorithm", that uses iterations to reach local maximum or minimum by using stochastically estimated gradients. At each optimization step, a small perturbation is added onto the current position, and the matric function of the output is examined. The estimated gradients are calculated based on the change of the matric function, and the control variables are updated along the same direction of the estimated gradients. Here, our goal is to achieve equal nonlinear-induced phase profiles for all the pulses in the burst. Since the amplified pulse shape is linked to its nonlinear phase shape, when the seed pulses are reshaped to produce equal nonlinear phase in the output burst, the pulse shapes should also be identical. In the SPGD algorithm, we aim to minimize the difference of nonlinear phase between the current pulse and the

target pulse. The target pulse can be either one of the real pulses in the burst, or a given pulse with arbitrary shape. The optimal target phase should be the one that allows maximum spectral bandwidth and energy, while minimizing the overall difference of nonlinear phase and pulse shape across the output burst. For example, in a burst of 81 pulses, the 41st output pulse is better than the 1st or the last pulse, and thus is preferred to be the target pulse. This is because the 1st or the 81st pulse shapes are significantly modulated by gain narrowing or gain saturation, while the 41st pulse has relatively flat amplitude and phase shape distortions. The metric function is chosen as,

$$J(x^{(n)}) = \sum_{m=1}^{M}(\emptyset(m,n) - \emptyset(m,N))^2 \tag{3.6}$$

$$x^{(n)} = [\boldsymbol{x}_A^{(n)}, \boldsymbol{x}_P^{(n)}] \tag{3.7}$$

$$\boldsymbol{x}_A^{(n)} = \left[x_A^{(n)}[1], x_A^{(n)}[2], x_A^{(n)}[3], x_A^{(n)}[4]\right] \tag{3.8}$$

$$\boldsymbol{x}_P^{(n)} = \left[x_P^{(n)}[1], x_P^{(n)}[2], x_P^{(n)}[3], x_P^{(n)}[4]\right] \tag{3.9}$$

$x^{(n)}$ is the input voltage value vector, sent to the DAC to control electro-optic modulators for reshaping the n-th pulse. $x^{(n)}$ has two components: $\boldsymbol{x}_A^{(n)}$ is the input value to the DAC for controlling the pulse shape, and $\boldsymbol{x}_P^{(n)}$ is for controlling the phase profile. Each component has four elements, since we have five controlling points in 1ns time window, and the last point always rem zero. $\emptyset(m,n)$ is the phase of the current pulse, where n is the current pulse number, and $\emptyset(\mathrm{m},\mathrm{N})$ is the phase of the target pulse, where N represents the target pulse number. Here, we choose 41st pulse as the target pulse, and so N = 41. M is the number of data points in a single pulse, determined by the oscilloscope specification, and m is the data-point number. Since the gain in the fiber amplifiers varies along the burst, and the gain seen by the later pulse is determined by the

cumulative effect by all the previous pulses, the burst is optimized from the first pulse to the last pulse, with independent optimization for each pulse. The procedure of the SPGD-based in-burst pulse shaping is,

For the n-th pulse,

Step 1: measure and calculate $J(x^{(n)})$

Step 2: give perturbation to the input amplitude and phase $x^p = x^{(n)} + \delta x^{(n)}$

Step 3: measure and calculate $J(x^p)$

Step 4: update input amplitude and phase $x^{(n+1)} = x^{(n)} + g[J(x^p) - J(x^{(n)})]\delta x^{(n)}$

Repeat step 1-4 until iteration stops

n = n +1

At the beginning of each iteration for the n-th pulse, the burst is read out from a fast oscilloscope, and the metric function for the current pulse is calculated. A small perturbation $\delta x^{(n)}$ is added onto each of the control variables $x^{(n)}$, and the metric function is examined. $\delta x^{(n)}$ are small values, that are randomly and independently chosen, and have the zero mean, and the standard deviation δx_0 [25]. The improvement (or decrease) of the matric function is calculated, and the input amplitude and phase magnitudes are updated, based on this improvement (or decrease), and accounting for the optimization parameter g (the gain) and $\delta x^{(n)}$. This procedure is repeated until the iteration stops when the required precision in the pulse phase shape is achieved, and the optimization then starts to work on the next pulse.

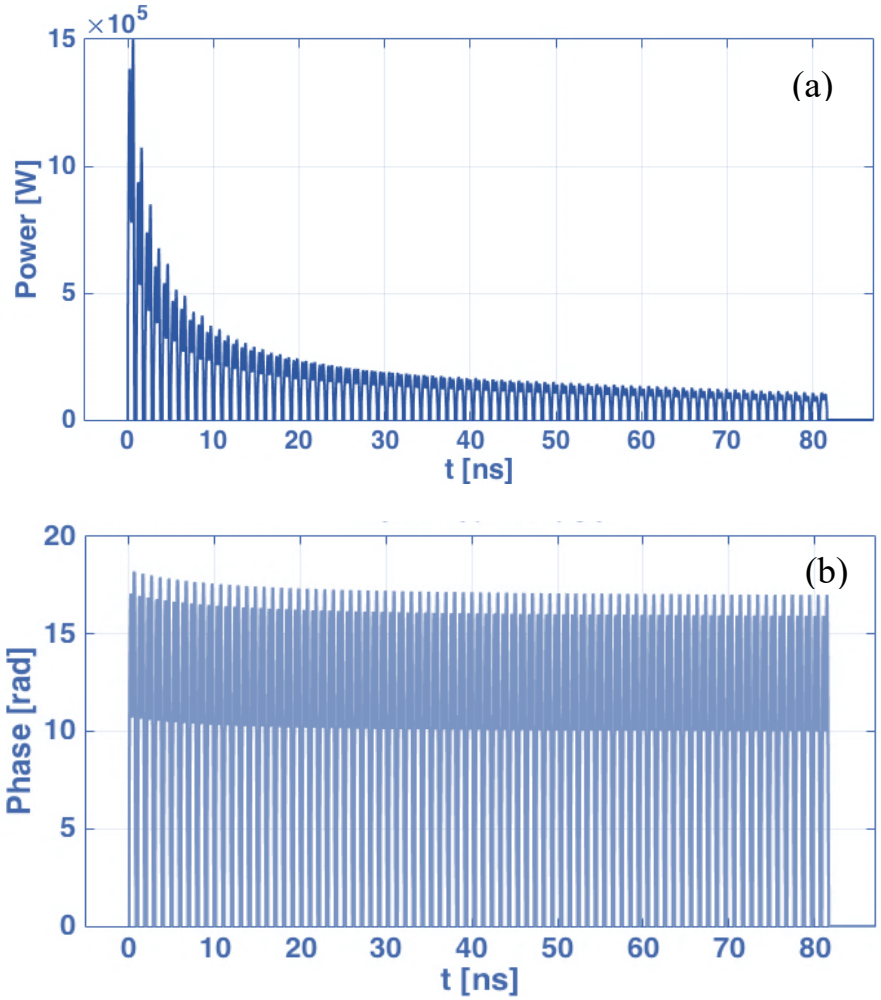

Figure 3.24 Optimized amplitude and nonlinear phase profile across the burst with shaping error correction

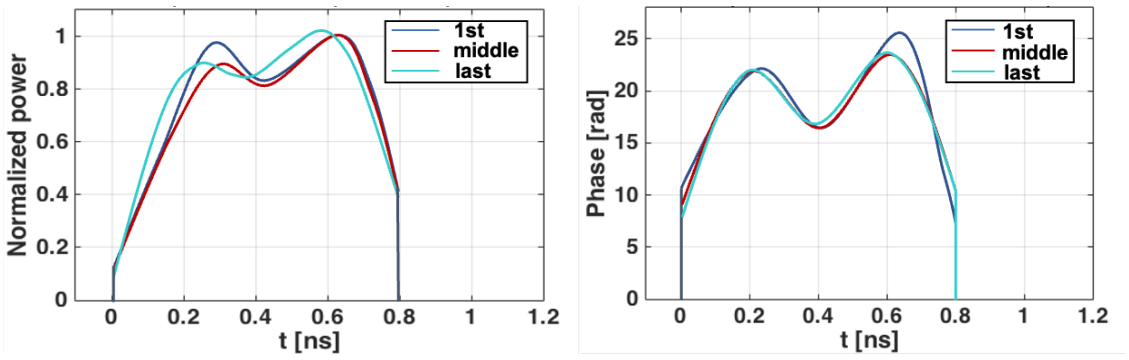

Figure 3.25 Comparison of individual pulse amplitude and nonlinear phase profiles in the amplified burst shown in figure 3.24

After implementing the SPGD-based optimization loop into the numerical code, as figure 3.24 and 3.25 shows, identical pulse shapes and nonlinearity-induced phase-shift profiles are achieved in the stacking burst. Identical pulse shapes obtained through the optimization confirms that, in a strongly saturated fiber amplifier, the amplified pulse shape is linked to the nonlinear phase profile. This is because both the pulse shape and the nonlinear phase are determined by the gain saturation in the fiber amplifier. The effects of the small deviations between individual pulses on the pulse stacking efficiency need to be examined, and further improvements are required if the effects are not negligible.

It is worth calculating the compressed pulse shape with the non-flat nonlinear phase profile in figure 3.25 to examine if this nonlinearity is acceptable. The spectrum can be obtained from the pulse shape in figure 3.25 due to the temporal-spectral mapping, and then the nonlinear phase profile in figure 3.25 is added onto this spectrum. By Fourier transforming the spectrum back to the time domain, the compressed pulse in figure 3.26 is obtained with 300fs FWHM duration, the same as the duration of bandwidth-limit pulse with 10nm bandwidth. But the side-wings aside the peak induced from this non-flat phase shape indicate that the acceptable nonlinearity should be lower, or have a more flat shape. Lower nonlinearity can be achieved by using either longer bursts (a preferable option), or reducing the amplified pulse energy somewhat (if longer bursts cannot be achieved).

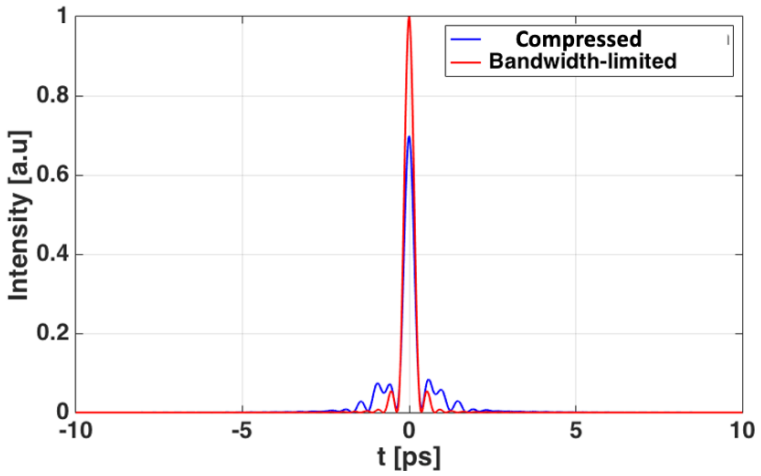

Figure 3.26 Calculated compressed and bandwidth-limit pulse shape of the amplitude pulse with nonlinear phase in the optimized stacking burst.

3.8 Experimental Validation of Gain-Saturation Control by In-Burst Pulse Amplitude and Phase Reshaping

On the basis of the above theoretical analysis, we conduct in-burst pulse shaping experiment to overcome gain saturation effects in our high energy CPSA system. Figure 3.27 shows the CPSA system experimental setup. Its electronic control system is shown in figure 3.28. 1GHz, ~100fs pulse train from the mode-locked Yb-doped fiber oscillator is modulated by a pair of 1GHz electro-optic modulators to have the equal nonlinearity burst profile, and the individual pulse phases required by the pulse stacker. These modulated pulses are stretched to 1ns in the stretcher, where the 10nm spectral bandwidth pulses centered at 1037nm are also cut out. After stretching these pulses are sent to the pair of 10GHz amplitude and phase electro-optic modulators for in-burst individual-pule reshaping. Then, the seed burst with the prescribed amplitude and phase profiles is amplified to ~10mJ energy in a sequence of single-mode fiber amplification stages, and the two

high power stages based on CCC large-core fibers. The SPGD-based feedback loop is implemented using FPGA (Field-programmable Gate Array) hardware, a pair of 10GHz amplitude and phase modulators, and a 50GHz oscilloscope and a lab computer. FPGA with 5Gsps DAC controls the 10GHz amplitude and phase electro-optic modulators. The output burst is measured by a fast detector at the end of the final CCC-stage, and the waveform data is readout from a 50 GHz oscilloscope through GPIB (General Purpose Interface Bus), and sent to a lab computer for analysis. Among the pulses in the waveform data, the current pulse is picked up to calculate the metric function, and the updated control parameters obtained from improvement of the metric function are then sent to the DAC to update again the pulse shapes and phase profiles in the seed burst.

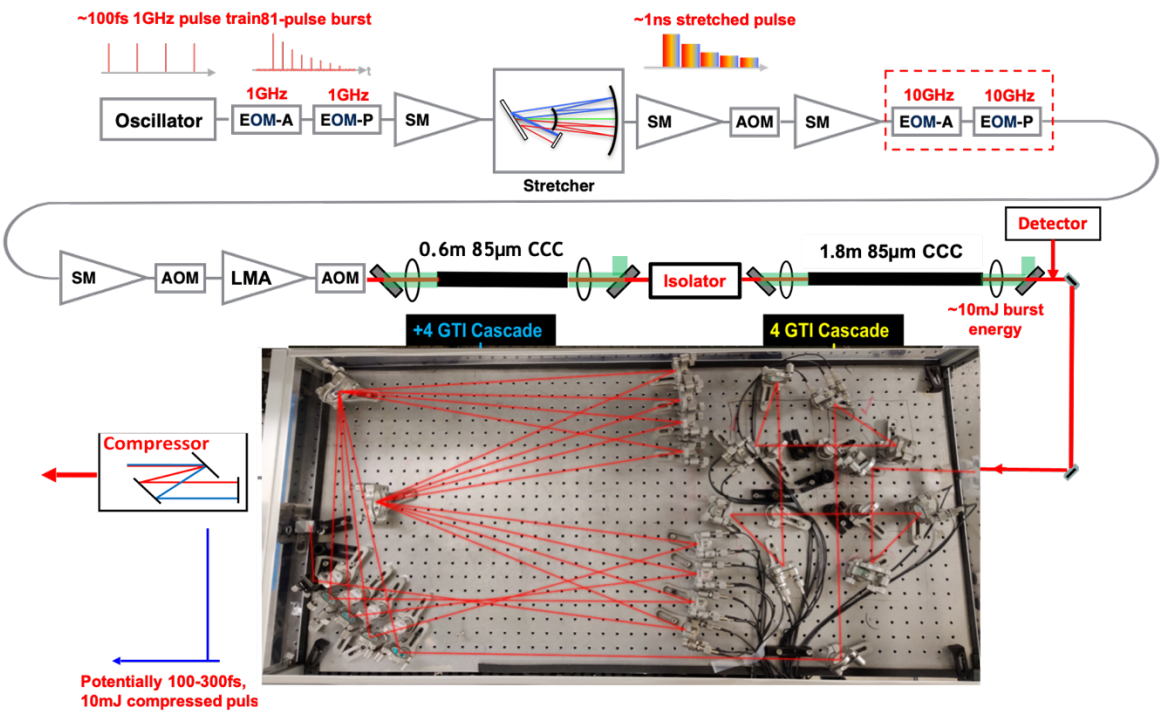

Figure 3.27 Experimental setup for in-burst pulse amplitude control in the CPSA system

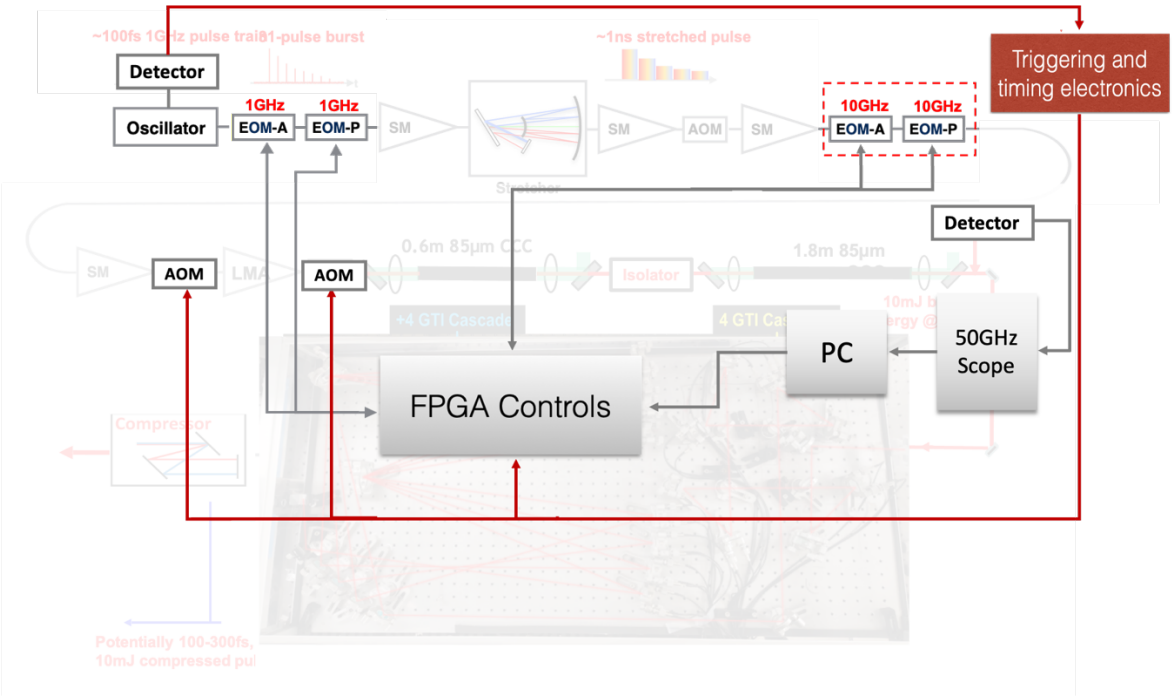

Figure 3.28 CPSA control system

As an initial step of in-burst reshaping to overcome gain-saturation effects, we did this in-burst reshaping experiment with pulse shape control only, to test equalizing the pulse shapes in the stacking burst, because the pulse shapes can be observed directly at the output end of the final amplification stage, while the phase profiles cannot be measured directly, and thus need to involve stacked pulse measurements at the system output. The SPGD-based optimization procedure is similar to the optimization for both pulse shapes and nonlinear phase profiles discussed in section 3.7, but the metric function is changed to be,

$$J\left(x^{(n)}\right) = \sum_{m=1}^{M}\left(\tilde{A}(m,n) - \tilde{A}(m,N)\right)^2 \tag{3.10}$$

$$\tilde{A}(m,n) = M\frac{A(m,n)}{\sum_{m=1}^{M} A(m,n)} \tag{3.11}$$

$$x^{(n)} = \left[x_A^{(n)}[1], x_A^{(n)}[2], x_A^{(n)}[3], x_A^{(n)}[4]\right] \tag{3.12}$$

Where A(m, n) is the amplitude of the n-th pulse. This time the control parameter $x^{(n)}$ has only amplitude components. The metric function is the square of the difference between the current and the target pulse shape, with each pulse shape normalized by its pulse area. The optimization procedure is

For the n-th pulse,

Step 1: calibrate amplitude EOM transmission at current pulse

Step 2: measure and calculate $J(x^{(n)})$

Step 3: give perturbation to the input amplitude and phase $x^p = x^{(n)} + \delta x^{(n)}$

Step 4: measure and calculate $J(x^p)$

Step 5: update input amplitude and phase $x^{(n+1)} = x^{(n)} + g[J(x^p) - J(x^{(n)})]\delta x^{(n)}$

Repeat step 2-5 until iteration stops

Step 6: calculate the desired $x^{n'}$ from x^n to maximize the pulse energy

n = n +1

The step 1, and the step 6 are needed because the amplitude electro-optic modulator controls the pulse shape by adjusting the transmission. Therefore, after several optimization iterations, the transmitted pulse energy is less than the initial pulse energy. Therefore, after the iterations stop, the pulse amplitude should be increased to have the maximum energy transmission, while simultaneously maintaining the optimized pulse shape. This cannot be done directly through multiplying by some factor the four input values, sent first to the DAC, and then to the electro-

optic modulator. There are two reasons: (1) dependence of the electro-optic modulator transmission vs the input voltage is nonlinear; (2) the gain of the amplifier is also nonlinear due to saturation. To find the correct input values, that allow maximum transmission while maintaining the optimal pulse shape, the relation between the input voltage sent to the DAC, and the amplified pulse amplitude needs to be calibrated. It should be noted that this calibration has to be done for each pulse independently, because the current DAC response from the same voltage values is dependent on its response at the previous times, and so changes over the burst. Also, the gain in the fiber amplifier is varying along the burst. Using the measured relationship, as shown in figure 3.29, the optimized pulse can achieve the maximum energy while maintaining the pulse shape. Although the transmission of the electro-optic modulator is a sinusoid, this relation is not an exact sinusoid due to the time-varying gain in the amplifier. Assuming x^{max} is the highest voltage in the current optimized pulse, and x^{k} is one of the other three voltages, the corresponding transmissions are T^{max} and T^{k} correspondingly. To maintain the maximum pulse energy, T^{max} needs to move to the point $T^{max'}$ which is at the top of the curve. And to maintain the pulse shape, T^{k} needs to move to the point $T^{k'}$, and its value should be,

$$T^{k\prime} = \frac{T^{max\prime}}{T^{max}} T^{k} \tag{3.13}$$

After changing the peak voltage to the value that has the maximum transmission and moving all the other three control voltages to the values obtained in equation (3.13), the resulting pulse can have simultaneously the maximum amplitude, and the optimized pulse shape.

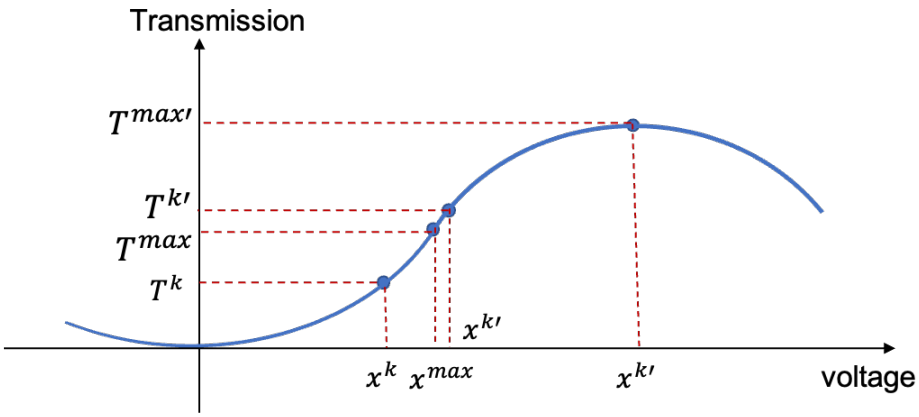

Figure 3.29 Schematic of amplitude electro-optic modulator transmission

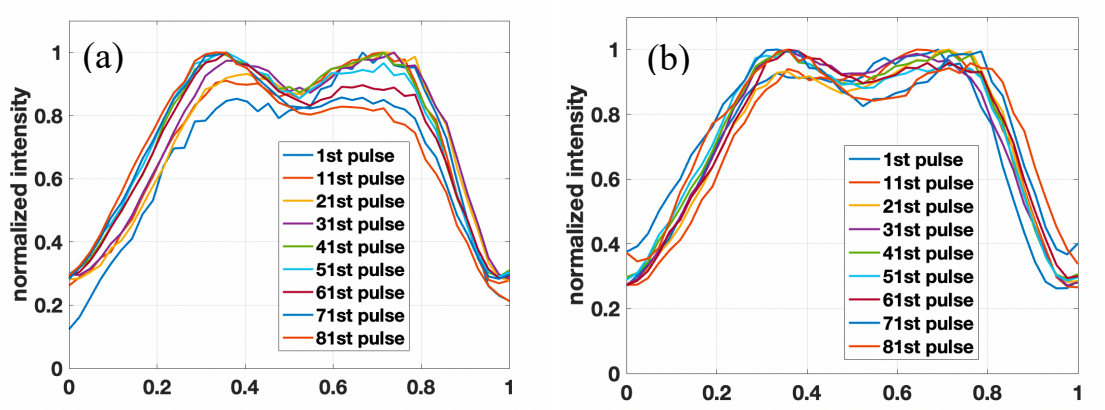

Figure 3.30 Experimental measurement of individual temporal shapes across the 6.2mJ amplified burst with (a) no saturation control, and (b) in-burst amplitude reshaping for saturation control.

The experimental results are shown in figure 3.30. At the output end of the last CCC-stage, 6.2mJ burst energy for 81 pulses is obtained at 2KHz repetition rate. Figure 3.30 (a) shows the measured pulse shapes with no saturation control. The differences between the broadband-pulse shapes along the burst are induced by the gain saturation. They are relatively mild in this case, because the spectral bandwidth is only 10nm, and the pulse output energy is relatively low, producing only a moderate degree of saturation. These distortions should be stronger for broader pulse spectra, and

for higher extracted energies. The optimized pulse shapes, obtained by this in-burst pulse reshaping, shown in figure 3.30 (b) are very close to each other. These results confirm that identical pulse shapes across the burst are achievable using this in-burst reshaping technique. In the near future, 30nm spectral bandwidth and higher pulse energies will be explored experimentally, at which point we anticipate a much stronger gain saturation effects, and thus the critical need for this in-burst amplitude reshaping technique.

CHAPTER IV

Gain Narrowing Compensation for Sub-100fs, Multi-mJ Energy Laser Systems

In addition to high pulse energy, broadband spectral width is also required to achieve short pulse duration (sub-100fs) at the end of a laser system, for generating multi-TW peak power pulses. This means that gain narrowing effects, which produce spectral narrowing on broadband pulses in a high-gain laser system, need to be considered. There have been multiple efforts for compensating gain narrowing effects in Yb-doped fiber laser systems. 120fs pulse duration with 10mJ energy is achieved by implementing two Fourier-domain pulse shapers in a spatial beam combining based Yb-doped fiber laser system [29]. Sub-100fs pulses with μJ-level energy are obtained by implementing filters that pre-shape the seed spectrum to overcome gain narrowing effects [30]–[32]. But the total gain in these systems is only ~ 40dB, while producing multi-mJ pulses require at least 100dB gain. Here, our goal is to explore the spectral shaping effects from gain narrowing in 30-100fs duration region under 100-150dB gain, and to examine the possibility of fully compensating gain narrowing effects in our CPSA system. Because of the complexity of the CPSA system, we first build a Regenerative-amplification fiber system that can provide controllable gain, while keeping the energy below the saturation energy, to explore the gain narrowing effects with the increasing gain. We then design a Lyot-based spectral filter to compensate gain narrowing effects. After gain narrowing compensation, spectral content corresponding to 42fs bandwidth-limited duration is experimentally obtained under 150dB gain. Subsequently, this spectral filter is inserted into the CPSA system to manage gain narrowing effects under real gain, and we

experimentally demonstrated 78fs duration with gain required for obtaining ~10mJ energies from the final amplifier.

4.1 Gain Narrowing Effects in Sub-100fs High Energy Fiber Laser Systems

Gain narrowing is the phenomenon that an amplified spectral bandwidth is reduced due to the limited gain bandwidth of a gain medium. Yb-doped fiber amplifiers have the advantage of a broadband gain window starting from 1015nm to longer than 1100nm. Such a broad gain has the potential to achieve sub-100fs (as shown in this work – from ~42fs - ~100fs) pulses in Yb-doped fiber amplification systems. However, the gain is not flat vs the wavelength, which makes the spectral components at the peak of the gain curve experience higher gain than the spectral components at the wings around the peak. Such gain difference induces narrowing effect of the spectral bandwidth, which increases with the total gain in a system. The total gain is the sum of the gain experienced by the signal in all amplifiers, whereas the net gain equals to the total gain minus by the total loss in a system. Note that this loss is usually very broadband and is thus not correcting the gain narrowing effects. A higher total gain usually induces a stronger gain narrowing effect.

Gain narrowing in a broadband Yb-doped fiber amplification system can be simulated by using the absorption and emission cross data (shown in Figure 4.1 (a)) to calculate the wavelength-dependent gain for different total-gain values in this system. Figure 4.1 (b) shows the spectra narrowing dependence on the total gain calculated using the fiber models described in chapter 2. A flat-top broadband input pulse with 1ns-long stretched duration is sent to a CCC-fiber amplifier, where it is amplified by 25dB of total gain. The input pulse energy is controlled to be much lower

than the saturation energy of the fiber, so that no gain saturation is involved, and the spectrum changes are only due to gain narrowing effect. This amplified pulse with a narrowed spectrum is then attenuated, to have the similar energy to the original input pulse, and is then sent to the fiber amplifier again to measure the effect of gain narrowing with increasing total gains. In this way, spectra of the pulses amplified to different gain values are obtained. The bandwidth-limited pulse duration of the input pulse is 50fs. As the total gain increases, the FWHM of the spectrum narrows to a larger degree. When the gain is 150dB, the FWHM of the spectrum is reduced to 6nm, which corresponds to a ~500fs bandwidth-limited pulse duration, ten times longer than the original pulse. Spectral filtering can be used to compensate this gain narrowing effects, but usually, the effectiveness of such compensation also decreases with increasing overall gain. For example, in [16], spectral-filter compensation allowed to achieve 91 fs pulses in a Yb-fiber CPA system, but with the total gain limited to only ~40dB. CPSA technique can extract 10mJ energy from fiber amplifiers, which requires total system gains of up to >100dB. In this chapter, gain narrowing effects is explored for 30-100fs pulses in 100-150dB gain Yb-doped fiber laser systems. We use a spectrally controllable device, consisting of a sequence of linear polarizers and birefringent plates, which allows to accurately and adjustably tailor its spectral filtering properties to achieve complete gain-narrowing compensation over 30-70nm of signal bandwidth for the total gain reaching 150dB. This opens a pathway towards sub-100fs duration and multi-mJ pulses from fiber CPSA systems.

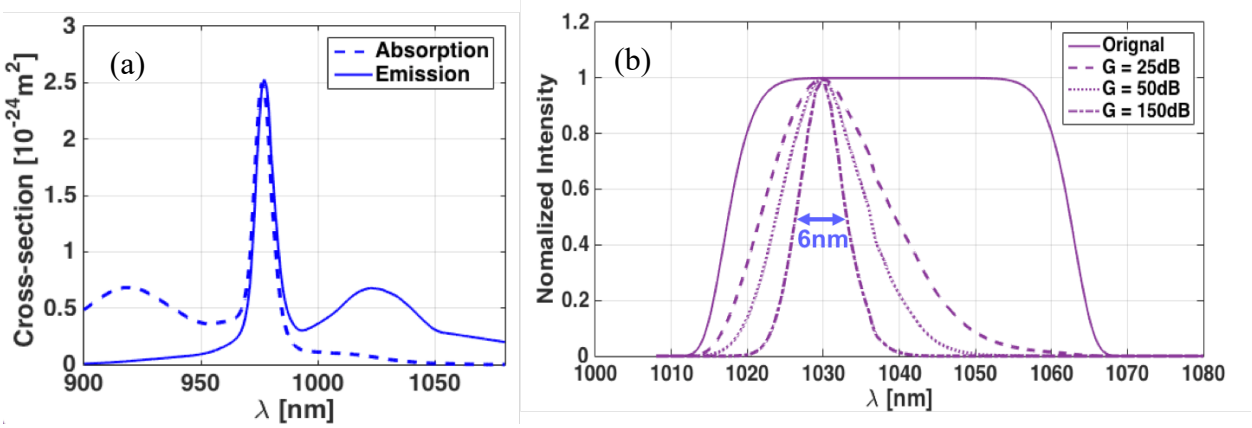

Figure 4.1 (a) absorption and emission cross section of Yb^{3+}; (b) narrowed spectra at different gain values.

4.2 Regenerative-Amplification Fiber System for Exploring Gain Narrowing Effects

To characterize gain narrowing effects in fiber amplifiers at very high total gain, we use the setup of a regenerative fiber-loop amplifier shown in figure 4.2 (a) to measure and compare spectra before and after amplification with the controllable gain. 1GHz input pulse train stretched to 1ns-long is sent into the acousto-optic modulator, where the 1st order picks up a burst with 10's pulses at 1MHz, which is injected into the fiber, while the rest of the pulse train goes out at the 0th order and get dumped at the PBS #3. The fast-electro-optic modulator selects one single pulse from the burst, and this pulse get amplified in a single-mode Yb-doped fiber, that provides 25dB gain per-pass, and then goes through the AOM for another roundtrip. The HWP #2 and the PBS #2 form an adjustable attenuator, which provides spectrally independent loss to compensate the single pass gain so that pulse energy remains constant after each roundtrip, while the total accumulated gain keeps increasing with each roundtrip. The AOM turns on again after a selected number of

roundtrips, to send the amplified signal out at the 1st order of the AOM, and the spectrum is measured after it transmits the PBS #3. The output beam, and the input beam are rejected by the AOM at the 0th order, and can be separated by the PBS #3, because the output beam is controlled to have the polarization perpendicular to the transmitted polarization of the PBS #1, while the input beam is polarization-controlled to have the maximum transmission of the PBS #1. By controlling how many roundtrips the pulse undergoes, we can explore gain narrowing effects corresponding to different total gains.

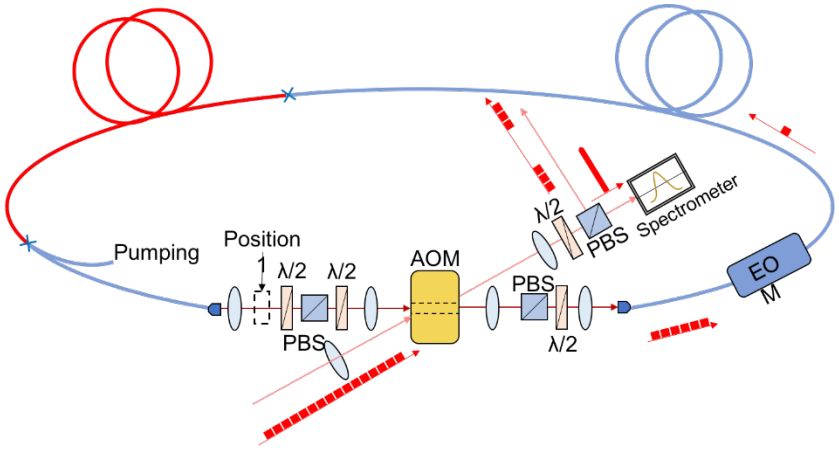

Figure 4.2 Regenerative-amplification fiber system configuration

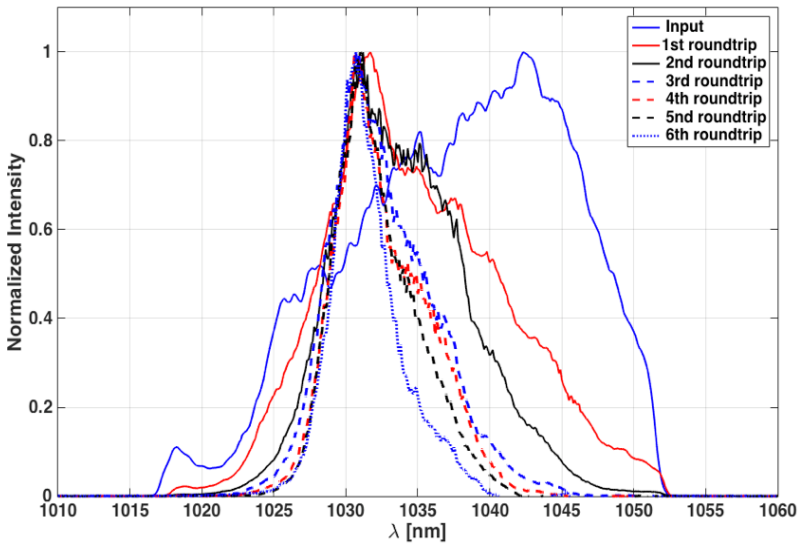

Figure 4.3 Measured spectra for different gain (25dB gain for each roundtrip)

Figure 4.3 shows the experimental results of strong spectral narrowing with increasing number of roundtrips. The input spectrum has 25nm FWHM bandwidth which corresponds to 100fs bandwidth-limited pulse duration. The FWHM narrows increasingly with increasing number of the roundtrips. It is reduced to merely 5nm, when amplified after 6 roundtrips by ~150dB, corresponding to the bandwidth-limited pulse duration of ~500fs. This measurement confirms the gain narrowing simulation results described earlier in the chapter and provides a conclusive demonstration of the strong gain narrowing effect in high gain Yb-doped fiber amplifiers.

4.3 Spectral Filter Based on Lyot Configuration

To overcome gain narrowing, we use Lyot spectral filters (figure 4.4(a)) to adjustably compensate the spectral loss. The device configuration is determined by three stages, where each of them has one birefringent crystalline quartz plate, and one polarizer. The transmission curve (transmission vs. wavelength) is a sinusoid for each stage. Therefore, for three stages the filter transmission is the multiplicity of three different sinusoidal functions. In each stage the thickness of the crystal determines the bandwidth, and the central wavelength is where the transmission dip is, while the angle between axis of each crystal and each polarizer determines modulation depth. The transmission of the spectral filters at frequency w can be calculated using equation (4.1), (4.2) and (4.3). At ith-stage, the linear polarized beam pass through a birefringent crystal with thickness

$P_i = OPL_i = \left(m + \frac{1}{2}\right)\lambda_0$ (m is the order of the multi-order HWP and λ_0 is the central wavelength) with an angle α_{i1} between the axis of the linear polarized beam and the crystal. This beam is then spectral-filtered by a linear polarizer, with an angle α_{i2} between the axis of the crystal and the linear polarizer. Figure 4.4 (b) are calculated transmission curves at different configurations, showing that by controlling the crystal thickness, and the angle between the two axes for three stages, the transmission curve can be adjusted over a wide range of shapes and bandwidths, and the extinction ratio can be as high as 40dB.

$$T_1 = \begin{bmatrix} 1 & 0 \\ 0 & 0 \end{bmatrix} \begin{bmatrix} cos\alpha_{12} & sin\alpha_{12} \\ -sin\alpha_{12} & cos\alpha_{12} \end{bmatrix} \begin{bmatrix} e^{-\frac{i}{2}P_1\left(\frac{nw}{c}\right)} & 0 \\ 0 & e^{\frac{i}{2}P_1\left(\frac{nw}{c}\right)} \end{bmatrix} \begin{bmatrix} cos\alpha_{11} & sin\alpha_{11} \\ -sin\alpha_{11} & cos\alpha_{11} \end{bmatrix} \begin{bmatrix} 1 \\ 0 \end{bmatrix} \quad (4.1)$$

$$T_2T_1 = \begin{bmatrix} 1 & 0 \\ 0 & 0 \end{bmatrix} \begin{bmatrix} cos\alpha_{22} & sin\alpha_{22} \\ -sin\alpha_{22} & cos\alpha_{22} \end{bmatrix} \begin{bmatrix} e^{-\frac{i}{2}P_2\left(\frac{nw}{c}\right)} & 0 \\ 0 & e^{\frac{i}{2}P_2\left(\frac{nw}{c}\right)} \end{bmatrix} \begin{bmatrix} cos\alpha_{21} & sin\alpha_{21} \\ -sin\alpha_{21} & cos\alpha_{21} \end{bmatrix} T_1 \quad (4.2)$$

$$T_3T_2T_1 = \begin{bmatrix} 1 & 0 \\ 0 & 0 \end{bmatrix} \begin{bmatrix} cos\alpha_{32} & sin\alpha_{32} \\ -sin\alpha_{32} & cos\alpha_{32} \end{bmatrix} \begin{bmatrix} e^{-\frac{i}{2}P_3\left(\frac{nw}{c}\right)} & 0 \\ 0 & e^{\frac{i}{2}P_3\left(\frac{nw}{c}\right)} \end{bmatrix} \begin{bmatrix} cos\alpha_{31} & sin\alpha_{31} \\ -sin\alpha_{31} & cos\alpha_{31} \end{bmatrix} T_2T_1 \quad (4.3)$$

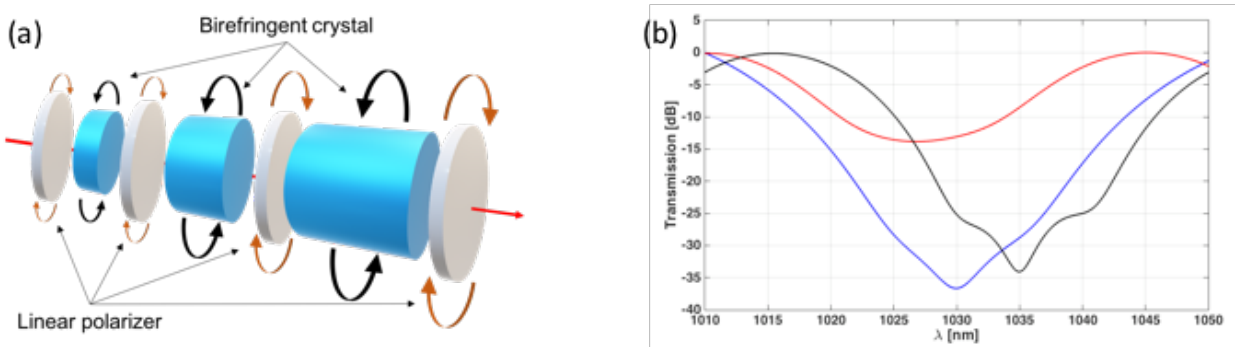

Figure 4.4 (a) spectral filter; (b) transmission of the spectral filter

The initial test of this spectral filter is done by inserting it inside the fiber loop, to compensate the gain narrowing. As figure 4.5 shows, the spectral filter is inserted right after the single-mode fiber amplifier. By controlling the parameters in the spectral filter, the measured compensated spectrum is obtained as shown in figure 4.6 (a). Figure 4.6(b) is the calculated bandwidth-limited pulse shape. It is clear that, after the compensation, the initial spectral width is recovered, and the bandwidth-limited pulse duration at the output is 104fs, the same as of the input pulse. This is an initial proof that the spectral filter can compensate strong gain narrowing in a broadband and high gain Yb-doped fiber amplifier system.

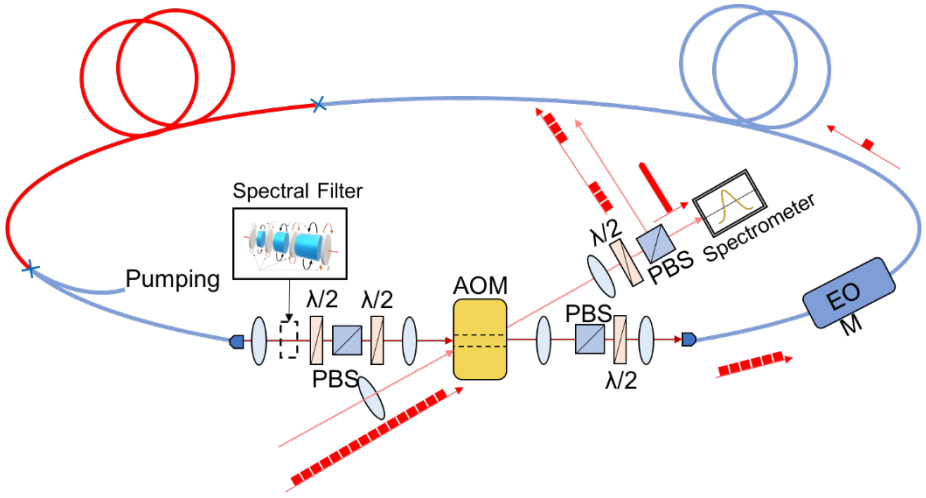

Figure 4.5 Regenerative-amplification fiber system configuration with gain narrowing compensation

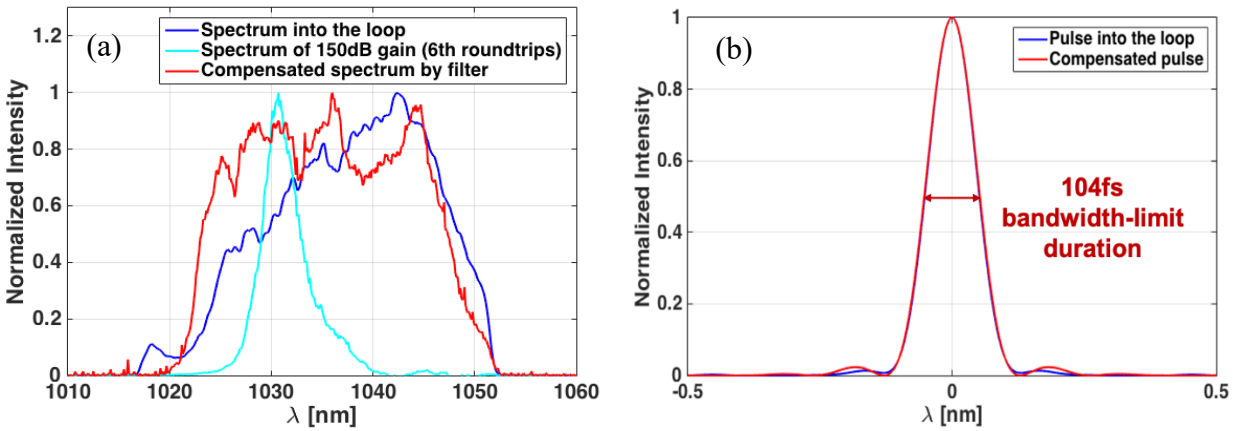

Figure 4.6 100fs gain narrowing compensation experimental results: (a) compensated spectrum by the spectral filters for 150dB gain compared with input spectrum and uncompensated spectrum narrowed by gain narrowing effects for 150dB gain; (b) calculated bandwidth-limited pulse shape of compensated spectrum and input spectrum.

4.4 Gain Narrowing Compensation to Below 50fs in the Regenerative-Amplification Fiber System

It is worthwhile to explore gain narrowing effects for broader bandwidth signal using regenerative-amplification fiber, since 30-50fs pulse duration are prefered for the applicastions of the envisioned multi-TW peak power laser systems. To obtain the ~30-50nm spectral bandwidth, corresponding to ~50fs bandwidth-limited durations, we spectrally broaden the pulses from the 1GHz oscillator using a nonlinear fiber amplifier. This nonlinear amplifier operstes in a so-called nonlinear-attractor regime [33], which broadens the spectrum by managing the nonliner effects and gain saturation in a single-mode fiber amplifier, so that the spectrum of the amplified pulse exceeds the gain bandwidth of the amplifier. A short pulse is sent to this fiber amplfiier, and then spectrally broadened by self-phase modulation effects due to its relative high peak power. This broadened spectrum is further broadened when the pulse passes through the saturated region in the fiber amplfiier. As discussed in Chapter 2, the two energy levels of Yb^{3+} are split into several

sublevels and different wavelengths, corresponding to different sublevels. When the Yb^{3+} fiber amplifier is saturated, the wavelength that sees the highest gain is saturated first, and so the gain at other wavelengths becomes higher than that of the peak wavelength, leading to spectral broadening.

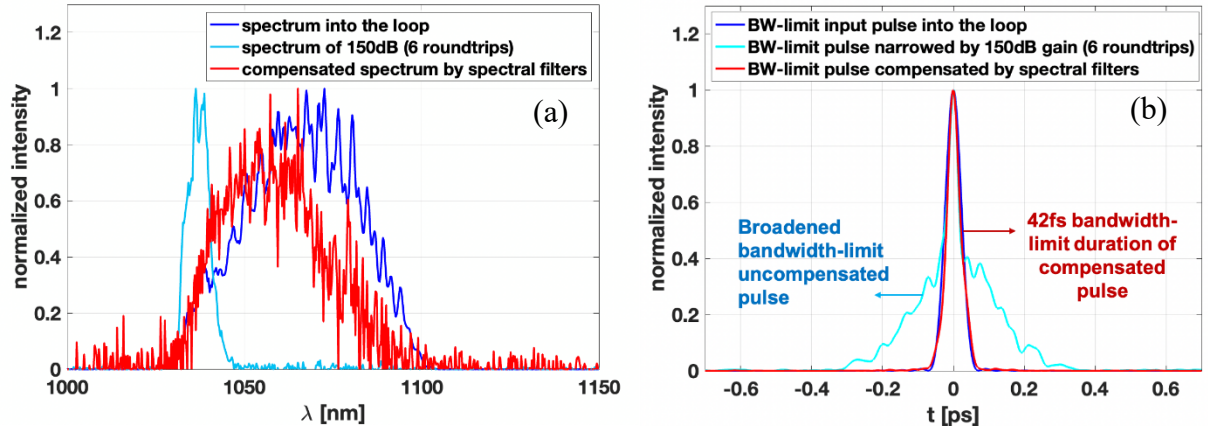

Figure 4.7 50fs gain narrowing compensation experimental results: (a) compensated spectrum by the spectral filters for 150dB gain compared with input spectrum and uncompensated spectrum narrowed by gain narrowing effects for 150dB gain; (b) calculated bandwidth-limited pulse shape of compensated spectrum and input spectrum.

The experimentally measured results are shown in figure 4.7. The compensated spectrum (red curve) is noisy, because the output spectrum after passing 6 roundtrips in the fiber loop is obtained by subtracting the input spectrum from the measured total spectrum. The loss in this fiber loop is large, and the compensated spectrum going out of the fiber loop after 6 roundtrips is relatively weak. In the meantime, the input pulse train with relatively high power, which is immediately rejected by the AOM, propagates along the same path as the output signal to the spectrometer.

Therefore, subtracting the input spectrum from the measured total spectrum allows to measure the compensated spectrum. The losses in the fiber loop can be optimized, and more accurate results can be obtained.

The calculated bandwidth-limited pulse shapes of the recovered spectrum, and the measured narrowed spectra due to the gain narrowing effects, as well as the measured input spectrum are shown in figure 4.7 (b). The bandwidth-limited pulse duration of ~42fs has been achieved for the gain-narrowing compensated bandwidth experimentally obtained after amplification with the total gain of 150dB. when there is no gain narrowing control, as the uncompensated spectrum (light blue) shows, the resulting narrowed spectrum can support approximately ten times longer pulses of 700-800fs.

4.5 Gain Narrowing Compensation Experiments in a CPSA System Producing 78fs Pulses

After the experiments of gain narrowing compensation in a regenerative-amplification fiber system, we conducted the gain narrowing compensation experiment in the actual CPSA system. The experimental setup is shown in figure 4.8. The oscillator generates ~100fs pulses with 60fs bandwidth-limited duration at 1GHz. The following amplitude electro-optic modulator carve out an equal amplitude burst of 81 pulses from the pulse train. To maintain broadband spectral content of 60fs duration, we replace the grating-based stretcher by 100m single-mode passive fibers to stretch the pulses in the burst to ~100ps. These stretched pulses are sent to the spectral filters to pre-shape the spectrum to overcome gain narrowing effects. Then, the shaped pulses are amplified

to 90μJ burst energy in the following four single-mode amplifier stages, one 25μm-LMA stage, and one 85μm-CCC stage, with AOMs between the stages to down-count the burst repetition rate, and to protect from ASE buildup between the stages. The gain at each amplification stage is measured, and the total gain is calculated by adding up the individual gain in each of the amplifiers, leading to a 100dB total gain in the CPSA system. The compensated spectrum with ~18nm bandwidth (FWHM) is obtained by controlling the parameters (angles and thickness of the crystals) of the spectral filters to maximize the spectral width. Its calculated bandwidth-limited pulse shape corresponding to 78fs duration (FWHM) is shown in figure 4.9, where it is also compared to the spectrum and calculated bandwidth-limited pulse shape of the 60fs seed pulses from the oscillator. It is worth noting that the compensated spectrum stops at ~1020nm, because there is no gain below 1020nm in a Yb-doped amplifier. This means that we fully compensated gain narrowing effects in the CPSA system with the 100dB total gain. It should be also noted that the achievable spectral width is dependent on the spectral shape output of the oscillator. The oscillator spectrum, plotted in a logarithmic scale (figure 4.10), shows that the ratio between the peak and the edge of the spectrum is 25dB.

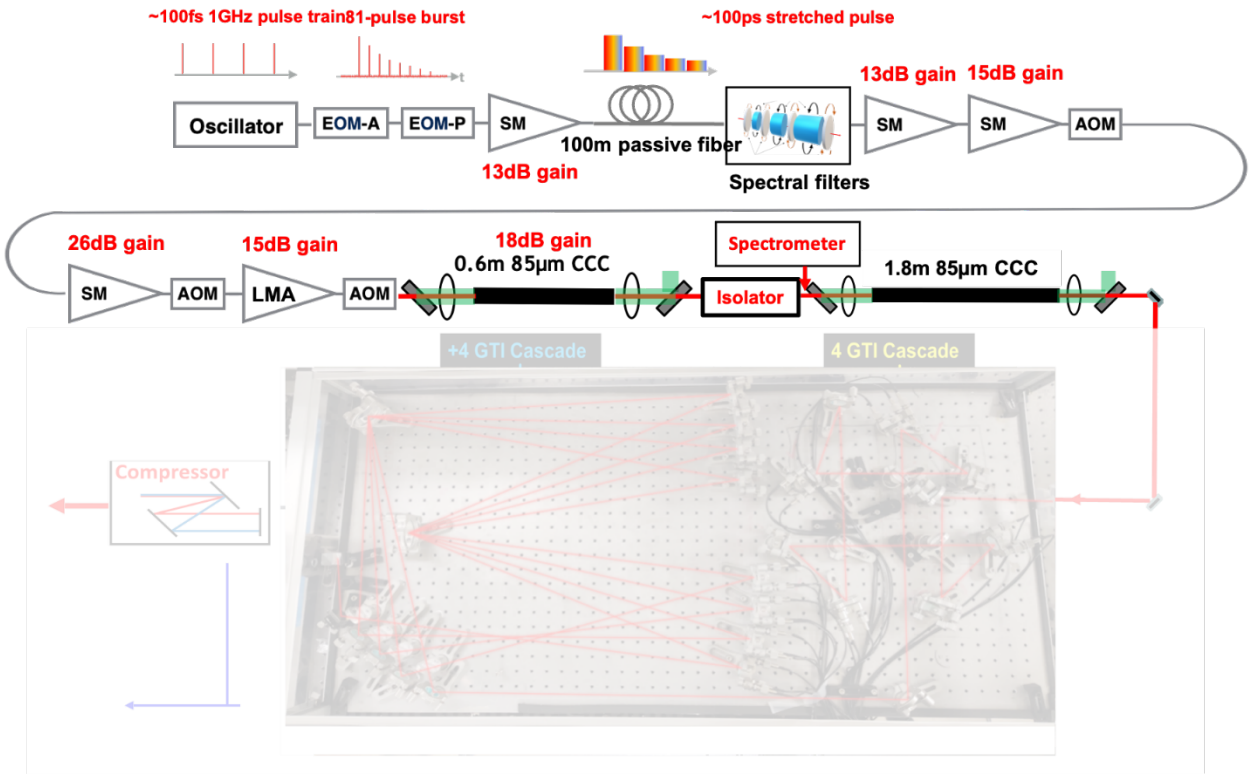

Figure 4.8 Experimental setup of CPSA system for gain narrowing compensation

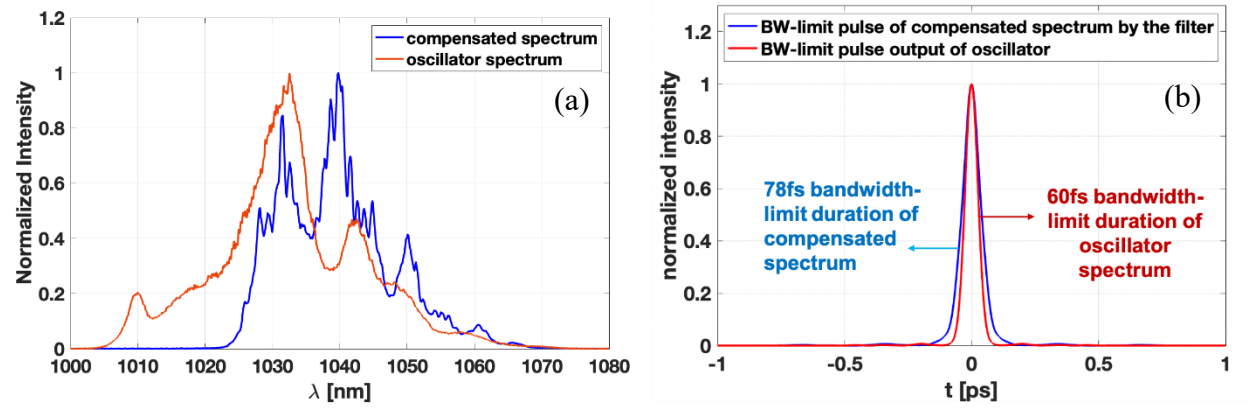

Figure 4.9 (a) measured compensated spectrum after amplified by 100dB gain in CPSA system, compared to the oscillator spectrum; (b) calculated bandwidth-limited pulse shapes based on the measured compensated spectrum and oscillator spectrum.

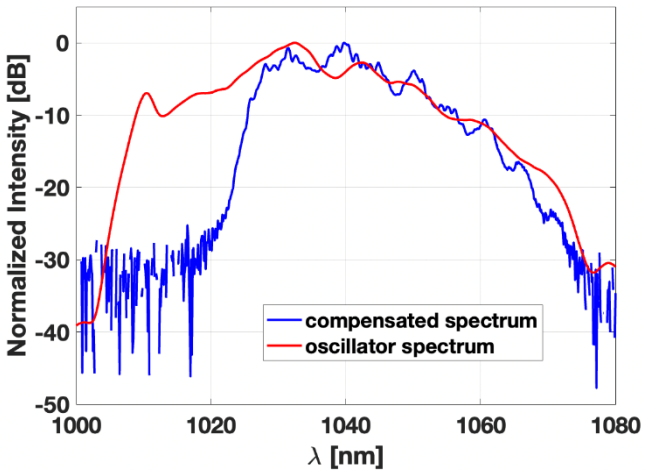

Figure 4.10 Measured spectra in a logarithmic scale of the oscillator output and the compensated pulse.

This means the actual gain that the spectral filter compensated is 125dB. This oscillator can be replaced by another 1GHz mode-locked oscillator that can generate nearly flat-top spectrum, which will allow to achieve broader compensated spectra. Also, in this experiment we only stretched the pulses to 100ps which limits the achievable energy. In the next step, we will use a grating-based stretcher that can maintain ~40fs spectral width for stretching the pulses from the 1GHz oscillator with the flat-top spectrum to 1ns duration. These 1ns stretched pulses will then be amplified in the sequence of the amplification stages including another 85µm-CCC stage (figure 4.8). Therefore, we anticipate achieving less than 78fs spectral content at the final amplifier output with the ~10mJ burst energy, after these modifications are implemented.

CHAPTER V

Broadband Femtosecond Dispersion Compensator for CPSA and Fiber CPA System Using Controlled Optical Aberrations

The previous chapters deal directly with challenges of maintaining broadband pulse spectra in CPSA, and ultrashort pulse fiber laser systems in general. This chapter deals with broadband challenges associated with pulse compression, since the shorter the pulse, the more challenging dispersion matching issues in the system are. And since previous chapters demonstrate a path to preserve bandwidths sufficient for ~40-100fs bandwidth-limited pulses from an Yb-doped high energy fiber system such as CPA or CPSA, which has not been achieved yet in the field, it becomes necessary to also develop new approaches to achieve compression of such short pulse durations in a fiber system, which is typically characterized by a very long propagation path in a dispersive fiber glass. For longer than 200-300fs pulses, only 2^{nd} and 3^{rd} dispersion orders in the system are necessary to compensate. In fiber laser systems or fiber delivery systems with less than ~100fs output pulses, 4^{th} order and even higher orders also need to be corrected. In CPSA and fiber CPA systems, where the optical pulses are stretched, amplified, and compressed, the stretcher and the compressor can be mutually misaligned in a prescribed way to achieve compensation of the 2^{nd} order and 3^{rd} order dispersion orders induced by the long propagation lengths in a fiber glass. This might be sufficient to achieve bandwidth-limited duration for pulses longer than ~150fs, when the 4^{th} order dispersion is usually not relevant. Such mismatch between stretcher and compressor works well for moderately short pulses from solid-state CPA systems, where signals propagate only centimeters in a gain medium. Such a small amount of material dispersion can be easily compensated for sub-100fs pulses by adjusting stretcher and compressor mutual alignment (becomes a challenge only for

pulses approaching ~30fs [34]). In a FCPA, with typically 10-100 meters of fiber in the path, this produces very large higher-order dispersion contributions, which cannot be compensated by such an approach. Many techniques have been developed for such dispersion compensation to solve this problem in fiber laser systems. But all of them are applicable only to relatively long (>100fs) pulses, since they are unable to compensate all relevant dispersion orders due to long fibers. For instance, Grism was introduced to provide 3rd order dispersion phase with the opposite sign of that of the fiber, but 4th order phase is still uncompensated [34], [35]. Fiber Bragg Gratings can provide higher order dispersions, but the magnitudes are fixed, and thus the required high accuracy is difficult to achieve [36]–[38]. Pulse shapers can provide real-time phases to correct the dispersion in laser systems. But the amount of dispersion they can provide is also limited.

In this chapter, we developed an optical-aberration-based dispersion compensator, which can provide a large amount of phase with 2nd, 3rd and 4th phase orders controlled independently. Therefore, it is well suited for fiber laser systems, and can compensate all the required dispersion orders for pulses around and much shorter than ~100fs. We experimentally demonstrated that in a fiber delivery system with 50m fiber, this device enables 70fs bandwidth-limited compressed pulses. Also, 136fs pulse duration was achieved utilizing this compensator in a CPA system, with a grating-based stretcher, 50m total fiber length in a system, and a grating-based compressor. Finally, we theoretical demonstrate that this compensator can be used in a CPA system with a specially-designed fiber stretcher, and a standard grating-based compressor to obtain 70fs compressed pulse duration, while compensating the 1ns stretched pulse duration.

5.1 Compensation Criteria for Higher-order Dispersion Terms

The phase accumulated due to dispersions from materials or dispersive optical components when an optical pulse propagates through a system can be expanded as Taylor series:

$$\phi(\omega) = \phi_0 + \phi_1(\omega - \omega_0) + \frac{\phi_2}{2!}(\omega - \omega_0)^2 + \frac{\phi_3}{3!}(\omega - \omega_0)^3 + \frac{\phi_4}{4!}(\omega - \omega_0)^4 + \ldots \quad (5.1)$$

Where ϕ_m are the phase coefficients and can be calculated as

$$\phi_m = \left(\frac{\partial^m \phi(\omega)}{\partial \omega^m}\right)_{\omega=\omega_0} \quad (5.2)$$

The phase can also be described by the propagation constant $\beta(\omega)$, that is

$$\phi(\omega) = \beta(\omega)\, z = \beta_0 z + \beta_1(\omega - \omega_0)z + \frac{\beta_2}{2!}(\omega - \omega_0)^2 z + \frac{\beta_3}{3!}(\omega - \omega_0)^3 z + \frac{\beta_4}{4!}(\omega - \omega_0)^4 z + \cdots \quad (5.3)$$

Here $\beta_m = \left(\frac{\partial^m \beta(\omega)}{\partial \omega^m}\right)_{\omega=\omega_0}$. In an optical system, the total β_m is the sum of β_m in different optical components. For example, the magnitude of β_2 in a FCPA system is the sum of β_2 in the stretcher, fiber and compressor. In an ideal system, $\beta_m = 0$ must be achieved for all orders, and the output pulse has bandwidth-limited pulse duration. Since different optical components have different dispersion, all the dispersion orders cannot be fully compensated simultaneously in a real optical system. Compensation of 2nd and 3rd phase order compensation can be achieved, for example, by adjusting the separation and the angles of incidence in the stretcher and compressor. But higher dispersion orders cannot be compensated in this way, and thus limit the shortest achievable pulse duration. To quantify this, it is necessary to analyze the effects of higher-order dispersion on the pulse duration. We carry-out this analysis by both numerical simulations and analytically.

In the numerical analysis, the pulse is chosen to have a square-shape spectrum centered at 1030nm, which is usually the case for optical systems where the spectrum is cut-off by hard-edge components such as a stretcher grating. In the frequency domain, different magnitudes of different dispersion terms are added onto the spectrum separately. Then, the corresponding stretched pulse shapes are obtained by Fourier transform. The broadening effects of different phase orders can be characterized by two factors: Strehl ratio and FWHM (full width at half maximum). Strehl ratio is the ratio between the compressed-pulse and bandwidth-limited pulse peak intensities. FWHM represents the pulse duration of the pulse. It should be noted that FWHM alone is not sufficient for characterizing the compressed pulse quality. Figure 5.1 shows the numerical results for 30nm and 60nm bandwidths, which correspond to 100fs and 50fs bandwidth-limited pulse durations. For each phase order, its value that is acceptable for a 50fs pulse without significant broadening is one order of magnitude lower than that for a 100fs pulse. Therefore, for a specific spectral width, the acceptable phase term values decrease by a factor of ten with every phase order increased.

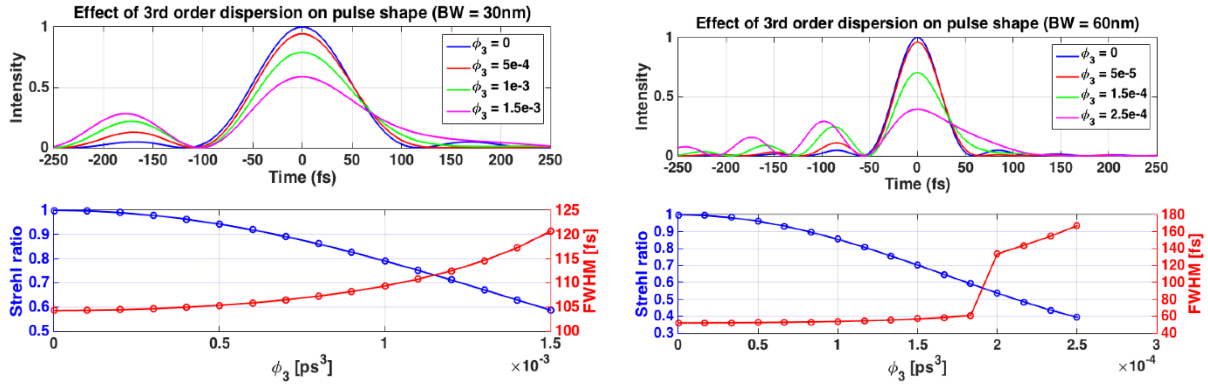

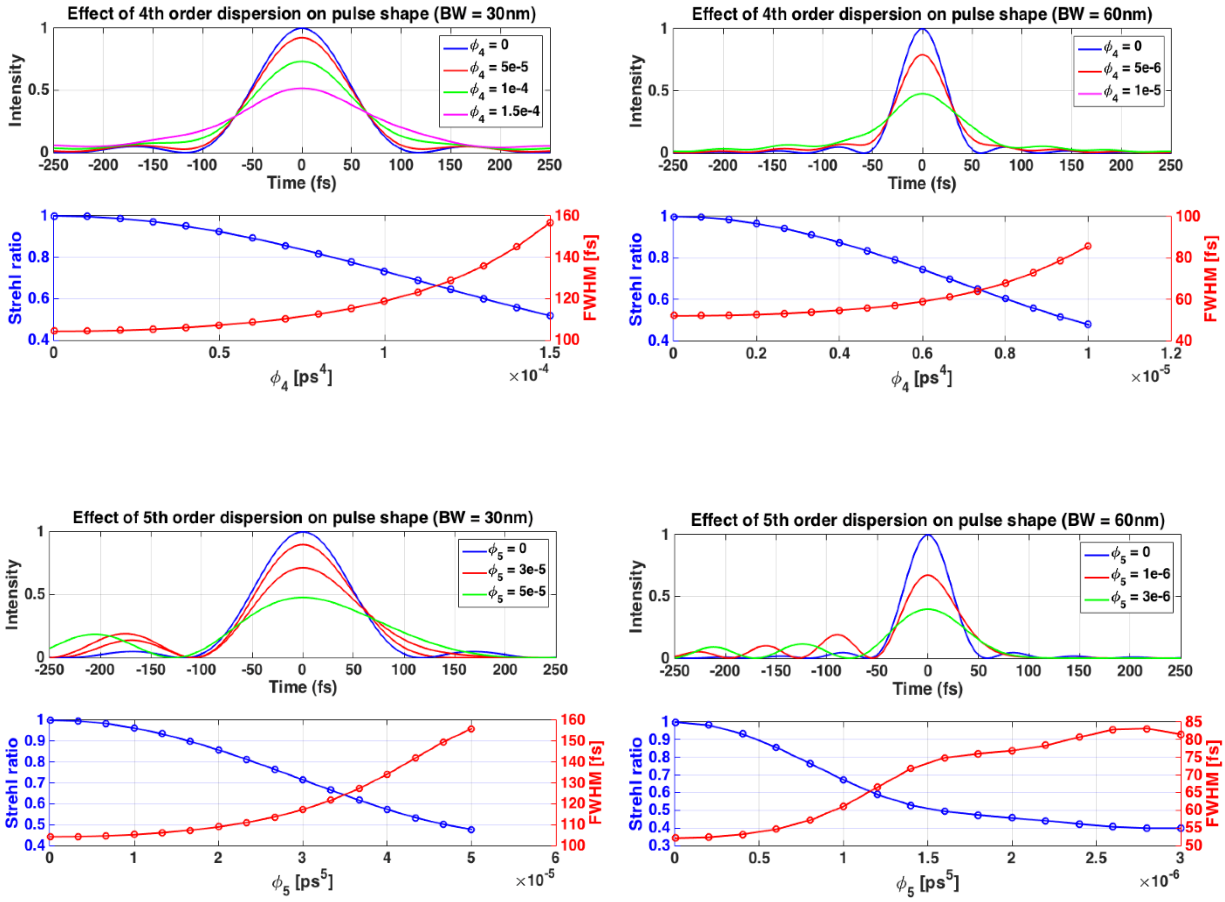

Figure 5.1 Pulse broadening effects of 3rd, 4th and 5th dispersion phase orders, assuming square-shape spectrum with 30nm and 60nm bandwidth.

Let's now consider the problem analytically. For a specific frequency ω, the time required to propagate a medium with length z is

$$\tau(\omega) = \frac{\partial\phi(\omega)}{\partial\omega} = \frac{\partial\beta(\omega)}{\partial\omega} z = \frac{z}{v_g(\omega)} \tag{5.4}$$

Here $v_g(\omega) = (\frac{\partial\beta(\omega)}{\partial\omega})^{-1}$ is the group velocity. The Taylor series of $\tau(\omega)$ is

$$\tau(\omega) = \tau_0 + \tau_1(\omega - \omega_0) + \frac{\tau_2}{2!}(\omega - \omega_0)^2 + \frac{\tau_3}{3!}(\omega - \omega_0)^3 + \frac{\tau_4}{4!}(\omega - \omega_0)^4 + \ldots \quad (5.5)$$

According to equations (5.4) and (5.5),

$$\tau_m = \left(\frac{\partial^{m+1}\beta(\omega)}{\partial\omega^{m+1}}\right)_{\omega=\omega_0} \times z = \left(\frac{\partial^{m+1}\phi(\omega)}{\partial\omega^{m+1}}\right)_{\omega=\omega_0} = \phi_{m+1} \quad (5.6)$$

The propagation time of frequency ω relative to frequency ω_0 is therefore

$$\Delta\tau(\omega) = \tau(\omega) - \tau(\omega_0) = \tau_1(\omega - \omega_0) + \frac{\tau_2}{2!}(\omega - \omega_0)^2 + \frac{\tau_3}{3!}(\omega - \omega_0)^3 + \frac{\tau_4}{4!}(\omega - \omega_0)^4 + \ldots$$
$$= \phi_2(\omega - \omega_0) + \frac{\phi_3}{2!}(\omega - \omega_0)^2 + \frac{\phi_4}{3!}(\omega - \omega_0)^3 + \frac{\phi_5}{4!}(\omega - \omega_0)^4 + \ldots \quad (5.7)$$

Since $\Delta\tau(\omega)$ is the time delay between frequency ω and ω_0, it represents the stretched pulse duration after a pulse propagates through a dispersive medium. Let $\Delta\omega = \omega - \omega_0$ be the half width at half maximum (HWHM) of the spectrum, where ω_0 is the central frequency. Each stretched pulse duration order can be calculated by

$$\Delta\tau_1(\omega) = \phi_2\Delta\omega, \quad \Delta\tau_2(\omega) = \frac{\phi_3}{2!}(\Delta\omega)^2,$$
$$\Delta\tau_3(\omega) = \frac{\phi_4}{3!}(\Delta\omega)^3, \quad \Delta\tau_4(\omega) = \frac{\phi_5}{4!}(\Delta\omega)^4 \quad (5.8)$$

That is

$$\Delta\tau_n(\omega) = \frac{\phi_{n+1}}{n!}(\Delta\omega)^n \quad (5.9)$$

To maintain the short pulse duration, $\Delta\tau_n$ (n = 1,2,…) should be very close to the bandwidth-limited pulse duration. Let τ_p represent the bandwidth-limited pulse duration, so that $\Delta\tau_n = \tau_p$. The time-bandwidth product of a pulse is

$$\frac{\Delta\omega\Delta\tau_p}{2\pi} = C_B \tag{5.10}$$

Here C_B is the factor that is dependent on specific pulse shape. Substituting the equation 5.10 to equation 5.9, we obtain

$$\phi_n = \frac{2\pi C_B(n-1)!}{(\Delta\omega)^n} \tag{5.11}$$

This formula can be used to calculate the acceptable residual higher-order dispersion terms for any spectral shape and spectral width. For square-shape pulses, $C_B = 0.885$. The analytical results for 50fs and 100fs square-shape pulses are shown in Table 1. Compared to the numerical results, the analytical results correspond to 90% of the Strehl ratio. Thus, the phase values ϕ_n obtained by equation 5.11 represent the criteria for residual phase values that are allowed in a system without causing significant broadening.

Phase order	50fs (60nm) pulse	100fs (30nm) pulse
$\phi_3(ps^3)$	7.5e-5	6.0e-4
$\phi_4(ps^4)$	4.3e-6	6.9e-5
$\phi_5(ps^5)$	3.2e-7	1.0e-5

Table 5.1 Theoretical results of criteria for higher-order dispersion terms.

5.2 Optical Aberration-Based Dispersion Compensator

Here we report a novel solution to this problem, which uses a specially-designed compact device, based on conventional diffraction-grating pair, with artificially induced controllable aberrations from an optical telescope inside this arrangement to achieve the required high-order dispersion compensation. We demonstrated this device experimentally with 30nm bandwidth femtosecond pulses, showing that 3rd and 4th order dispersion in a system with 50m-fiber path can be compensated for ~70fs – 150fs duration pulses.

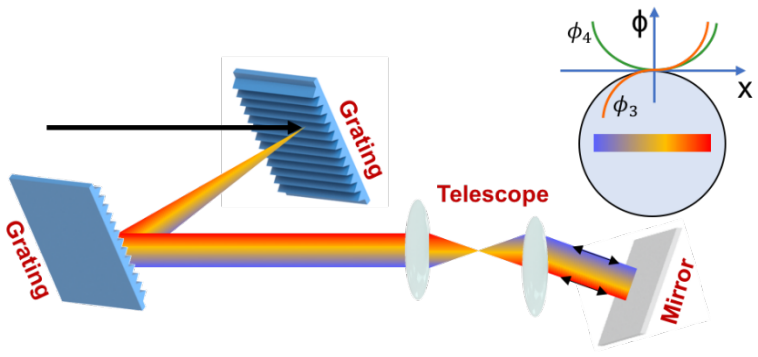

Figure 5.2. Layout of the aberration-based dispersion compensator

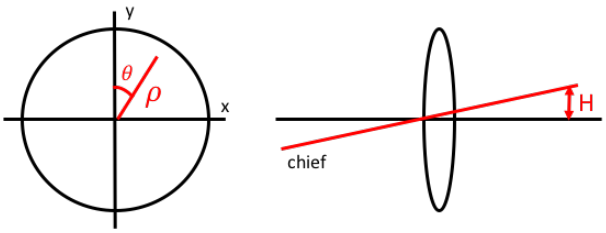

Figure 5.3 Aberration parameters

Figure 5.2 shows the layout of the dispersion compensator. The grating pair provides 2nd order phase by the separation between the two gratings, and the input angle to this grating pair is set at the Littrow angle. Lower groove density is desired due to the smaller higher order phase. To compensate the third and fourth order phase in the system, a telescope consists of a pair of lenses inserted right after the grating pair. Due to the spatially chirped collimated beam, a mapping from the wavelength to the position along the first of lens is achieved. It is known that optical aberrations can be described using Seidel polynomials [39]

$$W = \sum W_{ijk} H^i \rho^j \cos\theta^k \tag{5.12}$$

Where W is the optical path difference function obtained by comparing the aberrated wavefront to the ideal spherical wavefront. The Seidel polynomials is the series expansion of W. and each term represents a specific aberration. W_{ijk} is the wavefront aberration coefficient, whose value determines the maximum value this aberration term can achieve. W_{ijk} has unit of wavelength, and other factors are in normalized units. As shown in figure 5.3, ρ is the fractional radius ranging from 0 to 1, and H is the fractional image height whose range is also from 0 to 1. θ is the azimuth angle to the main axis and cos θ ranges from -1 to 1. Here we consider two of the fiber Seidel

aberrations, where i+j = 4: coma and spherical aberrations. These two kinds of aberrations can be described as ($\theta = 0$ in our case)

$$W_c = W_{131} H \rho^3 \cos\theta = W_{131} H \rho^3 \tag{5.13}$$

$$W_s = W_{040} \rho^4 \tag{5.14}$$

In our device, since the collimated beam going through the telescope is spatially chirped, we built a mapping from wavelength to ρ as shown in figure 5.2, where the spatial chirped beam goes through the lens. Thus, the phase terms from this telescope corresponding to coma and spherical aberrations at each surface are

$$\Phi_{coma} = \frac{\omega}{c} OPL(\omega) = \frac{\omega}{c} W_{131} H \left(\frac{\rho(\omega)}{\rho}\right)^3 = \frac{\omega}{c} W_{131} H \left(\frac{\omega - \omega_0}{\Delta\omega/2}\right)^3 = \frac{8 W_{131} \omega}{c(\Delta\omega)^3} H(\omega - \omega o)^3 \tag{5.15}$$

$$\Phi_{spherical} = \frac{\omega}{c} OPL(\omega) = \frac{\omega}{c} W_{040} \left(\frac{\rho(\omega)}{\rho}\right)^4 = \frac{\omega}{c} W_{040} \left(\frac{\omega - \omega_0}{\Delta\omega/2}\right)^4 = \frac{16 W_{040} \omega}{c(\Delta\omega)^4} (\omega - \omega o)^4 \tag{5.16}$$

ω is optical frequency and Δω is bandwidth. The total coma and spherical aberrations are the sum of four surfaces inside the telescope. Thus, this telescope provides 3rd and 4th phase from coma and spherical aberrations. W_{131} and W_{040} are determined by lenses characteristics. H can be controlled by shifting the second lens up and down, and ρ(ω) is determined by spatially chirped beam size, which can be tuned by shifting the second lens closer to, or further away from the first lens. Therefore, controlled magnitudes of 3rd and 4th order phase can be achieved with this telescope to compensate the corresponding dispersion orders.

5.3 Dispersion Compensation Experiments

i) Dispersion compensation in fiber delivery system

In our experimental setup, 160fs chirped pulses (with bandwidth-limited duration of 70fs) from an ytterbium-doped fiber oscillator are sent into the dispersion compensator. An Offner stretcher follows the compensator and stretches these pulses to ~1ns. The signal is then amplified by an ytterbium-doped single mode amplifier, with the total length of 50m from active and passive fibers. A compressor is then put after the amplifier, with the same grating as the one in the stretcher. The grating groove density is 1740/mm. The stretcher and compressor are configured to provide the same magnitude of dispersion, but with opposite signs, and so the net dispersion of the stretcher and the compressor is zero. The dispersion compensator is then configured to compensate all the dispersion orders originating from the fiber glass in the system.

The lenses inside this dispersion compensator are carefully chosen using ZEMAX, where the aberration coefficients are given for an extensive catalog of commercially available lenses. The magnitudes of the aberrations are controlled by the telescope alignment. The spherical aberration, and so the 4th order phase, is controlled by the distance between the two lenses, and the coma aberration, which is the 3rd order phase, is controlled by the height of the lenses. Figure shows the dependence of 4th order phase on the position of the second lens. By moving the second lens slightly off the theoretical focal point, a range of 4th order phase values is available for optimization.

Figure 5.4 (a) shows the measured autocorrelation of compressed pulses. The bandwidth-limited pulse duration is 70fs (the corresponding autocorrelation trace duration should be 97.6fs), while the measured pulse duration is 71.7fs (the measured autocorrelation duration is 111fs). To compare, figure 5.4 (b) shows the optimum pulse shape, achieved by optimizing the separation between the grating pair inside the compensator, when the telescope is removed so that no aberration is provided to compensate different dispersion orders. The duration between the two side peaks is close to 1ps.

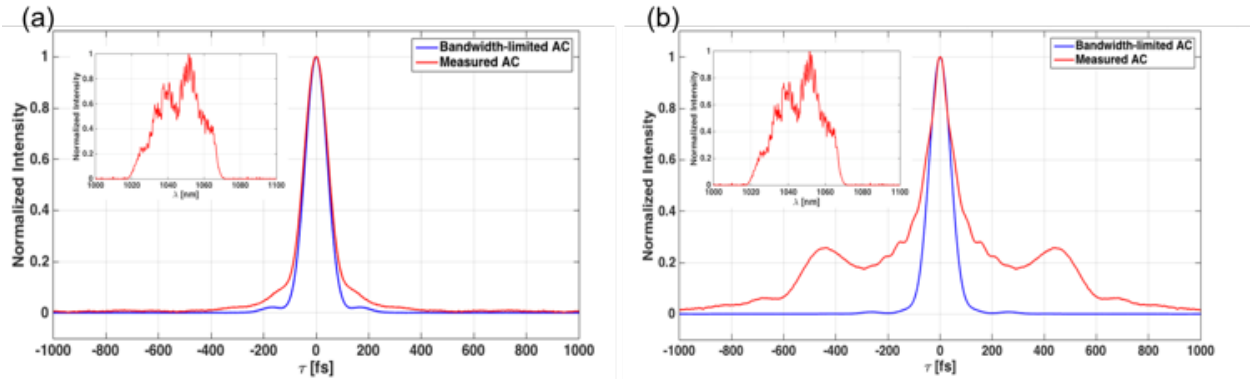

Figure 5.4. (a) measured and calculated autocorrelation traces; (b) measured and calculated autocorrelation traces without aberration compensating third and fourth order phase

ii)Dispersion compensation in FCPA system

In CPA system, there is another approach of dispersion control. Other than using compensator to compensate all the orders of dispersion of fiber, different phase orders can also be provided by mismatching the stretcher and compressor. Along with the phase orders provided by the compensator, this configuration can be more flexible, and can be used to compensate larger dispersion amounts.

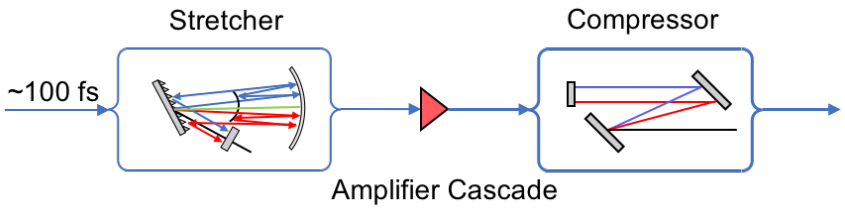

Figure 5.5 Configuration of Fiber CPA system

Figure 5.5 shows a typical configuration of a FCPA system. Pulses generated from a laser source going through a stretcher (the grating usually has high groove density) to stretch to 1-3ns, get amplified in a cascade of fiber amplifiers with 10's meter-fiber length, and are compressed when going through a compressor. The phase accumulated when going through the system and the total values of dispersion at each dispersion order are:

$$\phi^{tot}(\omega) = \phi\, s\,(\omega) + \phi\, f(\omega) + \phi\, c\,(\omega) \tag{5.17}$$

For each component, the phase can be expanded as Taylor series:

$$\phi^{i}(\omega) = \frac{\beta^{i}{}_{2}}{2!}(\omega-\omega_0)^2 z + \frac{\beta^{i}{}_{3}}{3!}(\omega-\omega_0)^3 z + \frac{\beta^{i}{}_{4}}{4!}(\omega-\omega_0)^4 z + \cdots \tag{5.18}$$

When there are ~50m-fiber in the system, only two of the three orders can be compensated to zero by mismatching the stretcher and compressor, and the rest one will remain very large, prohibiting compression to sub-100fs.

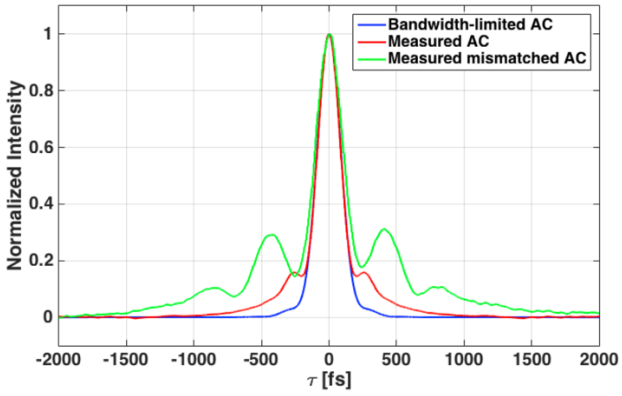

Figure 5.6 Measured autocorrelation trace of compressed pulse with dispersion compensator, and compressed pulse obtained by optimizing stretcher and compressor without compensator

Figure 5.6 shows the measured 100fs compressed pulses and bandwidth-limited pulse autocorrelation trace. The anticipated bandwidth-limited pulse duration is 136fs (autocorrelation duration should be 198fs), while the measured pulse duration is 136fs (measured autocorrelation duration is 198fs). The observed satellite pulses in the compressed pulses indicate that further improvement is possible, which is being pursued in the ongoing experiments.

5.4 Application of Aberration-Based Dispersion Compensator in CPA Systems with a Fiber Stretcher and Grating-Based Compressor

As shown in the previous section, aberration-based dispersion compensator can be applied to various optical systems. This section describes applying this dispersion compensator to CPA systems, which use a specially designed (and commercially available) fiber stretcher, and a standard grating-based compressor [11], [12], [40]–[42]. Compared to grating-based stretchers, which can be 1-2 m long for 1-2 ns pulses, a fiber stretcher is all fiber-based, and is thus much

more compact. Also, a fiber stretcher provides larger magnitudes of higher-order dispersion than normal fibers, and the signs of each order (up to 5th order phase) are opposite of the grating pair, while all the orders of normal fibers have the same sign as those of the grating pair, except for the 2nd order. These advantages make fiber stretchers a good option in CPA systems, especially high-energy CPA systems where a grating-based compressor is desired because of high output energies and powers. However, there are still mismatches of phase orders between the fiber stretcher and grating-based compressor, which limit the stretched pulse duration. This section shows that, when utilizing the aberration-based dispersion compensator to correct higher-order dispersion phases in CPA systems with a fiber stretcher and a grating-based compressor, 50-70 fs pulses can be stretched to 1 ns and still be able to be compressed to the bandwidth-limited durations. Without this correction, the acceptable stretched duration is one order of magnitude smaller.

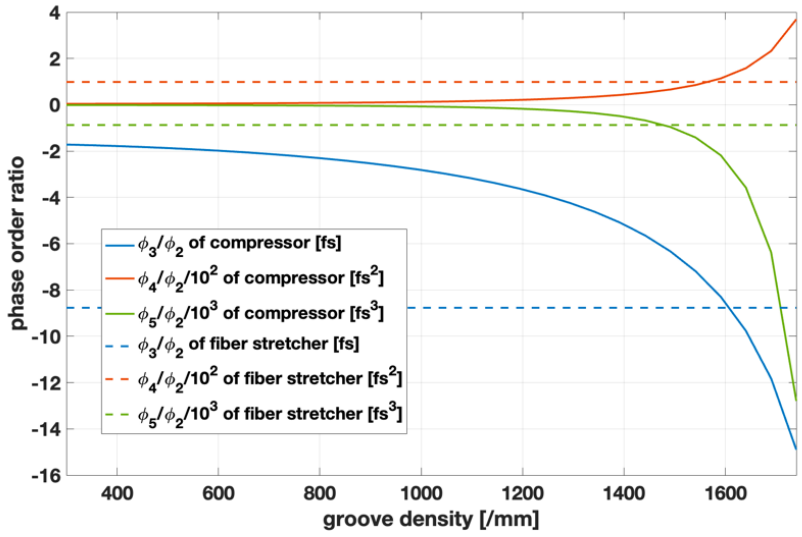

Figure 5.7 Calculated phase orders of the fiber stretcher and compressors with gratings of different groove density.

Phase order values of the fiber stretcher and compressors with gratings of different groove density are compared in figure 5.7. According to this comparison, phase orders of the fiber stretcher and the grating-based compressor cannot be matched at the same time. For instance, the 3rd order of the fiber stretcher matches the compressor with close to 1600/mm gratings while their 4th and 5th order doesn't match each other. In addition, since the groove densities of gratings are not continuous, and a small off from the desired groove density value can lead to large phase order mismatch, an additional dispersion compensation is required to achieve large stretching ratio. The achievable stretched pulse duration can be calculated based on the bandwidth-limited duration, and the ratios of higher-order to the 2nd order dispersion phase. The 2nd order phase needed to stretch the pulse to duration ΔT_{str} from a given bandwidth-limited pulse duration ΔT_{BL} is:

$$|\phi_2^{str}(\omega_0)| = \frac{\Delta T_{str}\Delta T_{BL}}{2\pi C_B} \tag{5.19}$$

According to equation (5.10) and (5.11), the maximum acceptable n-th order dispersion phase can be written as:

$$\phi_n = \frac{2\Delta T_{BL}{}^{n}(n-1)!}{(\pi C_B)^{n-1}} \tag{5.20}$$

Combining equation (5.19) and (5.20) and the maximum acceptable stretched pulse duration is:

$$\Delta T_{str} = 4\frac{\Delta T_{BL}{}^{n-1}(n-1)!}{(\phi_n/\phi_2^{str})(\pi C_B)^{n-2}} \tag{5.21}$$

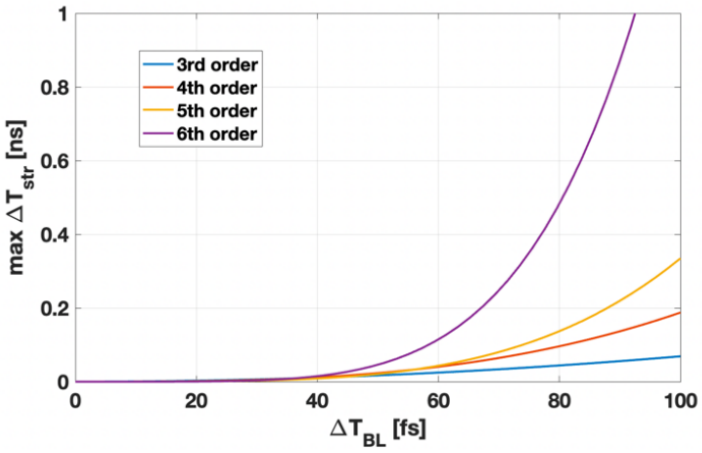

Figure 5.8 Maximum acceptable stretched duration from the given bandwidth-limited durations for different phase orders in the CPA system with the fiber stretcher and compressor with 1600/mm gratings.

Figure 5.8 shows the maximum stretched duration in the CPA system, with the fiber stretcher and compressor with 1600/mm gratings, when the phase orders lower than the current order are fully compensated. For example, the red curve in Figure 5.8 represents the maximum stretched duration, when the 2nd and 3rd order phase are zero, and the 4th order phase is the main limitation. We can tell from this plot that the stretched duration is limited to 1-10 ps by the 3rd order phase, which is very small and needs an additional device to correct the dispersion phases.

The aberration-based dispersion compensator provides 3rd and 4th order phase correct, and the magnitudes can be continually adjusted so that high-order phases can be fully compensated. The compressor with 1480/mm gratings is used because its 5th order is very close to that of the fiber stretcher, and 3rd and 4th order phase in the system are compensated by the aberration-based compensator.

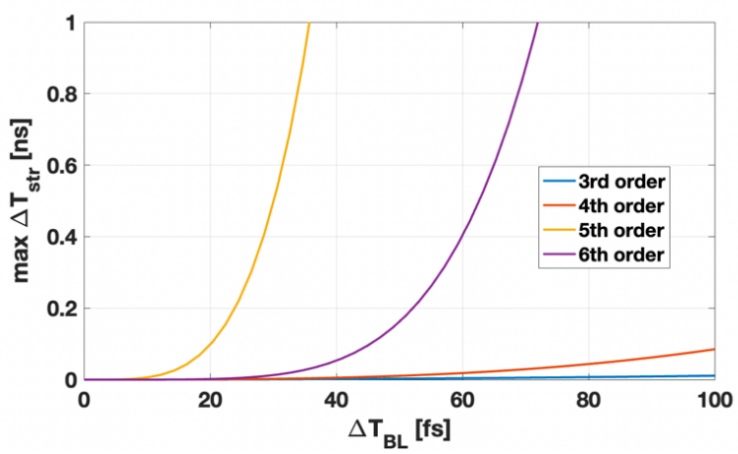

Figure 5.9 Maximum acceptable stretched duration from the given bandwidth-limited durations for different phase orders in the CPA system with the fiber stretcher and compressor with 1480/mm gratings.

Figure 5.9 shows the maximum acceptable stretched duration when the compressor 1480/mm gratings are used. This means when the 3rd and 4th order phase are compensated, the maximum acceptable stretched duration is determined by the 6th order phase in the system. Compared to only 1-10 ps stretched duration without the compensator, the pulse of 70 fs bandwidth-limited duration can be stretched to 0.8-1 ns. The dispersion compensator configuration is shown in figure 5.10. The grating pair is 1000/mm with the grating width of 2.5 cm. The input angle is chosen close to be Littrow angle, and the separation between the gratings is adjusted to have the desired spatially chirped beam size (1.1 cm). The first lens of the telescope is the bi-convex lens LE5183 from Thorlabs, which provides the positive 4th order phase. The second lens of the telescope is the bi-concave lens LD4931 from Thorlabs, which is off-axis to provide 3rd order phase.

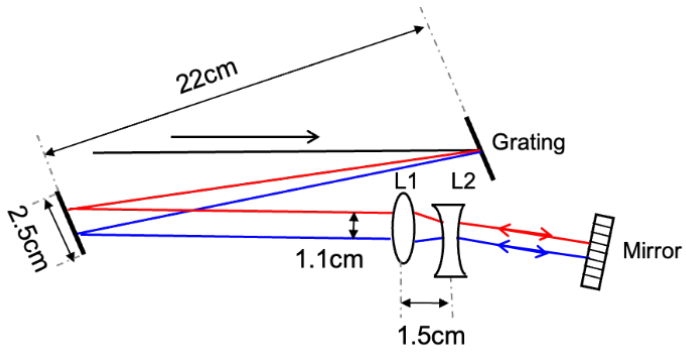

Figure 5.10 Dispersion compensator configuration (L1: bi-convex lens LE5183 from Thorlabs, L2: bi-concave lens LD4931 from Thorlabs, grating: 1000/mm).

In summary, we demonstrate theoretically and experimentally aberration-based device to compensate each dispersion order in a fiber CPA system with 10's meter-fiber length. And we experimentally compress down to close to bandwidth-limited pulse duration for 70fs.

BIBLIOGRAPHY

[1] L. Quinn *et al.*, "Infrared and Optical Masers," *Physical Review*, vol. 112, no. 6, pp. 1940–1949, Dec. 1958.

[2] T. H. Maiman, "Stimulated Optical Radiation in Ruby," *Nature*, vol. 187, no. 4736, pp. 493–494, 1960.

[3] A. J. Gross and T. R. W. Herrmann, "History of lasers," *World Journal of Urology*, vol. 25, no. 3, pp. 217–220, Jun. 2007.

[4] G. Mourou, T. Tajima, M. N. Quinn, B. Brocklesby, and J. Limpert, "Are Fiber-based Lasers the Future of Accelerators?," *Nuclear Instruments and Methods in Physics Research, Section A: Accelerators, Spectrometers, Detectors and Associated Equipment*, vol. 740, pp. 17–20, Mar. 2014.

[5] W. Leemans and E. Esarey, "Laser-driven Plasma-wave Electron Accelerators," *Physics Today*, vol. 62, no. 3, pp. 44–49, 2009.

[6] Donna Strickland and Gerard Mourou, "Compression of Amplified Chirped Optical Pulses," *Optics Communications*, vol. 55, no. 6, pp. 447–449, 1985.

[7] T. Zhou, J. Ruppe, C. Zhu, I.-N. Hu, J. Nees, and A. Galvanauskas, "Coherent Pulse Stacking Amplification using Low-finesse Gires-Tournois Interferometers," *Optics Express*, vol. 23, no. 6, p. 7442, Mar. 2015.

[8] Govind Agrawal, *Nonlinear Fiber Optics Fourth Edition*, 4th ed. 2006.

[9] H. Stark, M. Müller, M. Kienel, A. Klenke, J. Limpert, and A. Tünnermann, "Electro-optically Controlled Divided-pulse Amplification," *Optics Express*, vol. 25, no. 12, p. 13494, Jun. 2017.

[10] ANDREW M. WEINER, *Ultrafast Optics*. 2009.

[11] A. Fernández *et al.*, "High-fidelity, 160 fs, 5 μJ Pulses from an Integrated Yb-fiber Laser System with a Fiber Stretcher Matching a Simple Grating Compressor," *Optics Letters*, vol. 37, no. 5, pp. 927–929, 2012.

[12] D. v. Khudyakov *et al.*, "Application of Dispersion-Compensating Fiber with W-type Refractive Index Profile in Stretcher of Ultrashort Laser Pulses at a Wavelength of 103 μm," *Journal of the Optical Society of America B*, vol. 36, no. 11, p. 3066, Nov. 2019.

[13] Q. Han, T. Liu, X. Lü, and K. Ren, "Numerical Methods for High-power Er/Yb-codoped Fiber Amplifiers," *Optical and Quantum Electronics*, vol. 47, no. 7, pp. 2199–2212, Jul. 2015.

[14] Q. Han, J. Ning, and Z. Sheng, "Numerical Investigation of the ASE and Power Scaling of Cladding-Pumped Er-Yb Codoped Fiber Amplifiers," *IEEE Journal of Quantum Electronics*, vol. 46, no. 11, pp. 1535–1541, 2010.

[15] Q. Han, J. Ning, H. Zhang, and Z. Chen, "Novel Shooting Algorithm for Highly Efficient Analysis of Fiber Raman Amplifiers," *Journal of Lightwave Technology*, vol. 24, no. 4, pp. 1946–1952, Apr. 2006.

[16] Y. Wang and H. Po, "Dynamic Characteristics of Double-Clad Fiber Amplifiers for High-Power Pulse Amplification," *Journal of Lightwave Technology*, vol. 21, no. 10, pp. 2262–2270, Oct. 2003.
[17] X. Ma, C. Zhu, I.-N. Hu, A. Kaplan, and A. Galvanauskas, "Single-mode Chirally-coupled-core Fibers with Larger than 50μm Diameter Cores," *Optics Express*, vol. 22, no. 8, pp. 9206–9219, Apr. 2014.
[18] M. R. A. Moghaddam, S. W. Harun, and H. Ahmad, "Comparison between Analytical Solution and Experimental Setup of a Short Long Ytterbium Doped Fiber Laser," *Optics and Photonics Journal*, vol. 02, no. 02, pp. 65–72, 2012, doi: 10.4236/opj.2012.22010.
[19] D. Gloge, "Weakly Guiding Fibers," *Applied Optics*, vol. 10, no. 10, pp. 2252–2258, 1971.
[20] J. Stoer and R. Bulirsch, *Introduction to Numerical Analysis*. Springer New York, 1980.
[21] J. W. Thomas, "Numerical Partial Differential Equations Finite Difference Methods by J.W. Thomas (z-lib.org)".
[22] E. Desurvire, *Erbium-doped Fiber Amplifiers : Principles and Applications*. Wiley, 1994.
[23] X. Peng and L. Dong, "Temperature Dependence of Ytterbium-doped Fiber Amplifiers," *J.Opt.Soc.Am.B*, vol. 25, no. 1, pp. 126–130, 2007.
[24] M. J. F. Digonnet, E. Murphy-Chutorian, and D. G. Falquier, "Fundamental Limitations of the McCumber Relation Applied to Er-doped Silica and other Amorphous-host Lasers," *IEEE Journal of Quantum Electronics*, vol. 38, no. 12, pp. 1629–1637, Dec. 2002.
[25] J. M. Ruppe, "Theoretical and Experimental Foundations of Coherent Pulse Stacking Amplification," 2017.
[26] A. E. Siegman, *Lasers*. University Science Books, 1986.
[27] A. Galvanauskas, "Ultrafast Lasers Technology and Applications," 2003.
[28] M. A. Vorontsov and V. P. Sivokon, "Stochastic Parallel-gradient-descent Technique for High-resolution Wave-front Phase-distortion Correction," *J. Opt. Soc. Am. A*, vol. 15, no. 10, pp. 2745–2758, 1998.
[29] H. Stark, J. Buldt, M. Müller, A. Klenke, and J. Limpert, "100 fs Pulses Directly from a kW-class mJ-level Ytterbium-doped Fiber CPA Laser System," in *iber Lasers XVIII: Technology and Systems*, Mar. 2021, p. 48. doi: 10.1117/12.2579186.
[30] Y. Chiba, H. Takada, K. Torizuka, and K. Misawa, "65-fs Yb-doped Fiber Laser System with Gain-narrowing Compensation," *Optics Express*, vol. 23, no. 5, p. 6809, Mar. 2015.
[31] L. Lavenu *et al.*, "High-energy Few-cycle Yb-doped Fiber Amplifier Source Based on a Single Nonlinear Compression Stage," *Optics Express*, vol. 25, no. 7, p. 7530, Apr. 2017.
[32] K. Toda, K. Isobe, K. Namiki, H. Kawano, A. Miyawaki, and K. Midorikawa, "Temporal Focusing Microscopy Using Three-photon Excitation Fluorescence with a 92-fs Yb-fiber Chirped Pulse Amplifier," *Biomedical Optics Express*, vol. 8, no. 6, pp. 2796–2806, Jun. 2017.
[33] P. Sidorenko, W. Fu, and F. Wise, "Nonlinear Ultrafast Fiber Amplifiers Beyond the Gain-narrowing Limit," *Optica*, vol. 6, no. 10, pp. 1328–1333, Oct. 2019.

[34] S. Kane and J. Squier, “Grism-pair Stretcher-compressor System for Simultaneous Second-and third-order Dispersion Compensation in Chirped-pulse Amplification,” *J. Opt. Soc. Am. B*, pp. 661–665, 1997.
[35] L. Kuznetsova, F. W. Wise, S. Kane, and J. Squier, “Chirped-pulse Amplification Near the Gain-narrowing Limit of an Yb-doped Fiber Amplifier Using a Reflection Grism Compressor,” 2007.
[36] T. Bartulevicius *et al.*, “Compact Fiber CPA System based on a CFBG Stretcher and CVBG Compressor with Matched Dispersion Profile,” *Optics Express*, vol. 25, no. 17, pp. 19856–19862, Aug. 2017.
[37] J. Želudevičius, R. Danilevičius, and K. Regelskis, “Optimization of Pulse Compression in a Fiber Chirped Pulse Amplification System by Adjusting Dispersion Parameters of a Temperature-tuned Chirped Fiber Bragg Grating Stretcher,” *Journal of the Optical Society of America B*, vol. 32, no. 5, p. 812, May 2015.
[38] A. Galvanauskas, M. E. Fermann, D. Harter, K. Sugden, and I. Bennion, “All-fiber Femtosecond Pulse Amplification Circuit using Chirped Bragg gratings,” *Applied Physics Letters*, vol. 66, no. 9, pp. 1053–1055, Feb. 1995.
[39] Joseph M. Geary, *Introduction to Lens Design With Practical ZEMAX Examples*. Willmann-Bell, Inc., 2002.
[40] S. Kane and J. Squier, “Grating Compensation of Third-Order Material Dispersion in the Normal Dispersion Regime: Sub-100-fs Chirped-Pulse Amplification Using a Fiber Stretcher and Grating-Pair Compressor,” *IEEE JOURNAL OF QUANTUM ELECTRONICS*, vol. 31, no. 11, pp. 2051–2057, 1995.
[41] L. Grüner-Nielsen, D. Jakobsen, K. G. Jespersen, and B. Pálsdóttir, “A Stretcher Fiber for Use in fs Chirped Pulse Yb Amplifiers,” *Optics Express*, vol. 18, no. 4, pp. 3768–3773, 2010.
[42] L. Grüner-Nielsen *et al.*, “Polarization Maintaining Dispersion Compensating Fiber,” Nov. 2014.